UILU-ENG-85-2012

. ENGINEERING STUDIES

RAL RESEARCH SERIES NO. 521

ISSN: 0069-4274

A STUDY OF SEISMIC GROUND MOTION FOR LIFELINE RESPONSE ANALYSIS

By
A. ZERVA
A. H-S. ANG
and
Y. K. WEN

Technical Report of Research
Supported by the
NATIONAL SCIENCE FOUNDATION
(Under Grants INT 82-19528 and CEE 82-13729)

UNIVERSITY OF ILLINOIS
at URBANA-CHAMPAIGN
URBANA, ILLINOIS
OCTOBER 1985

50272-101

REPORT DOCUMENTATION PAGE	1. REPORT NO. UILU-ENG-85-2012	2.	3. Recipient's Accession No.

4. Title and Subtitle

A STUDY OF SEISMIC GROUND MOTION FOR LIFELINE RESPONSE ANALYSIS

5. Report Date: OCTOBER 1985

6.

7. Author(s)

A. Zerva, A. H-S. Ang and Y. K. Wen

8. Performing Organization Rept. No. SRS No. 521

9. Performing Organization Name and Address

Department of Civil Engineering
University of Illinois
208 N. Romine Street
Urbana, IL 61801

10. Project/Task/Work Unit No.

11. Contract(C) or Grant(G) No.

(C)
(G) NSF INT 82-19528
NSF CEE 82-13729

12. Sponsoring Organization Name and Address

National Science Foundation
Washington, DC

13. Type of Report & Period Covered

14.

15. Supplementary Notes

16. Abstract (Limit: 200 words)

An analytical model for determining the differential ground motion during an earthquake is developed. The ground motion is assumed to be a stationary random process, resulting from waves radiated from an underground source (fracture surface). The source motion is also modeled as a random process specified by a power spectral density. The spectral density of the ground motion is related to that of the source by a frequency transfer function. An analytical method for two-dimensional wave propagation is used to evaluate the displacements at the ground surface, from which the frequency transfer function is obtained through system identification. Power spectral densities of acceleration, cross-correlation and spatial variation coefficients, as well as power spectral densities of differential acceleration obtained through the model are compared with data from an actual earthquake, the earthquake of January 29, 1981, recorded at Lotung, Taiwan. The comparison indicates that the results of the model are in good agreement with the earthquake data.

Dynamic analyses of lifelines are also performed. The seismic input to the structures is considered to be either fully or partially correlated, and the results of the analytical stochastic ground motion model are used. The effect of the spatial variation of ground motions on the damage and reliability of horizontal systems is evaluated.

17. Document Analysis a. Descriptors

Earthquake
Ground Motions
Lifeline

b. Identifiers/Open-Ended Terms

c. COSATI Field/Group

18. Availability Statement	19. Security Class (This Report) UNCLASSIFIED	21. No. of Pages 137
	20. Security Class (This Page) UNCLASSIFIED	22. Price

ACKNOWLEDGMENTS

This report is based on the thesis of Dr. Aspasia Zerva submitted in partial fulfillment of the requirements for the Ph.D. in Civil Engineering at the University of Illinois at Urbana-Champaign.

The study is part of a cooperative research program with the National Taiwan University, Taipei, Taiwan suppported by the National Science Foundation under Grants INT 82-19528 and CEE 82-13729. These supports are gratefully acknowledged.

TABLE OF CONTENTS

Page

Page

LIST OF TABLES

Page

LIST OF FIGURES

Page

CHAPTER 1

INTRODUCTION

1.1 Introductory Remarks

Lifeline structures, such as pipelines, bridges, and communication transmission systems, are important infrastructure of cities and urban communities. The functional reliability of these lifeline systems during and after an earthquake and other natural hazards, therefore, is essential to the safety and health of the populace. However, lifelines have been heavily damaged during earthquakes (see, e.g., Jennings and Wood, 1971; U. S. Department of Commerce, 1973).

One major difference of lifelines from conventional structures is that lifelines extend essentially parallel to the ground for long distances compared to their other structural dimensions. Since an earthquake excitation consists of the superposition of a large number of waves with different characteristics, the different positions along a lifeline generally are subject to different motions. Although the coherent motion is a valid approximation for conventional structures, this same assumption may be unrealistic for long horizontal structures.

The spatial variation of seismic ground motions may be treated deterministically or stochastically. In the deterministic approach, a recorded accelerogram is used as the input motion at one point, and the differential motion between two points is obtained by a delay in the arrival of the seismic wave between the points (e.g., Nelson and Weidlinger, 1977; Johnson and Galletly, 1972). In the stochastic approach, a power spectral density for acceleration is assigned and the spatial

variation is considered to be an exponentially decaying function based on earthquake data (e.g., Hindy and Novak, 1980). In either case, recorded accelerograms are essential. Furthermore, the seismic evaluation of lifelines based on actual earthquake data requires observations from dense arrays of strong motion seismographs. Such a strong motion array has recently been installed in Lotung (Bolt, et al., 1982), in the northeast corner of Taiwan. The array is called SMART-1, for Strong Motion Array in Taiwan, and motions from several major earthquakes have been recorded. The data obtained from the SMART-1 array have also been analyzed; e.g., Bolt, et al. (1982); Loh, Ang, and Wen (1983); Loh (1984b); Harichandran and Vanmarcke (1984).

Models, however, based on results of a particular earthquake are difficult to generalize since earthquakes are different in intensity, duration and frequency content. Therefore, there is a need for analytical models that can yield results in agreement with available array data, in order to extrapolate the limited data to other sites and regions. In this regard, stochastic models may be particularly appropriate.

1.2 Objective and Scope

The objective of this study is to develop a stochastic model to represent the characteristics of earthquake excitations pertinent to lifelines, such as power and cross spectral density functions, cross-correlation and spatial variation. Empirical, closed form expressions are derived for the power spectral densities of differential ground motion; specifically, the form of the differential spectra depends on a few parameters that change with distance. The input data for the analytical stochastic model are the earthquake magnitude, the distance of the site from the existing faults and the velocities of the compressional and shear waves in the ground.

This study also examines the contribution of the spatially varying input ground motion to the response of lifelines (pipelines and long beams). The importance of bending stresses compared to axial stresses for

pipelines is discussed and the effect of differential motion on the response of long-span beams is presented.

1.3 Organization

In Chapter 2 the model for evaluating the stochastic characteristics of strong ground motion is summarized; the related work is reviewed and the general procedure of the model is described.

Chapter 3 gives the comparison of the results of the model with data obtained from the earthquake of January 29, 1981 recorded at the SMART-1 array in Taiwan; the results include the power spectral densities, cross-correlation coefficients, and spatial variations of ground motions in three directions.

Chapter 4 examines the effect of differential ground motion on the response of pipelines. Two different cases are considered; in the first case the effect of differential motions on the joints of a pipeline is examined, whereas for the second case a continuous pipeline on elastic foundations is analyzed.

Chapter 5 examines a single-span, simply-supported long beam subjected to partially and fully correlated support motions.

Finally, Chapter 6 summarizes the results, including the validation of the model and the main effects of differential motions on the response of lifelines.

CHAPTER 2

GROUND MOTION MODEL

2.1 Review of Current State

In earthquake resistant design of conventional structures, the key parameter used to quantify the seismic loading is usually the peak ground acceleration. Various attenuation equations for the peak ground acceleration have been proposed (see, e.g., Donovan and Bornstein, 1978). On a more sophisticated level the response spectrum has been used (Newmark and Hall, 1969). In the stochastic domain, an earthquake is approximated by a white noise or a filtered white noise process (Housner and Jennings, 1964). The underlying assumption in analyzing and designing conventional structures to resist earthquakes is that the ground motions over the entire plan area of a structure are the same or do not vary significantly from point to point.

However, the seismic design of long lifelines differs fundamentally from that of conventional structures. Whereas the foundations of conventional structures extend over a limited area and therefore the ground motion can be assumed to be coherent, i.e., the same, this is not the case for long lifelines, in which the structure extends over a great distance relative to its other dimensions. Whereas the coherent motion may not induce significant stresses in the structure, i.e., it may only cause rigid body motions, the incoherent motion may induce significant stresses within the structure.

Although the state-of-the-art of earthquake engineering has progressed rapidly in the past few decades, there are still areas associated with the analysis of horizontal systems that require further study, including improvements in the characterization and definition of the spatial variation of ground motions.

Differential earthquake ground motion can be the result of the following:

1. relative fault motion;
2. liquefaction of soil; and
3. wave propagation.

Only differential motions caused by wave propagation will be examined in this study.

In the stochastic approach for a point system (e.g., building), a power spectral density for acceleration is prescribed; often the Kanai-Tajimi spectrum (Kanai, 1957; Tajimi, 1960) is used. In the examination of long lifelines the spatial variation of ground motion is usually assumed to be an exponentially decaying function, which requires some previous knowledge of the earthquake characteristics. However these earthquake characteristics are difficult to obtain, because of the lack of dense instrument arrays that can provide information for evaluating the spatial variations of ground motions.

In order to evaluate the differential motion between two stations on the ground surface, Nelson and Weidlinger (1977) introduced the Interference Response Spectrum, which is the response of a two-degree of freedom pipeline subjected to a seismic excitation propagating along the axis of the pipeline. In the stochastic domain, Shinozuka and Kawakami (1977) introduced a one-dimensional model for evaluating the spatial variation of ground motions, namely a surface layer subjected to vertically incident shear waves in which the dominant frequency of the layer, as well as the incident wave, were considered to be random processes.

A stochastic model is proposed for determining the differential earthquake ground motions. The inputs to the model are:

1. the earthquake magnitude;
2. the depth and orientation of the existing fault;

3. the distance of the stations from the epicenter; and

4. the characteristics of the medium, namely the velocities of the compressional and shear waves in the intervening material.

The general description of the model is presented in the next section, followed by the various steps required in its implementation.

2.2 Description of Model

2.2.1 General Concept and Basis

The general approach for evaluating the strong ground motion may be summarized in the following steps:

1. Specification of the Earthquake Magnitude -- The earthquake magnitude depends on the particular site, the occurrence of earthquakes at the site, and on the structure itself, namely its lifetime.

2. Modeling of the Source Mechanism by a Random Process -- The motion at the source is considered to be a random process described by the power spectral density function. This power spectral density is a function of the earthquake magnitude and the characteristics of the surrounding medium.

3. Specification of the Frequency Transfer Function -- The frequency transfer function is the result of an analytical wave propagation solution and a system identification technique. The actual three-dimensional problem of the ground excitation during an earthquake is decomposed into two two-dimensional problems, namely a plane strain (dip-slip rupture) problem and an antiplane (strike-slip rupture) problem.

4. Evaluation of the Strong Ground Motion -- The characteristics of the surface ground motions include the power spectral densities and the cross spectral densities at various points on the ground surface, from which the spatial variations of the ground motions are determined.

2.2.2 Power Spectral Density of Source Motion

The motion at the source is likely to be far too complex to be represented by any simple mathematical function, and, therefore a statistical, rather than a deterministic, approach is more appropriate.

The random nature of the excitation at the source has been widely considered in the literature. Housner (1955) postulated that the earthquake mechanism occurs as a random ensemble of individual dislocations at the source. Haskell (1964, 1966) introduced the spatio-temporal autocorrelation function of the relative acceleration at the source, whereas Aki (1967) introduced the spatio-temporal autocorrelation function of the relative velocity at the source. Boore and Joyner (1978) examined the influence of rupture incoherence on seismic directivity by considering analytical and Monte Carlo studies of models of nonuniform rupture. Hanks (1979) and Hanks and McGuire (1981) proposed a stochastic source model with an ω-square spectrum and a corner frequency depended on the global stress drop at the fault to predict a variety of measures of strong ground motion. Andrews (1981) introduced a model of random fault motion by assuming that the slip velocity is a random function of time and position. Papageorgiou and Aki (1983a,b) constructed a source model by assuming that the fault surface is composed of an aggregate of circular cracks at which rupture occurs, and the stationary occurrence of such localized ruptures generates the strong motion. Recently, Joyner (1984) introduced a stochastic kinematic model, in which the spectrum is controlled by the rupture length and width.

The decomposition of the three-dimensional wave propagation problem into a plane strain and an antiplane problem implies the simultaneous occurrence of the rupture over the entire length of the source. Therefore, the autocorrelation function and the power spectral density of the motion at the source should also be independent of the spatial component along the length of the fault. Accordingly, only the temporal variability of the excitation as presented in Haskell's (1966) or Aki's (1967) source model can be included; in either source model, the rupture at the fault is correlated only for small time lags.

The autocorrelation function of a stationary random process X(t) is defined as (Bendat, 1977):

$$R_{xx}(\tau) = \lim_{T' \to \infty} \frac{1}{2T'} \int_{-T'}^{T'} x(t)x(t+\tau)\, dt \tag{2.1}$$

where: T',t denote time; and τ is the elapsed time difference. Alternatively, the autocorrelation function of a stationary process may be defined as the ensemble average of individual autocorrelation functions of arbitrary time records ${}^{j}x(t)$ of finite durations, namely (Bendat, 1977),

$$R_{xx}(\tau) = \frac{1}{2T_1} \int_{-T_1}^{T_1} < {}^{j}x(t)\ {}^{j}x(t+\tau) >_{Av} dt$$

$$= \frac{1}{2T_2} \int_{-T_2}^{T_2} < {}^{j}x(t)\ {}^{j}x(t+\tau) >_{Av} dt \tag{2.2}$$

where j denotes the particular dependence on the arbitrary time record ${}^{j}x(t)$, T_1 and T_2 denote finite time intervals, and $< >_{Av}$ denotes average.

Therefore, the autocorrelation function of the relative velocity at the source during an earthquake may be defined as,

$$R_{vv}(\tau) = \lim_{T' \to \infty} \frac{1}{2T'} \int_{-T'}^{T'} \dot{D}(t)\ \dot{D}(t+\tau)\, dt$$

$$= \frac{1}{2T} \int_{-T}^{T} < \dot{D}(t)\ \dot{D}(t+\tau) >_{Av} dt$$

$$= \frac{k_T}{2} \int_{-k_T^{-1}}^{k_T^{-1}} < \dot{D}(t)\ \dot{D}(t+\tau) >_{Av} dt \tag{2.3}$$

where:

v = velocity;

τ = the time lag;

D = the relative displacement at the source;

T = the total rise or fracture time at which the displacement at the source reaches its final value D_o;

k_T^{-1} = the correlation time, implying that the motion at the source is correlated only for time intervals $k_T^{-1} < \tau < k_T^{-1}$.

The superscript j has been omitted for simplicity.

According to Aki (1967), the autocorrelation function of the relative velocity is of the negative exponential form. Based on this assumption, the integration of Eq. 2.3 yields

$$R_{vv}(\tau) = \frac{k_T}{2} \chi_o (1 - k_T|\tau|) e^{-k_T|\tau|} \tag{2.4}$$

where χ_o is a constant determined from the characteristics of the fault and the surrounding medium. The term $(1 - k_T|\tau|)$ in Eq. 2.4 has been included as a window in order to eliminate the tail contribution of the exponential term for time lags $\tau > k_T^{-1}$.

The power spectral density of the relative velocity has the following form:

$$S_{vv}(\omega) = \frac{k_T^2 \chi_o}{2\pi(k_T^2+\omega^2)^2} \{2\omega^2 + e^{-1}[(k_T^2-\omega^2) \cos(\frac{\omega}{k_T}) - 2k_T\omega \sin(\frac{\omega}{k_T})]\} \tag{2.5}$$

The determination of the parameters χ_o and k_T is discussed below.

Evaluation of χ_o and k_T -- Following Haskell (1966) the parameter χ_o may be defined as follows. Let $A(\omega)$ be the Fourier transform of the average relative velocity at the fault, i.e.:

$$A(\omega) = \frac{1}{2\pi} \int_{-\infty}^{\infty} < \dot{D}(t) >_{Av} e^{-i\omega t} \, dt \tag{2.6}$$

where:

ω = the circular frequency; and

$\dot{D}(t)$ = the relative velocity at the source.

For $\omega = 0$, the above equation becomes

$$A(0) = \frac{1}{2\pi} \int_{-\infty}^{\infty} < \dot{D}(t) >_{Av} dt = \frac{D_o}{2\pi} \tag{2.7}$$

where D_o is the final value of the displacement or dislocation at the source.

It can be shown that

$$|A(\omega)|^2 = \frac{T}{\pi} S_{vv}(\omega) \tag{2.8}$$

where:

T = the rise time; and

$S_{vv}(\omega)$ = the power spectral density of the relative velocity at the source, as defined by Eq. 2.5.

For $\omega = 0$ and making use of Eq. 2.5, Eq. 2.8 gives

$$\chi_o = \frac{D_o^2}{2T\ e^{-1}} \tag{2.9}$$

For an infinite fault with infinite rupture velocity, Kanamori (1972) showed that:

$$\dot{u} = \frac{D_o}{2T} = \sigma \frac{v_s}{\mu} \tag{2.10}$$

where:

$\dot{u}$ = the particle velocity;

σ = the effective stress;

μ = the rigidity of the medium; and

v_s = the shear wave velocity of the bedrock.

The assumption of the equality of the effective stress σ to the static stress drop $\Delta\sigma$, i.e.,

$$\sigma = \Delta\sigma \tag{2.11}$$

is reasonable for a relatively smooth motion at the fault (Kanamori, 1972). The stress drop $\Delta\sigma$ is generally given by the equation

$$\Delta\sigma = C\ \mu\ \frac{D_o}{\Lambda} \tag{2.12}$$

where, C is a nondimensional factor, and Λ is a measure of length, both depending on the geometry of the fault. A summary of the values of these parameters for certain fault geometries may be found in Kanamori and Anderson (1975). For a finite rectangular fault Eq. 2.12 holds only approximately as discussed in Sato (1972).

Throughout this study, the following value of the stress drop for a dip-slip fault is used (Sato, 1972):

$$\Delta\sigma = \frac{8(\lambda+\mu)}{\pi(\lambda+2\mu)}\ \mu\ \frac{D_o}{W} \tag{2.13}$$

where:

λ,μ = the Lame' constants; and

W = the width of the source.

Combining Eqs. 2.10, 2.11 and 2.13, the rise time is given by

$$T = \frac{\pi\ W(\lambda+2\mu)}{16\ v_s(\lambda+\mu)} \tag{2.14}$$

Equations 2.9 and 2.14 indicate that the parameter X_o depends on the final dislocation at the source D_o, the width of the rupture W, and the velocities of the compressional and shear waves.

Based on worldwide data and a statistical analysis, Mohammadi and Ang (1980) obtained analytical expressions for characterizing the fault rupture as a function of the earthquake magnitude. On this basis, the rupture width and displacement may be determined as follows:

Width of rupture (in km):

$$W = \exp(1.38\ M_s - 7.32) \tag{2.15}$$

Rupture displacement (in m):

$$D_o = \exp(1.78\ M_s - 12.31) \tag{2.16}$$

where M_s is the surface wave magnitude.

Equations 2.9, 2.14, 2.15 and 2.16 completely define the source parameter X_o.

Kanamori and Anderson (1975) proposed that the correlation time k_T^{-1} is proportional to the rise time T, namely,

$$\varepsilon = \frac{T}{k_T^{-1}} \tag{2.17}$$

where ε is a proportionality constant.

As an indication of which values of the proportionality constant ε should be acceptable, the values of k_T/v_s obtained from Haskell (1966) were plotted in Fig. 2.1 as functions of M_s; similar values of k_T/v_s obtained from the model are also presented for ε = 1, 3, 5, 10, 20 and 100. The values of ε in the range of 1 to 10 appear to be appropriate. As can be seen in Fig. 2.2, ε controls the shape of the power spectral density at the source; the smaller the value of ε the more the spectrum approaches a delta

function at frequency $\omega = 0$, whereas for large values of ε the spectrum approaches a white noise process.

Whereas ε controls the decay of the spectrum, χ_o controls its maximum value, namely the value at $\omega = 0$. χ_o grows exponentially with the surface wave magnitude, M_s, as can be seen from Fig. 2.3.

2.2.3 Determination of Frequency Transfer Function

The motions at the ground surface induced by an earthquake are the result of the fault rupture at the source and the propagation of the resulting waves through the intervening strata. The latter effects may be represented by means of a frequency transfer function. This frequency transfer function is obtained through an analytical wave propagation solution and a system identification technique. Although the interaction of the motion at the source and the propagating waves is not taken into account, the separate examination of the excitation at the source and the transmission of the resulting waves is a good approximation (Aki, 1967).

The analytical wave propagation method used in this study is the method of self-similar potentials (Seyyedian-Choobi and Robinson, 1975), and a time-domain system identification technique (Beck, 1978) is used.

The Method of Self-Similar Potentials -- The method of self-similar potentials, or functionally invariable solutions, is a powerful technique for solving equations of motion in two-dimensional elasticity with initial or boundary conditions that are given as homogeneous functions of the space and time variables. An extensive description of the method with applications to certain contact problems is given in Thompson and Robinson (1969). The application of the same method for solving dynamic problems in a three-dimensional space is presented in Johnson and Robinson (1972) and Farewell and Robinson (1974), whereas Seyyedian-Choobi and Robinson (1975) solved the problem of a buried dislocation pulse in a layered half-space by a combination of self-similar solutions. In all cases, the medium is assumed to be elastic, homogeneous and isotropic.

For an elastic, homogeneous and isotropic solid, under the assumption of infinitesimal strain, Navier's equations of motion become:

$$\mu\, u_{i,jj} + (\lambda+\mu)\, u_{j,ji} = \rho\, \ddot{u}_i \qquad ; \qquad i,j = 1,\ 2 \text{ or } 3 \tag{2.18}$$

where, $u_{i,j}$ denotes the partial derivative of the i^{th} component of the displacement vector $\underset{\sim}{u}$ with respect to the j^{th} Cartesian coordinate and ρ is the mass density.

By the Stokes-Helmholz resolution, the displacement vector $\underset{\sim}{u}$ can be expressed as the sum of the gradients of a scalar potential ϕ and the curl of a vector potential $\underset{\sim}{\psi}$, i.e.,

$$\underset{\sim}{u} = \underset{\sim}{\nabla}\phi + \underset{\sim}{\nabla} \times \underset{\sim}{\psi} \tag{2.19}$$

where $\underset{\sim}{\psi}$ satisfies the condition:

$$\underset{\sim}{\nabla} \cdot \underset{\sim}{\psi} = 0 \tag{2.20}$$

For the equations of motion (Eq. 2.18) to be satisfied, it is both a necessary and sufficient condition that the respective potentials satisfy the wave equations; namely,

$$\phi_{,ii} - \frac{1}{v_p^2}\ddot{\phi} = 0$$

$$\psi_{i,jj} - \frac{1}{v_s^2}\ddot{\psi}_i = 0 \tag{2.21}$$

where $v_p = \sqrt{\frac{\lambda+2\mu}{\rho}}$ and $v_s = \sqrt{\frac{\mu}{\rho}}$ are the velocities of the compressional (or P-) wave and shear (or S-) wave, respectively.

The general approach for evaluating the displacements in an unbounded medium may be summarized as follows:

1. Introduce appropriate complex potentials, displacements and stresses.

2. Determine the equations for the characteristic surfaces. The characteristic surfaces are uniquely defined by the variables θ_1 and θ_2; these equations map the x,y,t space into the complex planes θ_1 and θ_2.

3. Express the complex displacements and stresses as functions of the complex potentials in the θ_1 and θ_2 planes.

4. Any loading that is homogeneous in space and time can be represented by an appropriate differentiation or integration of the equations obtained in Step 3. Obtain the expressions for displacements and stresses according to the degree of homogeneity.

5. Apply Cauchy's integral formula for the half-space to evaluate the complex expressions of the boundary conditions.

6. Equate the expressions obtained in Steps 4 and 5 at the boundaries and determine the corresponding complex potentials.

7. Substitute the complex potentials obtained in Step 6 into the equations for displacements and stresses obtained in Step 4. The real parts of the expressions represent the required displacements and stresses.

In general, the motions at the ground surface resulting from an earthquake of fault rupture origin are the result a three-dimensional problem. Seyyedian-Choobi and Robinson (1975) approximated the three-dimensional problem with two two-dimensional ones, namely a plane strain and an antiplane problem.

The plane strain problem, which corresponds to a dip-slip motion (Fig. 2.4a), results in the displacement time histories along the epicentral direction (u_y) and the vertical direction (u_x), whereas the antiplane problem, which corresponds to a strike-slip rupture (Fig. 2.4b), leads to the displacement time histories normal to the epicentral direction (u_z). In both problems, the solutions are independent of the z-direction.

For the general case of a half-space medium, the method considers:

(i) the boundary conditions at the free surface and at the rupture surface;

(ii) the effect of the reflected waves at the free surface; and

(iii) the possibility of the formation of a head wave and the effect of head wave disturbances when a shear wave reaches the free surface in the plane strain case.

The different parameters associated with the model are (see Fig. 2.4):

(i) The source parameters; namely, the width of the rupture W, the focal depth H (depth of earthquake source), the angle γ representing the orientation of the rupture surface relative to the free surface, the speed of rupture propagation α, and the fault displacements D_x and D_z for dip-slip and strike-slip motions, respectively.

(ii) The velocities of the compressional and shear waves in the medium.

Evaluation of the Impulse Response Function -- Consider a half-space with a fault rupture displacement u_B (Fig. 2.5). Using the method of self-similar potentials the displacement time histories at various stations at the ground surface (e.g., stations 1,2,3, ..., n) may be obtained. The system transmitting the excitation from the source to the free surface may be approximated by a linear N-degree of freedom system. The base excitation for each of these systems is the rupture displacement u_B, and the response at the surface (top mass) is the corresponding displacement time history obtained through the method of self-similar potentials.

The impulse response function of each of the N-degree of freedom systems may be assumed to consist of a negative exponential term and a sinusoidal term; this is consistent with observed displacement time histories. Although the method of self-similar potentials deals with an elastic, homogeneous and isotropic half-space, damping can be included in the analysis to represent the effect of radiation damping.

A normal mode approach was considered in the analysis, and the modes can, therefore, be examined one at a time. Recall that the impulse response function of an ordinary single-degree of freedom system has the form (e.g., Thomson, 1981)

$$h_o(t) = \frac{1}{\omega\sqrt{1-\zeta^2}}\, e^{-\zeta\omega t}\, \sin(\omega\sqrt{1-\zeta^2}\, t) \qquad (2.22)$$

where:

ω = the natural frequency; and

ζ = the damping coefficient.

Equation 2.22 satisfies both requirements of the system transmitting the fault excitation to the displacement at the free surface. It implies, however, that the base excitation is a point source, which is not the case of the fault displacement during an earthquake. The method of self-similar potentials considers that the following occurs at the source (Fig. 2.6). The motion is considered to start at time t = 0 at the middle of the width of the fault as a step function in displacement of infinite duration and magnitude equal to D_x for dip-slip faulting and D_z for strike-slip faulting. This step function propagates towards both ends of the fault with speed equal to the speed of rupture propagation α until it reaches the ends of the fault where it suddenly stops (bilateral faulting).

Therefore, the motion at the source is considered to consist of a series of unit impulses distributed over the width of the fault (Fig. 2.7), each occurring at time $t_i = |x_i|/\alpha$ and transmitted to the ground surface by the impulse response function of Eq. 2.22. Accordingly, the total impulse response function of the system has the form:

$$h(t) = \frac{1}{W}\int_{-W/2}^{W/2} h_o\left(t - \frac{|x_i|}{\alpha}\right) d|x_i|$$

$$= \frac{-1}{\kappa\omega\omega_d}\left\{\exp(-\zeta\omega t)(\zeta \sin \omega_d t + \sqrt{1-\zeta^2}\cos \omega_d t)\right.$$

$$\left. - \exp[-\zeta\omega(t-\kappa)][\zeta \sin \omega_d(t-\kappa) + \sqrt{1-\zeta^2}\cos \omega_d(t-\kappa)]\right\} \quad (2.23)$$

where:

$\kappa = W/2\alpha$; and

$\omega_d = \omega\sqrt{1-\zeta^2}$, the damped natural frequency.

A system identification technique allows the evaluation of the characteristics of the system, namely its natural frequencies, damping coefficients and participation factors. The input to the system under

consideration is a step function in displacement of infinite duration and magnitude equal to D_x for dip-slip faulting and D_z for strike-slip faulting. The output of the system, e.g., the response at the N^{th} degree of freedom, is the displacement time history obtained by the method of self-similar potentials, whereas the impulse response function is given by Eq. 2.23.

The system identification technique used in this study is an extension of an iterative approach (Beck, 1978) to minimizing a function $J(a_1, \ldots, a_n)$, whereby a series of one-dimensional minimizations are performed with respect to each a_i. In the basic approach, J is minimized with respect to a_1 while keeping the rest of the a_i's equal to their initial values. Then a_1 is changed to its new value and J is minimized with respect to a_2 with the remaining parameters held constant, and so on. After one sweep through the parameters, giving new estimates of the a_i's that minimize J, successive sweeps are performed until convergence is achieved.

In the present case J is the error function, namely;

$$J(\omega_1, \omega_2, \ldots, \omega_N, \zeta_1, \zeta_2, \ldots, \zeta_N, \phi_1^N, \phi_2^N, \ldots, \phi_N^N)$$

$$= \int_{t_a}^{t_f} [x_o(t) - x(t)]^2 \, dt \qquad (2.24)$$

where:

$\phi_1^N, \phi_2^N, \ldots, \phi_N^N$ = the participation factors at the N^{th} degree of freedom of the system;

t_a = the starting time of the record;

t_f = the final time of the record;

$x_o(t)$ = the displacement time history as obtained from the method of self-similar potentials; and

$$x(t) = \sum_{i=1}^{N} \frac{\phi_i^N}{\kappa\omega_i\sqrt{1-\zeta_i^2}} \left\{\exp\left[-\zeta_i\omega_i(t-\kappa)\right] \sin \omega_i\sqrt{1-\zeta_i^2}\,(t-\kappa)\right.$$

$$\left. - \exp(-\zeta_i\omega_i t) \sin \omega_i\sqrt{1-\zeta_i^2}\, t\right\} \qquad (2.25)$$

is the response of the system, with impulse response function defined earlier in Eq. 2.23.

During the first step of the minimization process, the parameters of all modes except one are held constant. Then J is minimized with respect to the natural frequency of the particular mode. During the second phase of the modal minimization the natural frequency is held constant and equal to the optimized value, while minimization takes place with respect to the damping coefficient. The participation factor is obtained by equating the derivative of the error function with respect to the participation factor to zero. After convergence for the mode under examination is achieved, J is minimized with respect to the following mode. The sweeps over all modes are continued until total convergence occurs. The advantage of the method is that it does not require initial values for the participation factors. It also allows the addition of one mode at a time by updating the number of modes in x(t) (Eq. 2.25) after each successful global minimization. Therefore, the iterations may be terminated, when an additional mode does not contribute considerably to the minimization of the error function.

The frequency transfer function for each mode is simply the Fourier transform of the impulse response function (Thomson, 1981). For the present purpose, this may be expressed as,

$$H_j(\omega) = \int_{t_a}^{t_f} h_j(t)\, e^{-i\omega t}\, dt \qquad (2.26)$$

where, $t_f - t_a$ is the duration of strong ground motion.

With the impulse response function of Eq. 2.23, Eq. 2.26 gives,

$$H_j(\omega) = \frac{-1}{\kappa\omega_j^2\sqrt{1-\zeta_j^2}} \cdot \frac{1}{\omega_j^2 - \omega^2 + 2\zeta_j\omega_j\omega i}$$

$$\cdot \{\exp[-(\zeta_j\omega_j + i\omega)t_f][(\omega_j - 2\zeta_j\omega_j - i\zeta_j\omega)(\sin \omega_d t_f$$

$$- \exp(\zeta_j\omega_j\kappa) \sin \omega_d(t_f-\kappa)) - \sqrt{1-\zeta_j^2}\ (2\zeta_j\omega_j + i\omega)$$

$$\cdot (\cos \omega_d t_f - \exp(\zeta_j\omega_j\kappa) \cos \omega_d(t_f-k))]$$

$$- \exp[-(\zeta_j\omega_j + i\omega)t_a][(\omega_j - 2\zeta_j\omega_j - i\zeta_j\omega)(\sin \omega_d t_a$$

$$- \exp(\zeta_j\omega_j\kappa) \sin \omega_d(t_a-\kappa)) - \sqrt{1-\zeta_j^2}\ (2\zeta_j\omega_j + i\omega)$$

$$\cdot (\cos \omega_d t_a - \exp(\zeta_j\omega_j\kappa) \cos \omega_d(t_a-k))]\} \qquad (2.27)$$

2.3 Stochastic Characteristics of Ground Motion

Absolute Ground Motion -- The power spectral densities and the cross spectral densities of ground motion at various points on the ground surface may be evaluated as follows.

Let $u_j(t)$ and $u_\ell(t)$ denote the displacement time histories at any two stations (or two directions) j and ℓ, respectively. The input to the system is the displacement at the source, for which the power spectral density of the velocity is given by Eq. 2.5. The expression for the displacement time history at station j is given by:

$$u_j(t) = \sum_{k=1}^{N} \phi_k^{(j)} \int_0^t h_k^{(j)}(t-\tau)\left[2\zeta_k^{(j)}\omega_k^{(j)}V(\tau) + (\omega_k^{(j)})^2 U(\tau)\right] d\tau \quad (2.28)$$

where:

$\phi_k^{(j)}$ = the participation factor for the k^{th} mode at station j;

$h_k^{(j)}(t)$ = the impulse response function for the k^{th} mode at station j as given by Eq. 2.23; and

$V(\tau)$, $U(\tau)$ = the velocity and displacement at the source.

The cross spectral density between stations (or directions) j and ℓ may be evaluated as follows:

$$S_{u_j u_\ell}(\omega) = \sum_{k=1}^{N}\sum_{m=1}^{M} \frac{\phi_k^{(j)}\phi_m^{(\ell)}}{\omega^2}\left[4\zeta_k^{(j)}\zeta_m^{(\ell)}\omega_k^{(j)}\omega_m^{(\ell)}\omega^2 - i2\zeta_k^{(j)}\omega_k^{(j)}(\omega_m^{(\ell)})^2\omega + i2\zeta_m^{(\ell)}\omega_m^{(\ell)}(\omega_k^{(j)})^2\omega + (\omega_k^{(j)})^2(\omega_m^{(\ell)})^2\right] H_k^{(j)*}(\omega)\, H_m^{(\ell)}(\omega)\, S_{vv}(\omega) \quad (2.29)$$

where * denotes the complex conjugate, N and M are the number of modes used in the analysis,

$H_k^{(j)}(\omega)$ = the frequency transfer function for mode k at station (or direction) j (see Eq. 2.27); and

$S_{vv}(\omega)$ = the power spectral density for the velocity at the source (Eq. 2.5).

If $j = \ell$, $N = M$, and Eq. 2.29 yields the power spectral density at station j; whereas if $j \neq \ell$, $N \neq M$, and Eq. 2.29 represents the cross spectral density of the displacement between stations (or directions) j and ℓ.

For a stationary process the cross spectral densities for velocity and acceleration are given by (Lin, 1976)

$$S_{\dot{u}_j \dot{u}_\ell}(\omega) = \omega^2 S_{u_j u_\ell}(\omega) \tag{2.30}$$

and

$$S_{\ddot{u}_j \ddot{u}_\ell}(\omega) = \omega^4 S_{u_j u_\ell}(\omega) \tag{2.31}$$

where $\dot{u}_j$ and $\ddot{u}_j$ denote velocity and acceleration, respectively.

Differential Ground Motion -- The cross-correlation coefficient of the motions between two different stations (or two different directions) is defined as:

$$\rho_{u_i u_j}(\omega) = \frac{\mathrm{Re}[S_{u_i u_j}(\omega)]}{\sqrt{S_{u_i u_i}(\omega)\, S_{u_j u_j}(\omega)}} \tag{2.32}$$

where Re denotes the real part. Through Eqs. 2.30 and 2.31, it can be shown that the cross-correlation coefficient for displacement, velocity, or acceleration is of the same form.

The spatial correlation coefficient is defined as:

$$\rho(\xi) = \frac{\int_{-\infty}^{\infty} \mathrm{Re}[S_{u_i u_j}(\omega)]\, d\omega}{\int_{-\infty}^{\infty} \sqrt{S_{u_i u_i}(\omega)\, S_{u_j u_j}(\omega)}\, d\omega} \tag{2.33}$$

where ξ is the distance between stations i and j, and $S_{u_i u_j}(\omega)$, $S_{u_i u_i}(\omega)$ and $S_{u_j u_j}(\omega)$ are given by Eq. 2.29.

Let $\Delta u(t) = u_i(t) - u_j(t)$ be the differential ground motion between stations i and j on the ground surface. The power spectral density of the differential ground displacement is,

$$S_{\Delta u,\Delta u}(\omega) = S_{u_i u_i}(\omega) + S_{u_j u_j}(\omega) - 2\,\mathrm{Re}[S_{u_i u_j}(\omega)] \tag{2.34}$$

where $S_{u_i u_i}(\omega)$ and $S_{u_j u_j}(\omega)$ are obtained from Eq. 2.29, whereas the real part of the cross spectrum $\mathrm{Re}[S_{u_i u_j}(\omega)]$ can be obtained directly from Eq. 2.29 or from Eq. 2.32.

The spectra for differential velocities and accelerations may then be evaluated as follows

$$S_{\Delta\dot{u},\Delta\dot{u}}(\omega) = \omega^2 S_{\Delta u,\Delta u}(\omega) \tag{2.35}$$

and

$$S_{\Delta\ddot{u},\Delta\ddot{u}}(\omega) = \omega^4 S_{\Delta u,\Delta u}(\omega) \tag{2.36}$$

where $\Delta\dot{u}$ and $\Delta\ddot{u}$ denote differential velocity and acceleration, respectively.

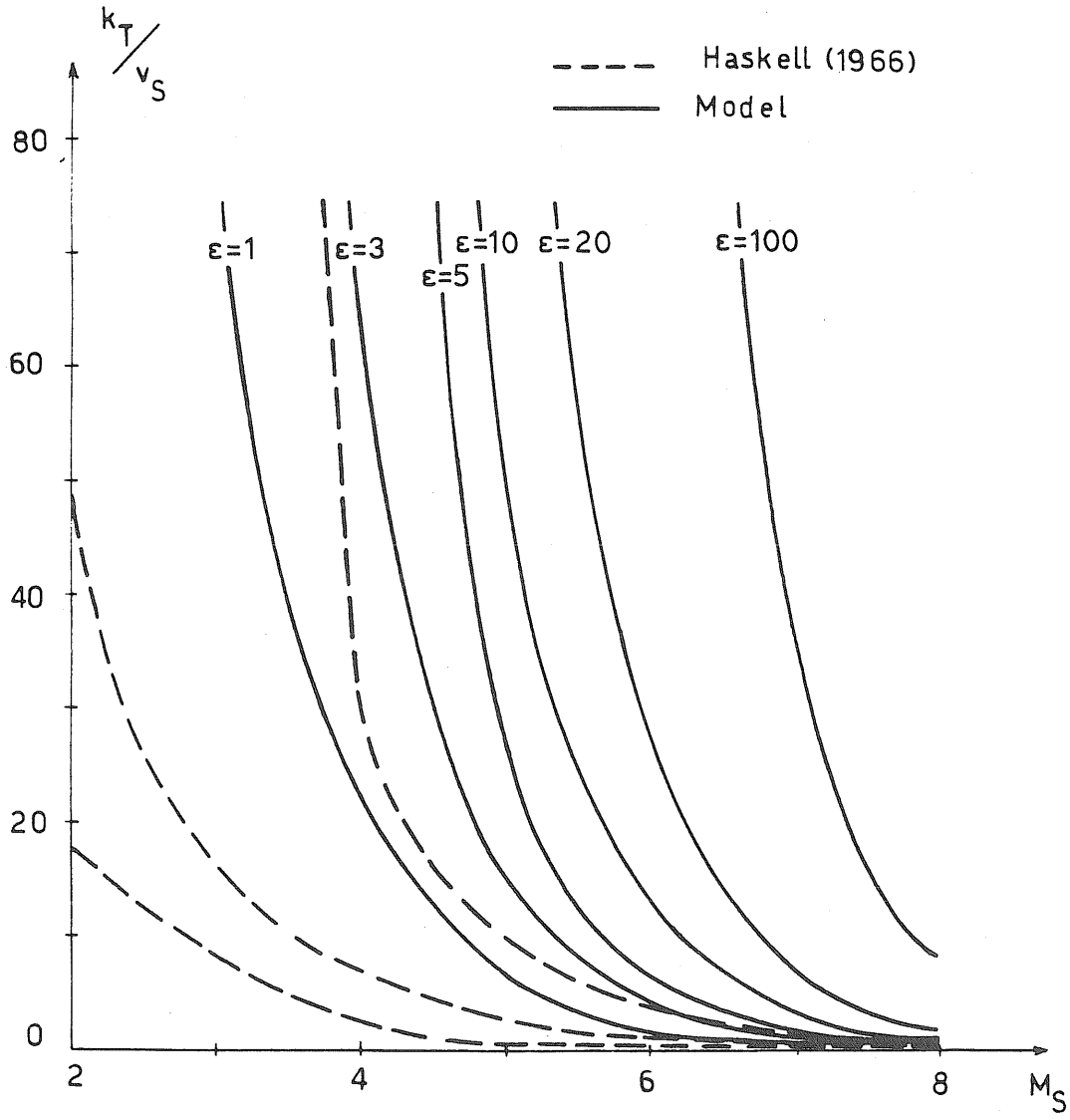

Figure 2.1 Values of $\frac{k_T}{v_s}$ for Different Earthquake Magnitudes

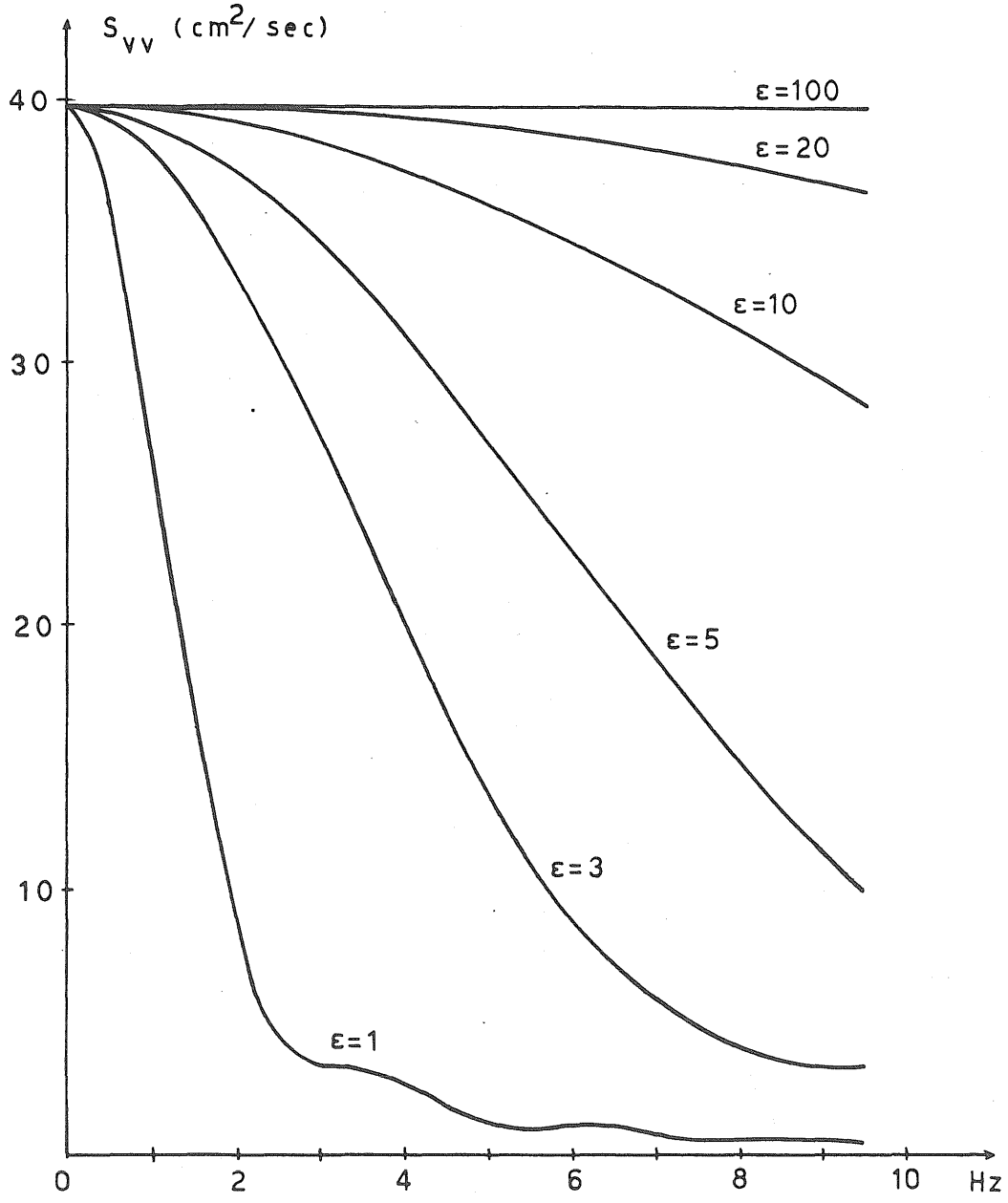

Figure 2.2 Effect of k_T on the Power Spectral Density at the Source

(v_s = 2.0 $\frac{km}{sec}$; M_s = 6.0)

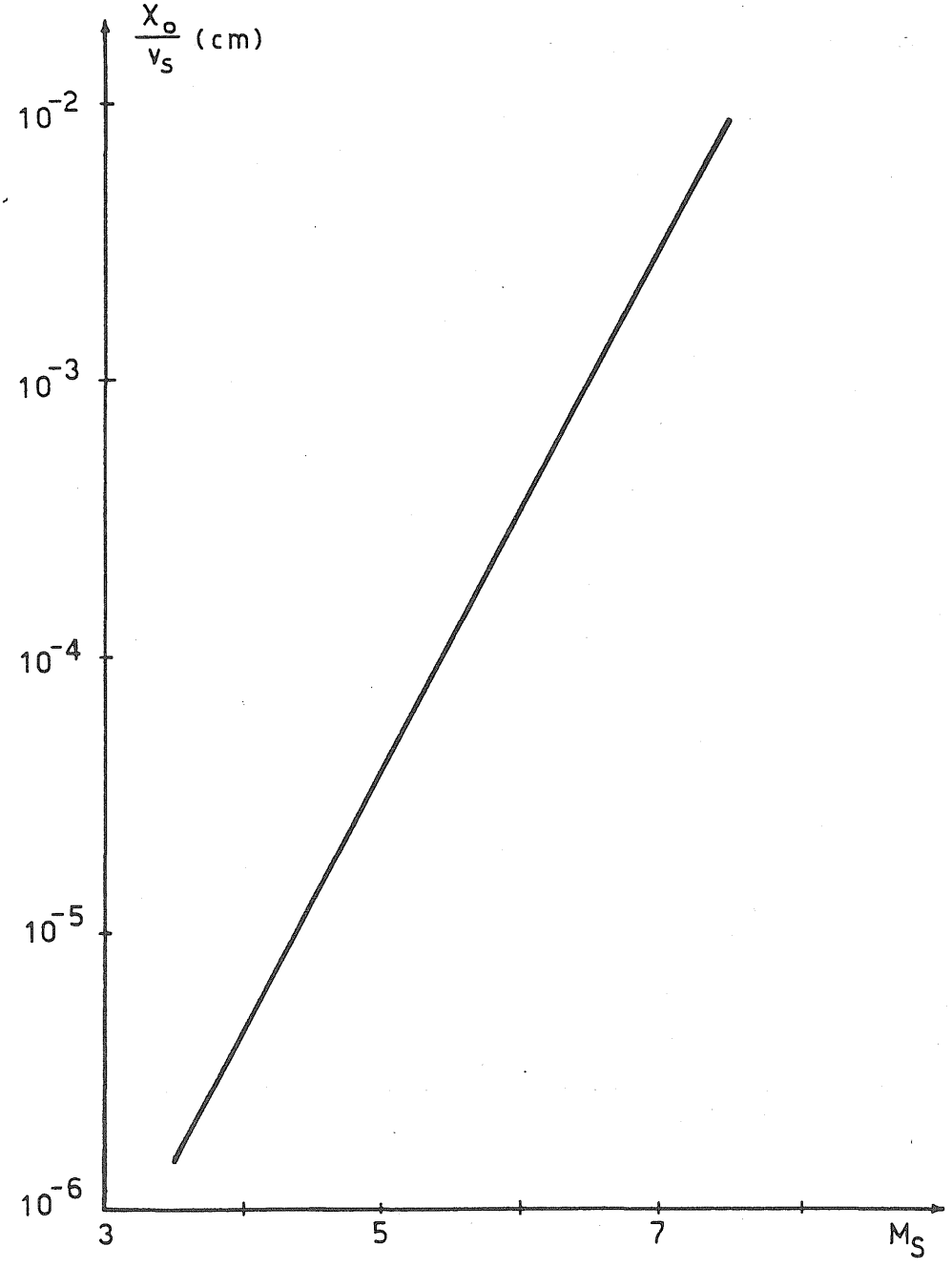

Figure 2.3 Dependence of X_o on Earthquake Magnitude

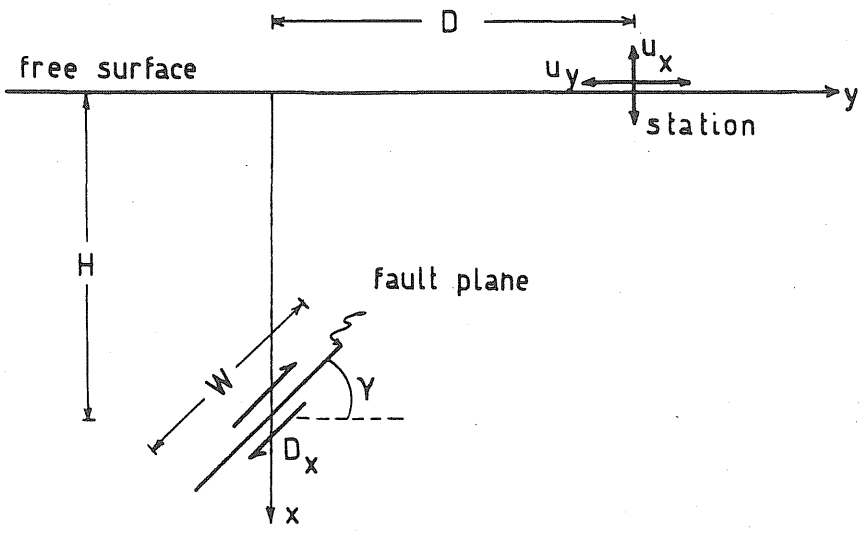

(a) Dip - Slip Rupture

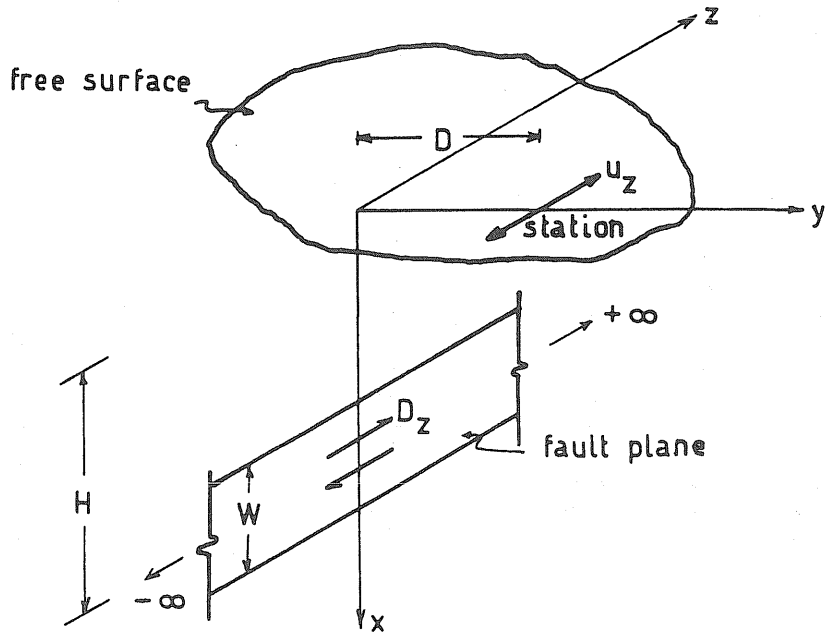

(b) Strike - Slip Rupture

Figure 2.4 Two-Dimensional Fault Model for a Half-Space Medium

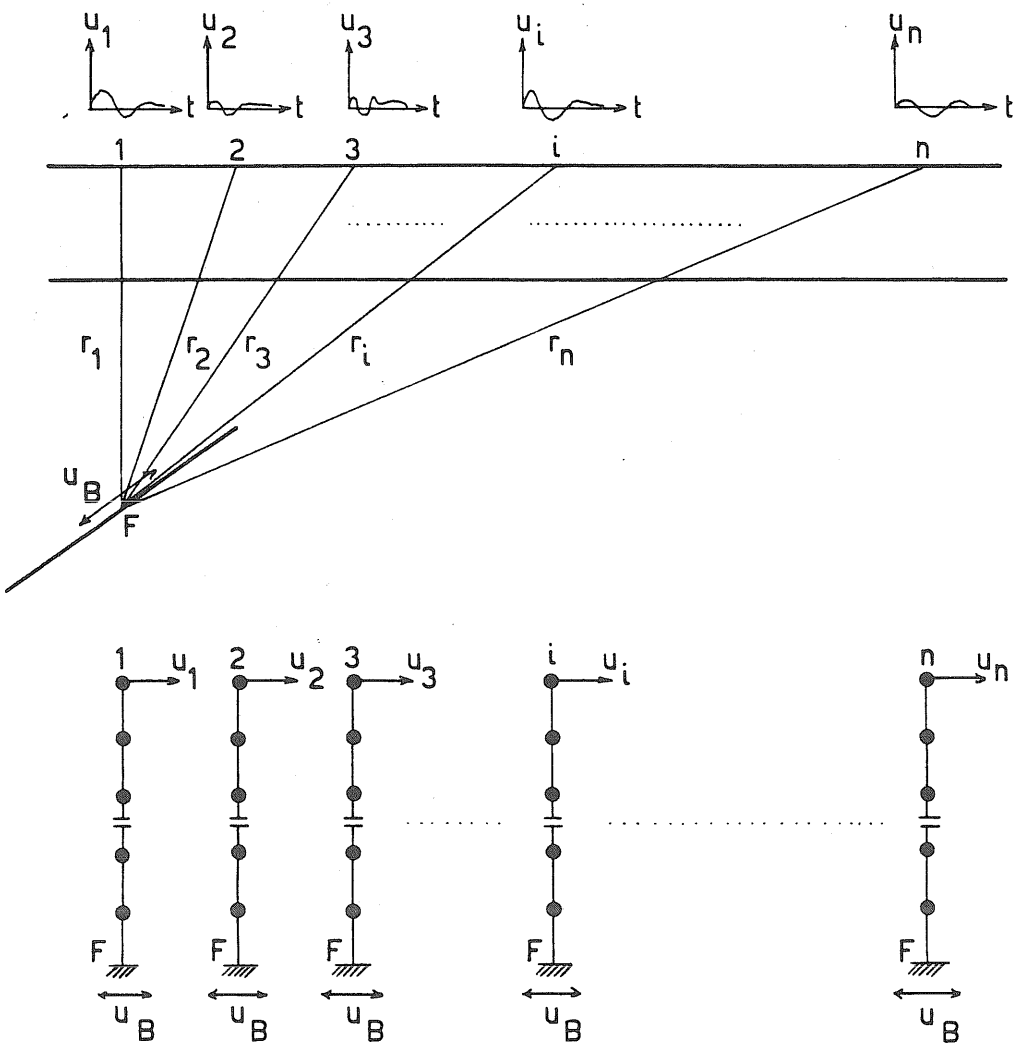

Figure 2.5 Approximation of Rays by Linear N-Degree of Freedom Systems

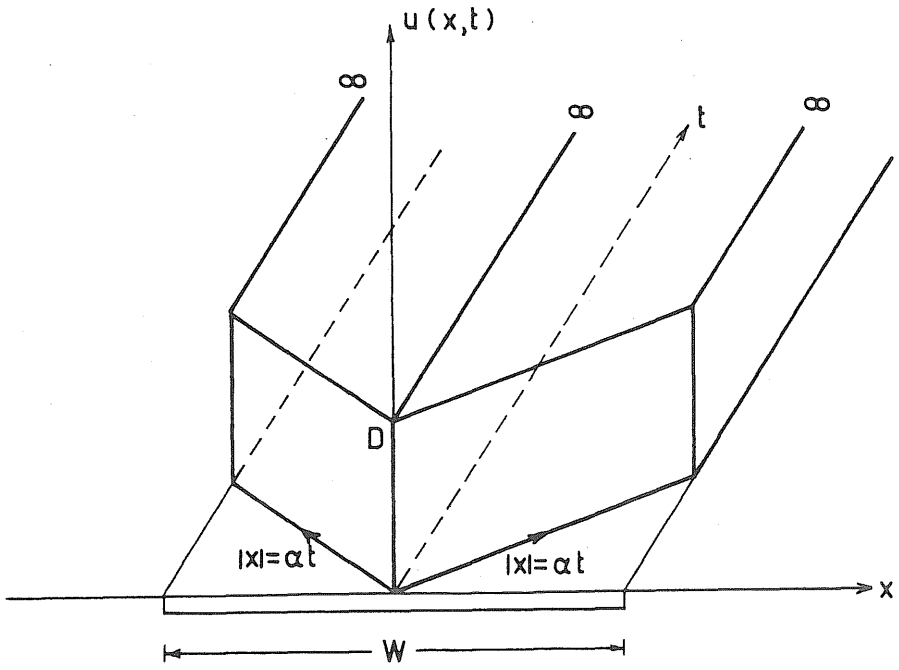

Figure 2.6 Motion at the Fault for the Method of Self-Similar Potentials

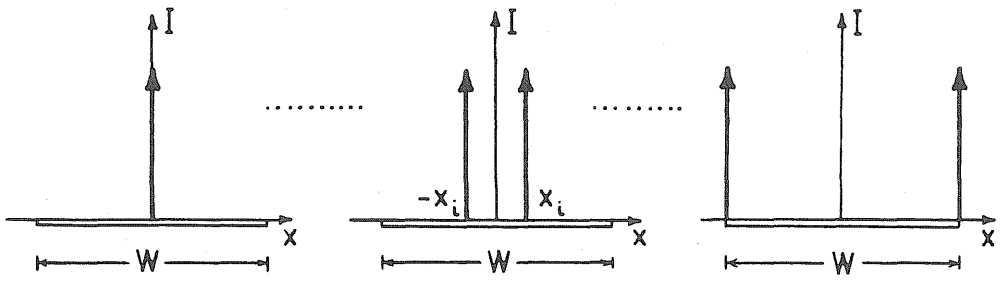

Figure 2.7 Superposition of Unit Impulses at the Source

CHAPTER 3

VALIDATION AND PRACTICAL SIGNIFICANCE OF MODEL

3.1 Introduction

This chapter presents the results of the stochastic model described in Chapter 2. In order to provide a basis for comparison and validation, the model is used to reproduce ground motions simulating the earthquake of January 29, 1981 recorded at Lotung, Taiwan.

Earthquake ground motions recorded by the dense instrument array (SMART-1, i.e., Strong Motion Array in Taiwan) in Lotung, in the northeast corner of Taiwan, provide information about the spatial variation of surface ground motions. The array (Fig. 3.1) consists of a center instrument C00 and other instruments arranged on three concentric circles (the inner denoted by I, the middle by M and the outer by O), with radii of 0.2 km, 1.0 km and 2.0 km, respectively; along the circumference of each of these circles are 12 strong-motion seismographs having a common time basis.

The comparison of the analytical results with the empirical data from the earthquake (Loh, Ang, and Wen, 1983; Loh, 1984b; Harada, 1984) includes power spectral density functions of acceleration along and normal to the epicentral direction for the stations located on the diameter from 006 to 012 (Fig. 3.1), cross and spatial correlation coefficients, as well as power spectral density functions of differential motions.

The power spectral density functions of differential motions are of great importance to the seismic safety evaluation of lifelines. For this reason, empirical and closed form expressions for the spectral densities

are also evaluated; specifically, the empirical expressions depend on a few parameters that change with the separation distance.

3.2 The Earthquake of 29 January 1981

The local magnitude of the 29 January 1981 earthquake was 6.3; in this range of magnitudes, the local magnitude, M_L, is equal to the surface wave magnitude, M_s (Hanks and Kanamori, 1979). Therefore,

$$M_s = 6.3 \tag{3.1}$$

The epicentral distance of the earthquake was 30 km from Lotung, with a focal depth of 11 km. According to Eqs. 2.15 and 2.16, the width of the rupture would be 3.95 km with a rupture dislocation of 33.4 cm. The contributions to the final fault offset were assumed to be equal from the dip-slip and strike-slip faulting. Therefore,

$$D_x = D_z = \frac{33.4}{\sqrt{2}} = 23.6 \text{ cm} \tag{3.2}$$

The velocity of compressional waves is (Loh, 1984a)

$$v_p = 3.33 \frac{\text{km}}{\text{sec}} \quad , \tag{3.3}$$

whereas the shear wave velocity would be (Newmark and Rosenblueth, 1971)

$$v_s = \frac{v_p}{\sqrt{3}} = 1.92 \frac{\text{km}}{\text{sec}} \tag{3.4}$$

The speed of rupture propagation at the fault is assumed to be 1.60 km/sec (which is equal to 0.83 v_s).

The epicentral direction of the earthquake almost coincides with the direction from Station 006 to Station 012 (Fig. 3.1).

The power spectral density of the excitation at the source is shown in Fig. 3.2. The value of the proportionality constant is $\varepsilon = 3$.

Typical displacement time histories in three directions -- vertical, along epicentral and normal to epicentral, -- obtained from the method of self-similar potentials are shown in Fig. 3.3 together with the results of the system identification technique; the results are almost indistinguishable. The number of modes used in the analysis ranged from 29 to 38; the iterations were stopped when an additional mode would not contribute significantly to the minimization of the error function. The initial values of the frequencies were taken from the peaks of a Fourier transform analysis of the displacement time histories.

As can be seen from Fig. 3.3 the excitation in the normal to the epicentral direction starts later than the other two. This is due to the fact that the excitation in this direction is the solution of the antiplane problem, which consists only of SH-waves. The excitations in the vertical and the along epicentral direction are the solution of the plane strain problem and consist of compressional, SV- and head waves.

3.3 Comparison of Results

The assumptions underlying the idealized model relative to reality may be summarized as follows:

1. In the model the medium is considered to be elastic, homogeneous and isotropic; in reality the ground is inelastic, inhomogeneous and anisotropic.

2. The medium is considered to be a uniform half-space; at the site of the SMART-1 array there are three shallow dipping layers (total depth approximately 500 m) right underneath the array.

3. The method is a two-dimensional approximation of a three-dimensional problem; in this way the interaction of reflected and refracted waves in the three-dimensional domain, as well as the effect of

the propagating disturbance along the length of the rupture and the end effects of the rupture are lost.

4. The source parameters are values obtained from world-wide data and may not be accurate for the reference earthquake.

Power Spectral Density for Acceleration -- The power spectral densities of acceleration at the stations on the diameter from 006 to 012 (Fig. 3.1) may be evaluated through Eqs. 2.29 and 2.31.

Figures 3.4 to 3.8 show the power spectral densities for acceleration at Stations 006, I06, C00, I12 and M12, respectively, along and normal to the epicentral direction; corresponding empirical results (Loh, Ang, and Wen, 1983) are also shown in these figures. Figure 3.9 shows the results of the model in the direction along the epicentral direction at Station M06 and normal to the epicentral direction at Station 012 together with the empirical results; no empirical results were available for the direction normal to the epicentral direction at Station M06, nor for the direction along the epicentral direction at Station 012.

The results of the model are in reasonable agreement with the empirical results obtained by Loh, Ang, and Wen (1983). However, in general, the results of the model underestimate the spectra at the higher frequencies along the epicentral direction, whereas they overestimate the spectra at the lower frequencies in the direction normal to the epicentral direction. These may be explained in part by the existence of the dipping layers; as Dravinski (1984) indicated, the existence of such layers results in the amplifications or reductions of the amplitudes of the incoming waves. These amplifications or reductions depend on the particular wave, the frequency of the wave, the number of layers and the characteristics of the layers; the effect of the layers is more obvious in the direction along the epicentral direction at Station M12 (Fig. 3.8a), where the maximum value of the spectrum occurs at a much higher frequency than at any other station, and in lesser degree in the spectra normal to the epicentral direction at Stations I06, C00 and 012, where the maximum values of the spectra occur at higher frequencies.

In addition, the model examines displacement time histories and not acceleration time histories, which, in general, results in the

overestimation of the spectra at the lower frequencies and underestimation at the higher frequencies. Furthermore, perfect correlation in the direction along the length of the fault reduces the high-frequency content of the source motion; as was indicated by Hanks (1979) the high-frequency strong ground motion depends strongly on the irregularities at the fault, particularly on the nature and extent of localized dynamic stress differences that develop during faulting. The dissipative nature of the soil may also be a reason for the overestimation of the spectra at the lower frequencies.

As indicated by Loh, Ang, and Wen (1983), and later by Loh (1984b), the dominant frequency in the disturbance along the epicentral direction is between 1.10 ÷ 1.30 Hz, whereas the dominant frequency in the disturbance normal to the epicentral direction ranges between 2.80 ÷ 3.10 Hz; the former is due to surface waves, whereas the latter is due to shear waves. In the model presented herein, the participating waves in the direction along the epicentral direction are longitudinal (P-), shear (SV-) and head waves, whereas in the normal to the epicentral direction the only participating wave is the shear (SH-) wave. Figures 3.4 through 3.9 show that the dominant frequencies as well as the amplitudes of the spectra, compare well with the empirical data.

Cross-Correlation and Spatial Variation -- Equations 2.32 and 2.29 allow the evaluation of the cross-correlation coefficient. Figure 3.10 shows the mean value of the cross-correlation coefficient along and normal to the epicentral direction at Stations 006, C00 and 012 averaged over four frequency ranges; the results of the model are in good agreement with the empirical results.

The spatial correlation coefficients (obtained from Eqs. 2.33 and 2.29) in three directions, namely vertical, along and normal to the epicentral direction, are shown in Figs. 3.11, 3.12 and 3.13. Lack of data in the vertical direction does not allow comparison of the spatial variation of the motion in this direction; the shape of the variation (Fig. 3.11), however, exhibits the characteristics of a spatial variation function, namely sinusoidal with exponential decay. The spatial variation along the epicentral direction (Fig. 3.12) is in reasonable agreement with

the data obtained from both Loh (1984b) in the direction along the epicentral direction and Harada (1984) in the NS direction (Fig. 3.1); considerable scatter in the data can be observed from the results of both authors. The spatial correlation in the direction normal to the epicentral direction (Fig. 3.13) is also in agreement with the empirical results reported by Loh (1984b).

Power Spectral Density of Differential Motion -- The power spectral density of differential acceleration may be obtained from Eqs. 2.36, 2.34 and 2.29. Empirical data for the power spectral density of differential acceleration along the epicentral direction could be deduced from Loh, Ang, and Wen (1983). Figure 3.14 shows the power spectra of differential accelerations for separation distances of 0.2 km, 0.4 km, 0.8 km, and 1.8 km, respectively, along the epicentral direction; corresponding results obtained from Loh, Ang, and Wen (1983) are also shown.

The theoretical results show the same trend as the empirical spectra. The spectral amplitudes, however, are underestimated at the lower frequencies, overestimated at the middle range, and approach zero at the higher frequencies faster than the empirical data.

Equations 2.36, 2.34 and 2.32 indicate that the power spectral densities of differential acceleration depend on the cross-correlation coefficient. For the actual earthquake, multiple reflections and refractions at the shallow layers, and the anisotropy of the ground result to a higher loss of coherence than for the model, which considers an elastic, homogeneous and isotropic half-space. The differences in the lower and middle frequency range of the model and the actual earthquake may be attributed to this fact. The differences in the higher frequency range result from the assumption that the actual three-dimensional problem of wave propagation may be decomposed into a plane strain and an antiplane problem, as was also explained in the case of the power spectral densities of the absolute acceleration in this direction.

3.4 Proposed Power Spectral Density of Differential Motion

The power spectral density of differential motions is of great importance to the seismic safety evaluation of long lifelines. For practical purposes, approximate power spectral densities of differential acceleration are introduced; these empirical expressions are obtained through a least-square minimization of the results of the half-space model (Eqs. 2.34 and 2.36).

The form of the differential spectra of acceleration in the vertical direction and the direction along the epicenter suggests that an expression similar to the Kanai-Tajimi spectrum (Kanai, 1957; Tajimi, 1960) is appropriate, namely

$$S^{e}_{x,y}(f) = S_o(\xi) \frac{1 + 4(\zeta_g(\xi))^2(\frac{f}{f_g(\xi)})^2}{(1 - (\frac{f}{f_g(\xi)})^2)^2 + 4(\zeta_g(\xi))^2(\frac{f}{f_g(\xi)})^2} \tag{3.5}$$

where f denotes frequency, $S_o(\xi)$, $f_g(\xi)$, $\zeta_g(\xi)$ are the spectral ordinate, main frequency and damping coefficient of the spectrum, respectively, and ξ denotes separation distance.

The differential spectra of acceleration in the normal to the epicentral direction show two dominant frequency ranges. Therefore, the form of the approximate spectra in this direction is

$$S^{e}_{z}(f) = S_o(\xi) \frac{1 + 4(\zeta_{g_1}(\xi))^2(\frac{f}{f_{g_1}(\xi)})^2}{(1 - (\frac{f}{f_{g_1}(\xi)})^2)^2 + 4(\zeta_{g_1}(\xi))^2(\frac{f}{f_{g_1}(\xi)})^2}$$

$$\cdot \frac{1 + 4(\zeta_{g_2}(\xi))^2(\frac{f}{f_{g_2}(\xi)})^2}{(1 - (\frac{f}{f_{g_2}(\xi)})^2) + 4(\zeta_{g_2}(\xi))^2(\frac{f}{f_{g_2}(\xi)})^2} \tag{3.6}$$

Figures 3.15, 3.17 and 3.19 show the comparison of the approximate power spectral densities with the results of the half-space model. The spectral amplitudes of the approximate expressions are higher than those of the half-space model in the lower frequency range; this provides a better approximation for the spectra of the actual earthquake, which are higher than the results of the half-space model in this frequency range as well (Sect. 3.3).

The variation of the parameters of the approximate power spectral densities with separation distance are shown in Figs. 3.16, 3.18 and 3.20. The variation of $S_o(\xi)$ starts from zero and decreases as distance increases, because of loss of correlation. The parameter $f_g(\xi)$ varies linearly for the case of the vertical motions and the motions along the epicentral direction, whereas $\zeta_g(\xi)$ is constant for the motions along the epicentral direction and varies slightly in the vertical direction. For the motions in the normal to the epicentral direction, the parameters vary sinusoidally.

The approximation may be further simplified by introducing linear variations of the parameters of Eqs. 3.5 and 3.6 with separation distance (see Figs. 3.16, 3.18 and 3.20). The equations representing the linear approximation may be summarized as follows:

(i) motions in vertical direction:

$$S_o(\xi) = \begin{cases} 4.50\xi & 0 \leq \xi \leq 0.4 \\ 13.67\xi - 3.67 & 0.4 \leq \xi \leq 1.0 \\ -2.29\xi + 12.29 & 1.0 \leq \xi \leq 2.2 \end{cases}$$

$$\left.\begin{aligned} f_g(\xi) &= -0.44\xi + 2.24 \\ \zeta_g(\xi) &= -0.04\xi + 0.32 \end{aligned}\right\} \quad 0 \leq \xi \leq 2.2 \qquad (3.7)$$

(ii) motions along epicentral direction:

$$S_o(\xi) = \begin{cases} 7.50\xi & 0 \leq \xi \leq 0.2 \\ 24.14\xi - 3.33 & 0.2 \leq \xi \leq 1.07 \\ -6.64\xi + 29.60 & 1.07 \leq \xi \leq 2.2 \end{cases}$$

$$\left.\begin{aligned} f_g(\xi) &= -0.56\xi + 2.50 \\ \zeta_g(\xi) &= 0.25 \end{aligned}\right\} \quad 0 \leq \xi \leq 2.2 \tag{3.8}$$

(iii) motions normal to epicentral direction:

$$S_o(\xi) = \begin{cases} 30\xi & 0 \leq \xi \leq 0.2 \\ 51.67\xi - 4.33 & 0.2 \leq \xi \leq 0.5 \\ -5.88\xi + 24.44 & 0.5 \leq \xi \leq 2.20 \end{cases}$$

$$\left.\begin{aligned} f_{g_1}(\xi) &= -0.40\xi + 2.79 \\ f_{g_2}(\xi) &= -0.72\xi + 6.19 \\ \zeta_{g_1}(\xi) &= 0.08\xi + 0.40 \\ \zeta_{g_2}(\xi) &= -0.03\xi + 0.59 \end{aligned}\right\} \quad 0 \leq \xi \leq 2.2 \tag{3.9}$$

where the separation distance ξ is in km, $S_o(\xi)$ in cm^2/sec^3, and $f_g(\xi)$, $f_{g_1}(\xi)$ and $f_{g_2}(\xi)$ in Hz.

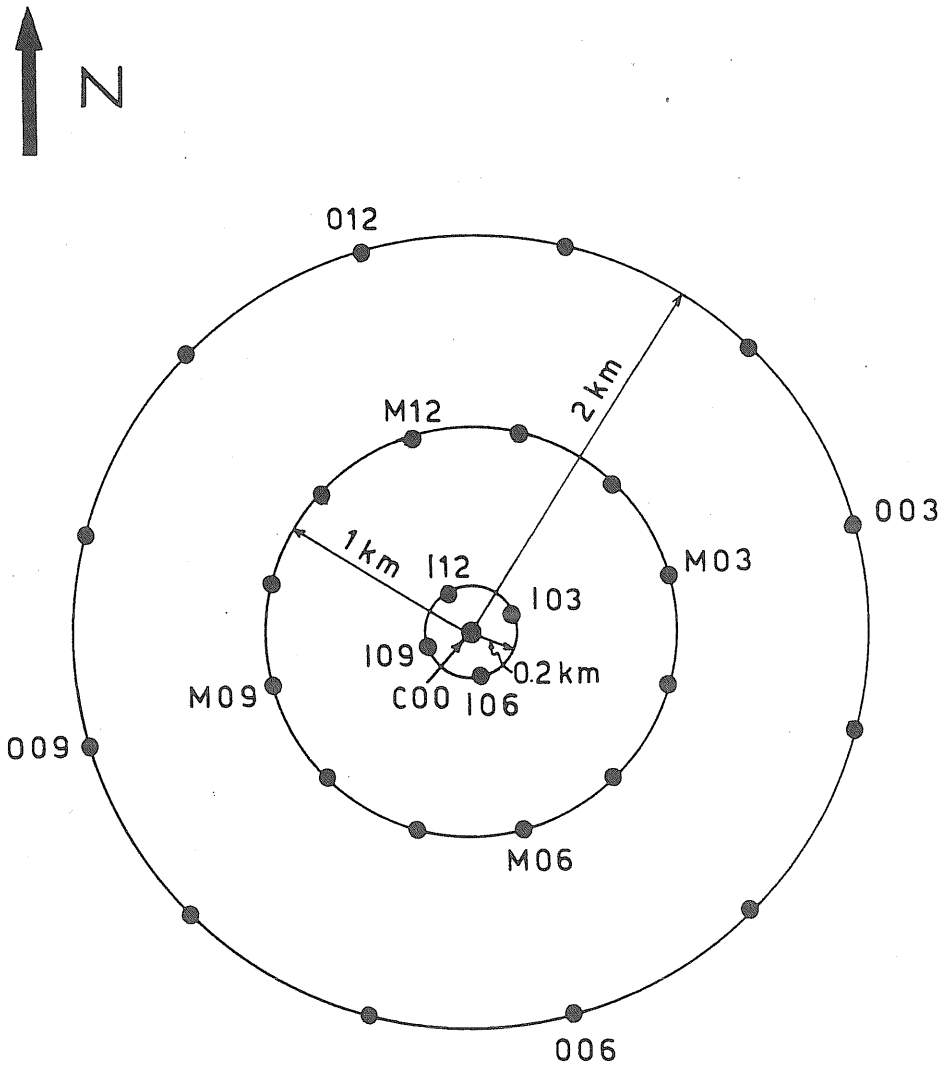

Figure 3.1 . The SMART-1 Array

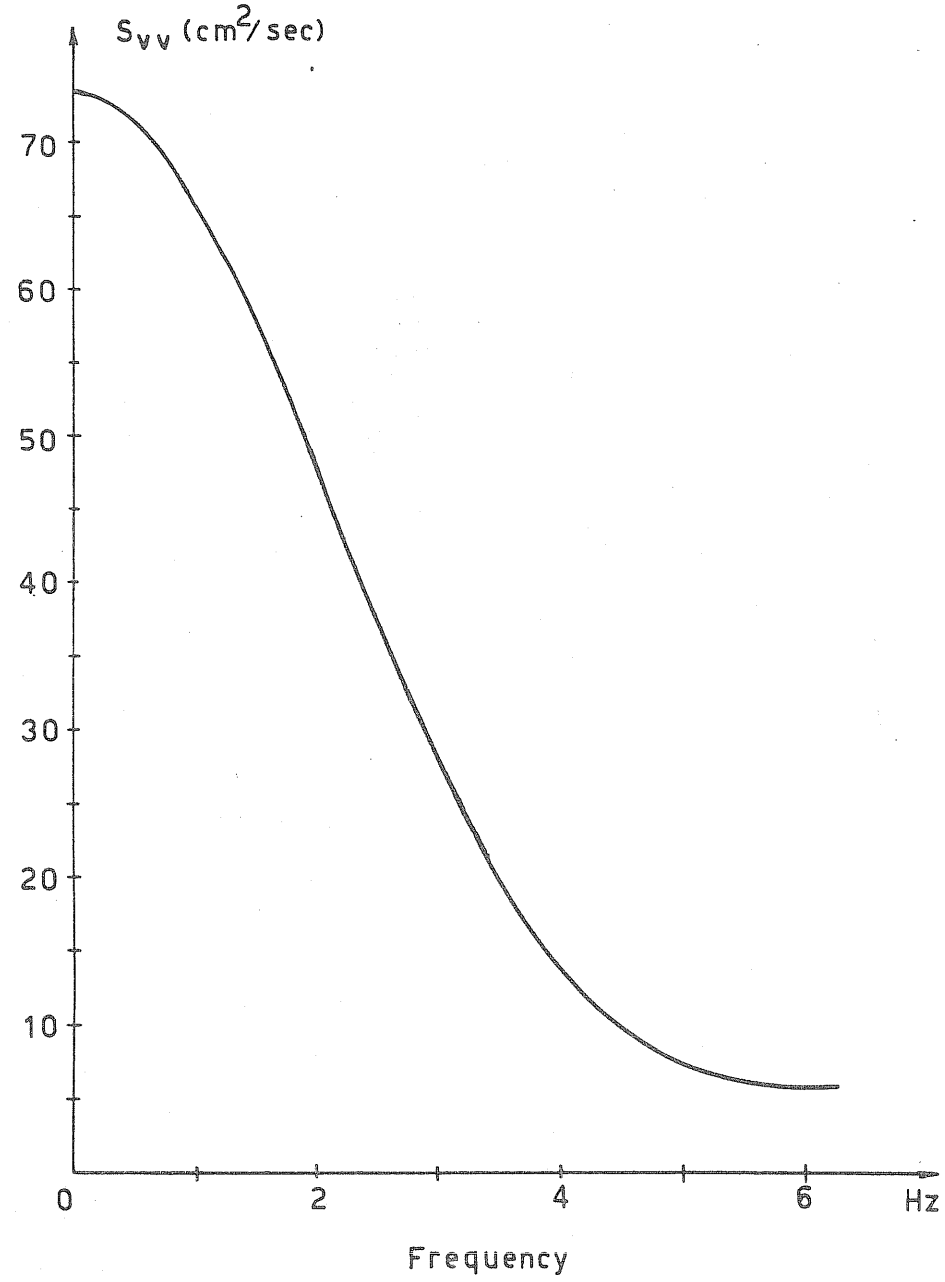

Figure 3.2 Power Spectral Density of the Excitation at the Source

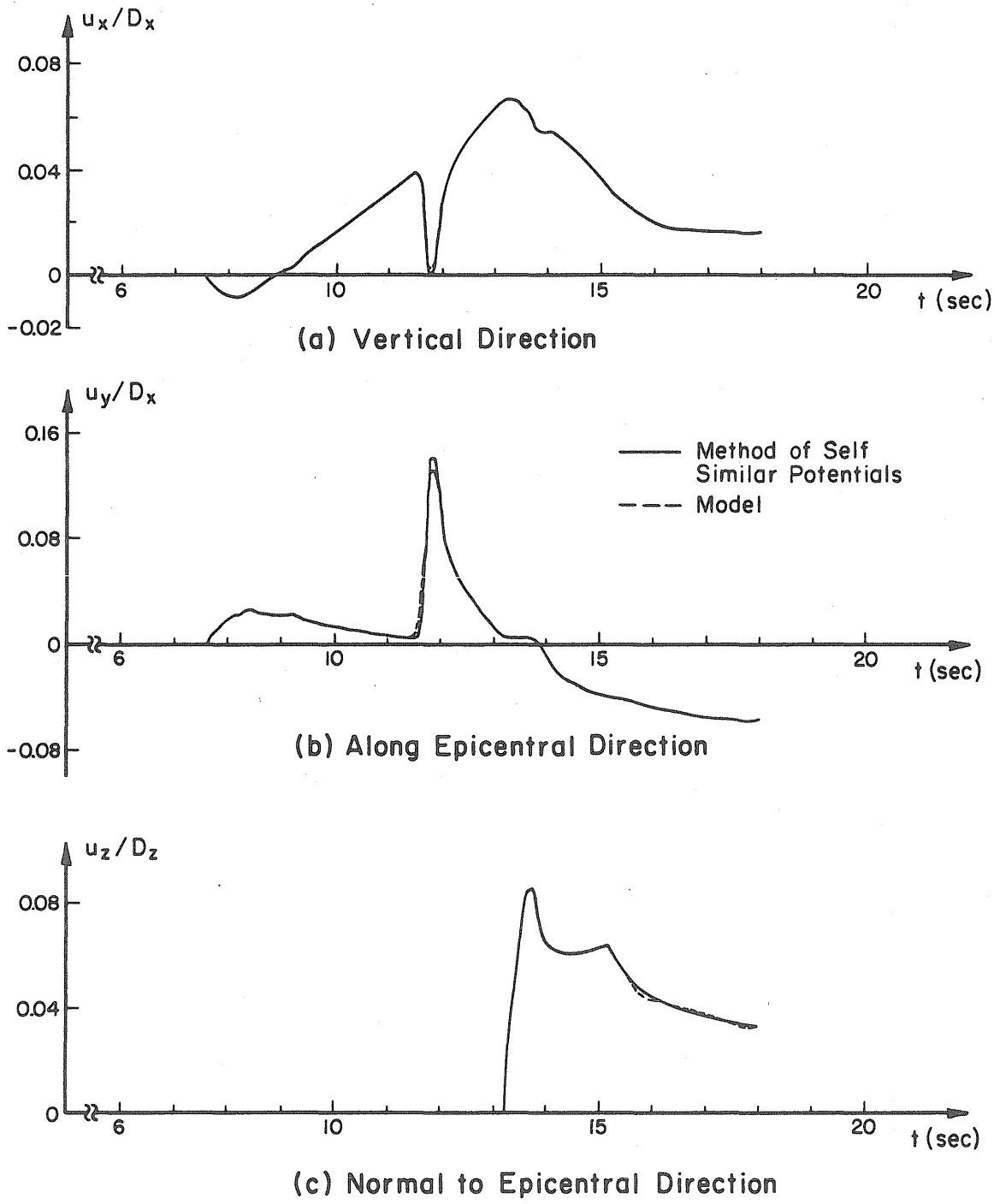

Figure 3.3 Displacement Time Histories at Station C00

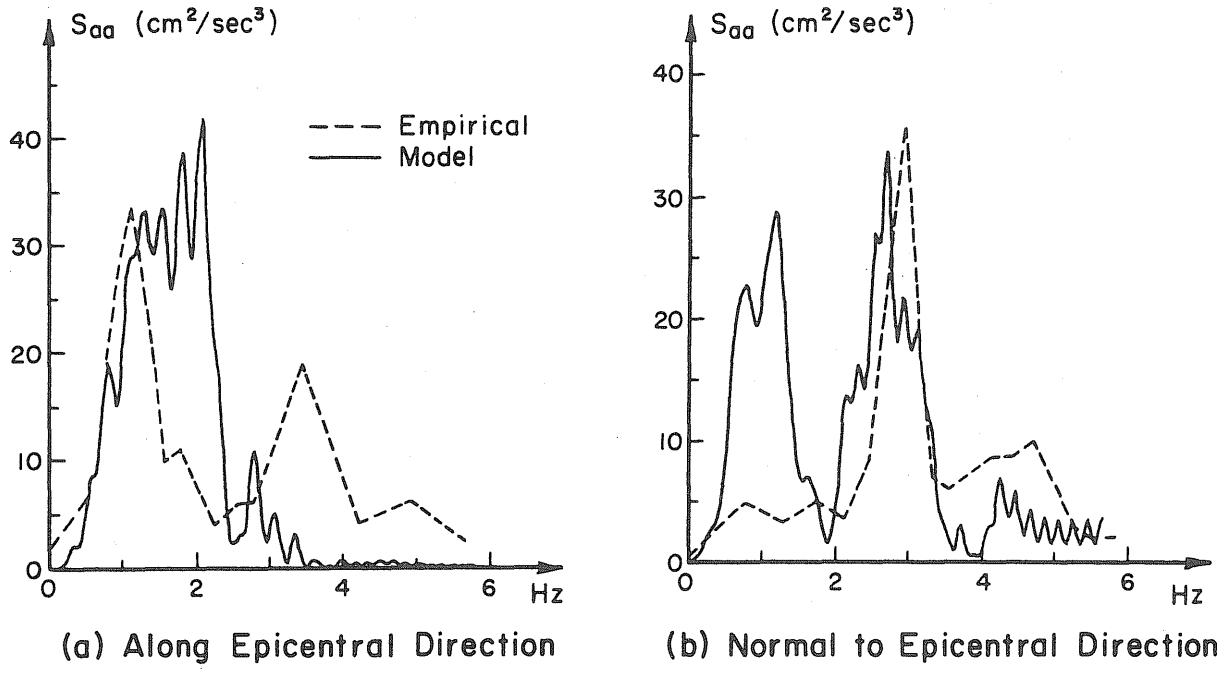

Figure 3.4 Power Spectral Densities of Acceleration at Station 006

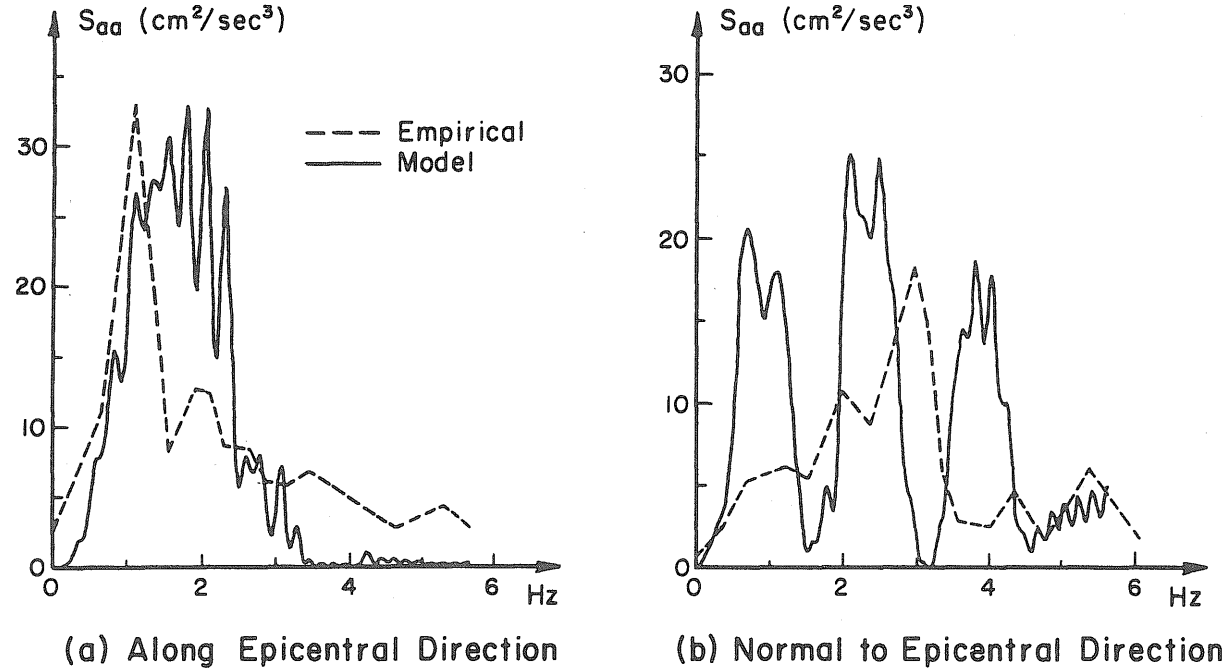

Figure 3.5 Power Spectral Densities of Acceleration at Station I06

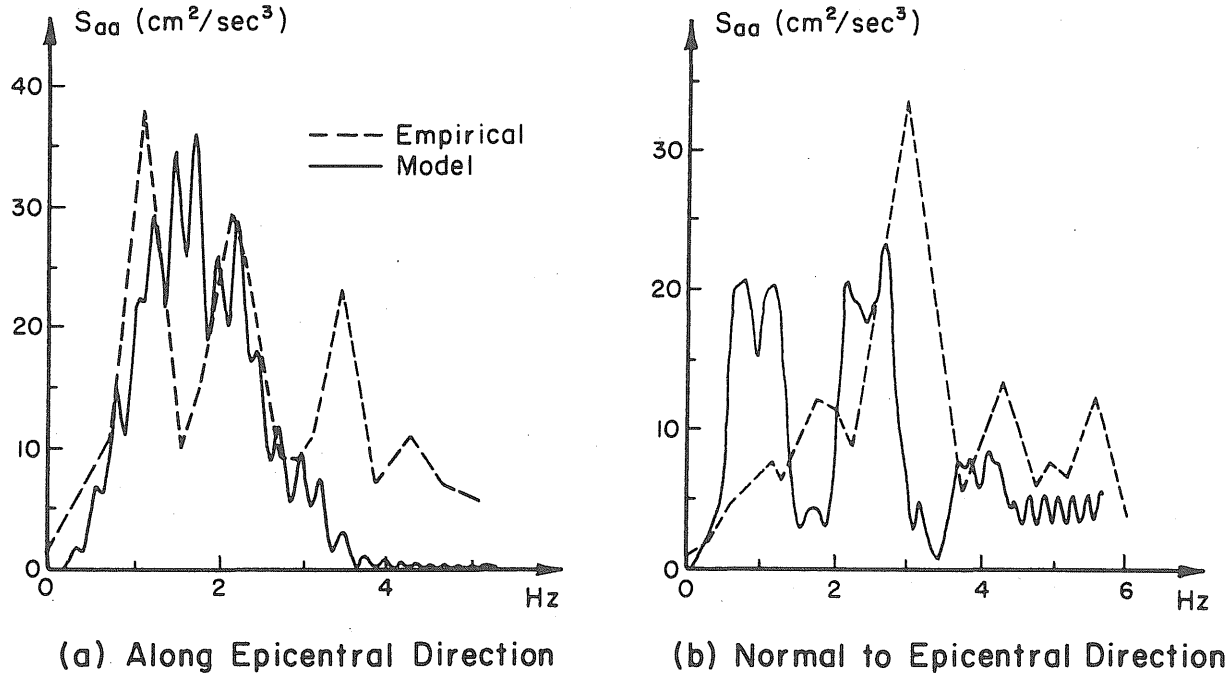

Figure 3.6 Power Spectral Densities of Acceleration at Station C00

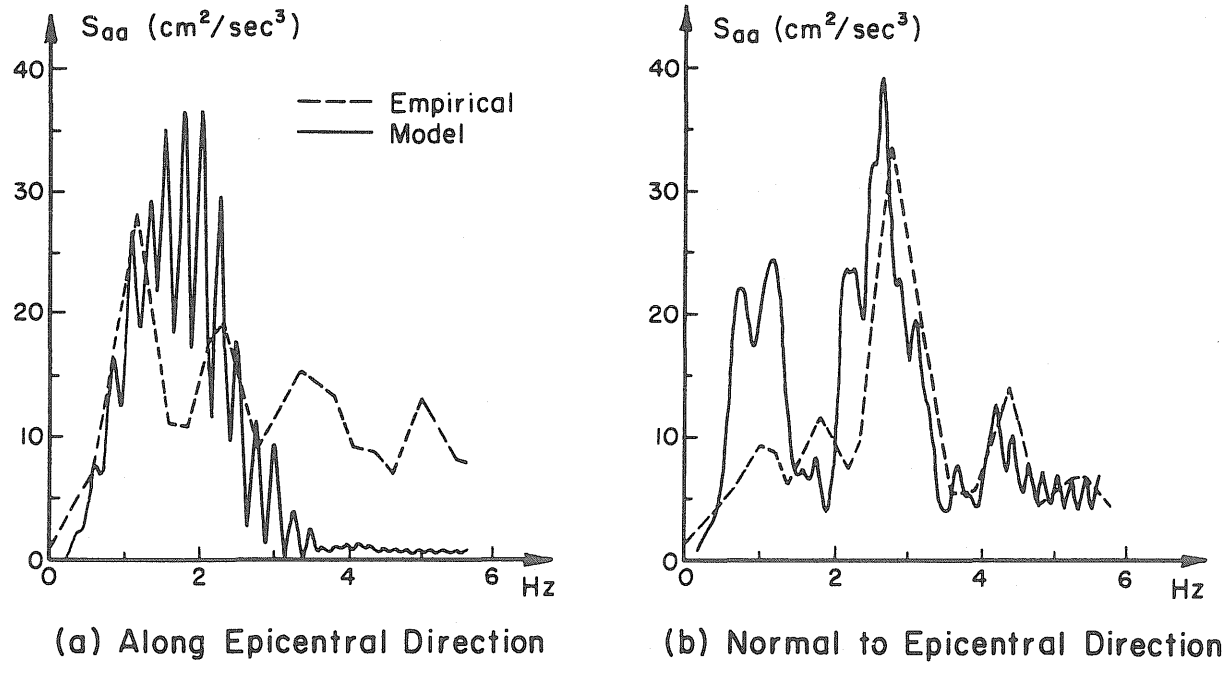

Figure 3.7 Power Spectral Densities of Acceleration at Station I12

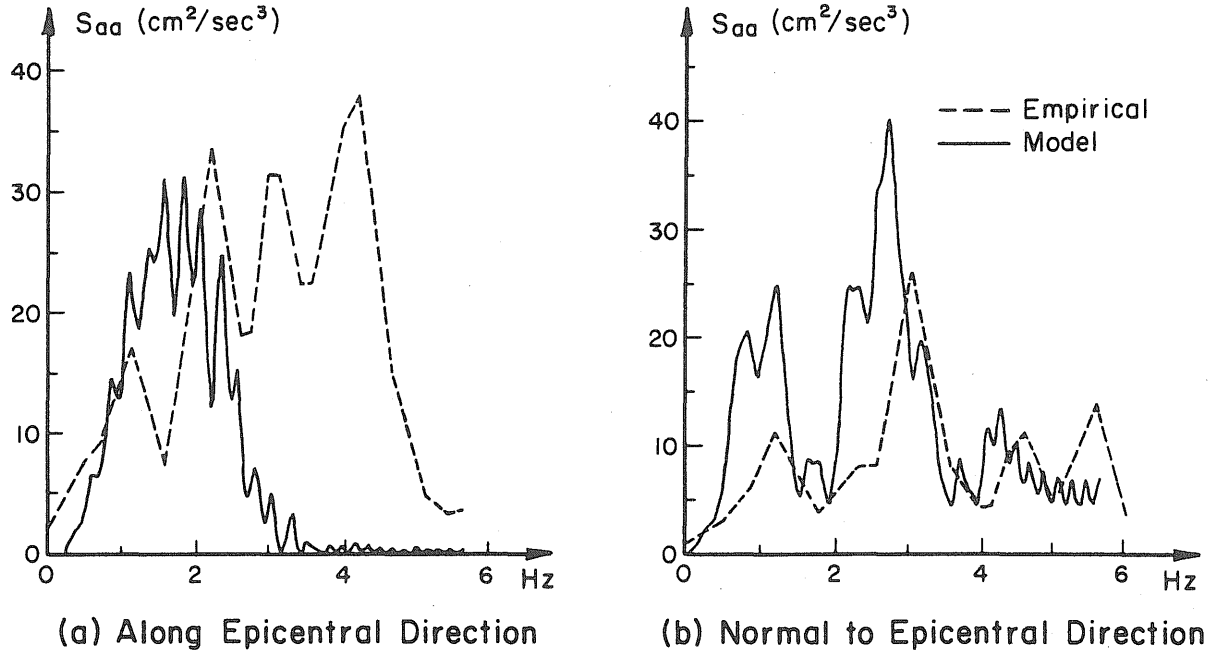

Figure 3.8 Power Spectral Densities of Acceleration at Station M12

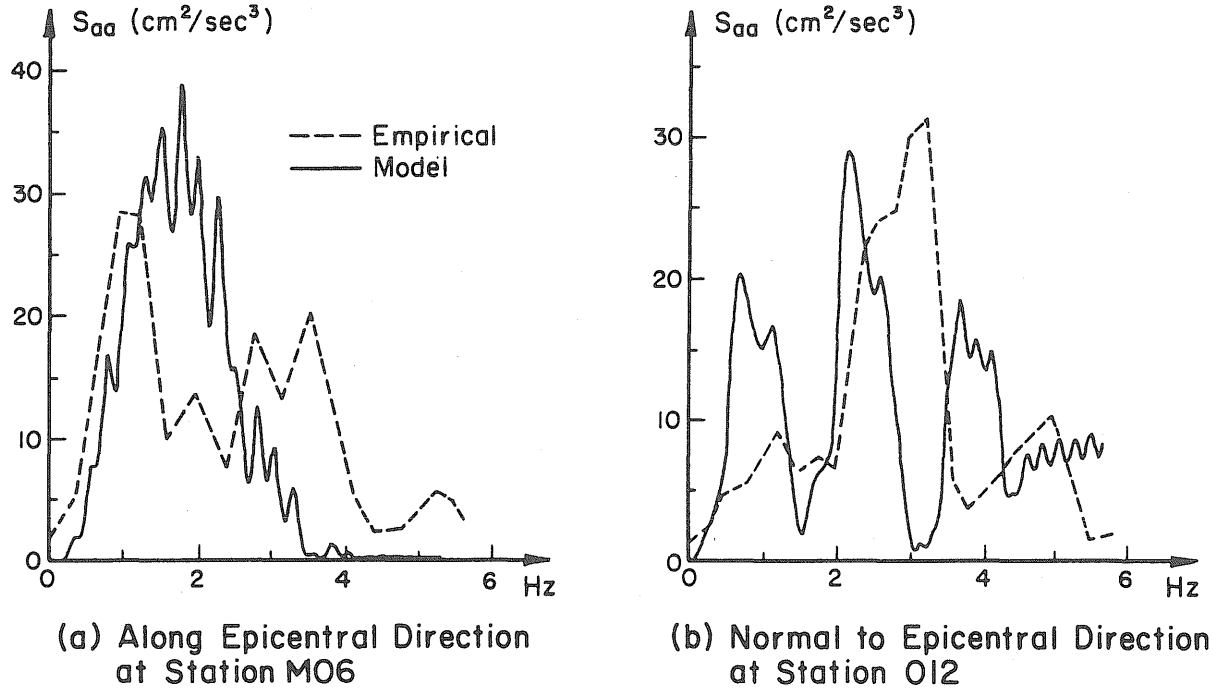

Figure 3.9 Power Spectral Densities of Acceleration

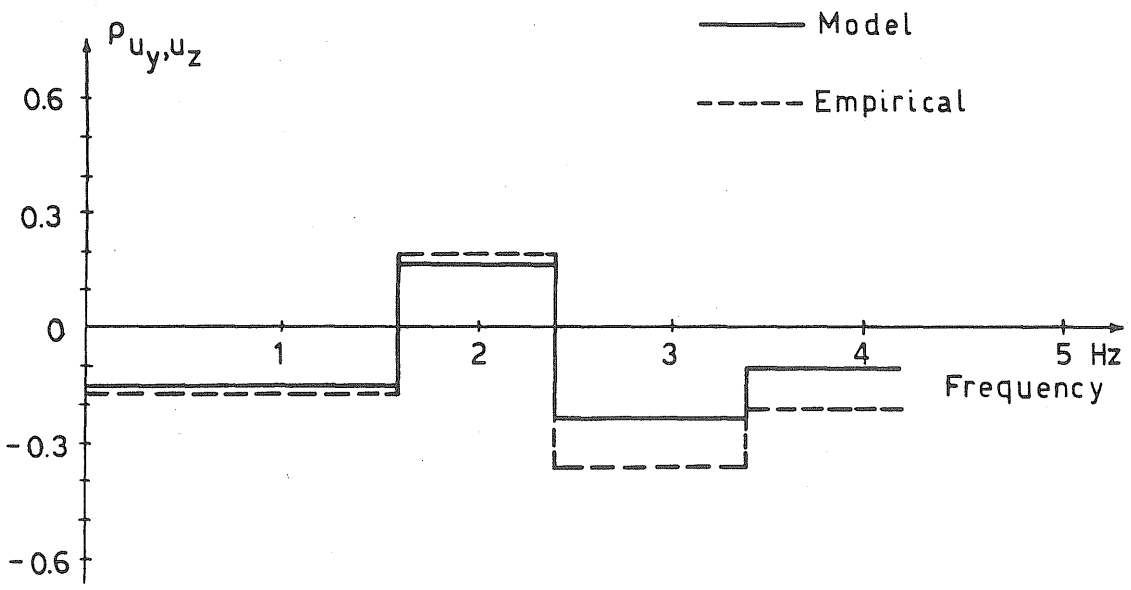

Figure 3.10 Cross-Correlation Coefficient Along and Normal to Epicentral Direction at Stations 006, C00 and 012

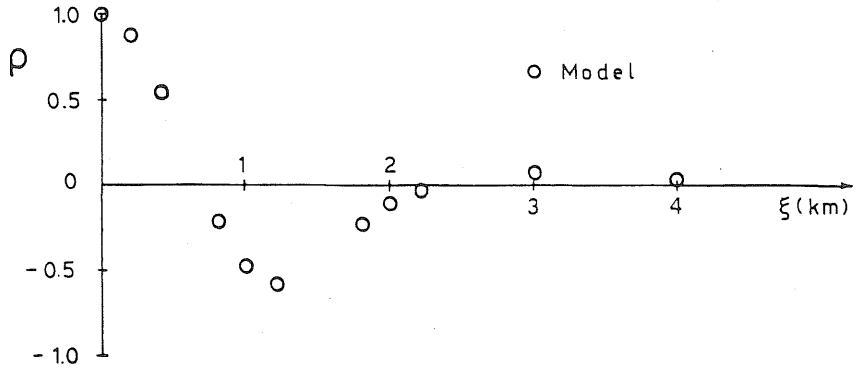

Figure 3.11 Spatial Correlation Coefficient in Vertical Direction

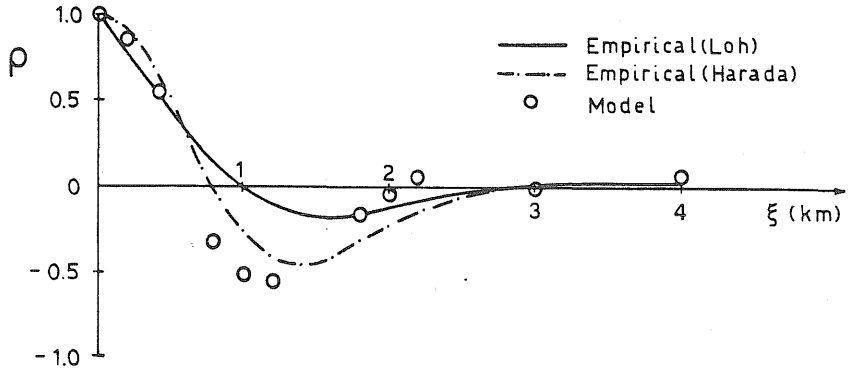

Figure 3.12 Spatial Correlation Coefficient Along Epicentral Direction

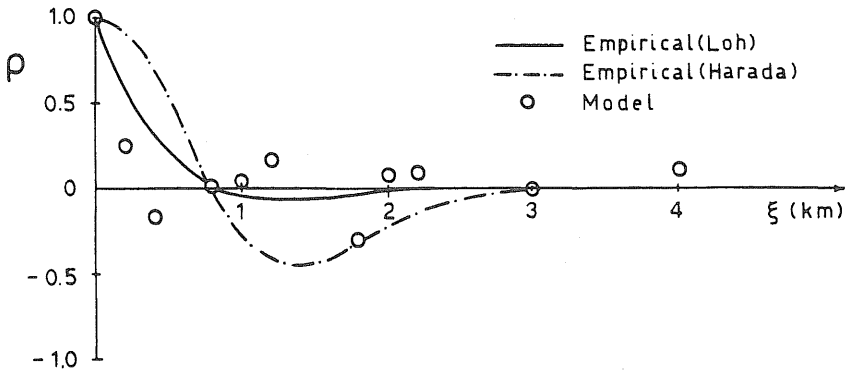

Figure 3.13 Spatial Correlation Coefficient Normal to Epicentral Direction

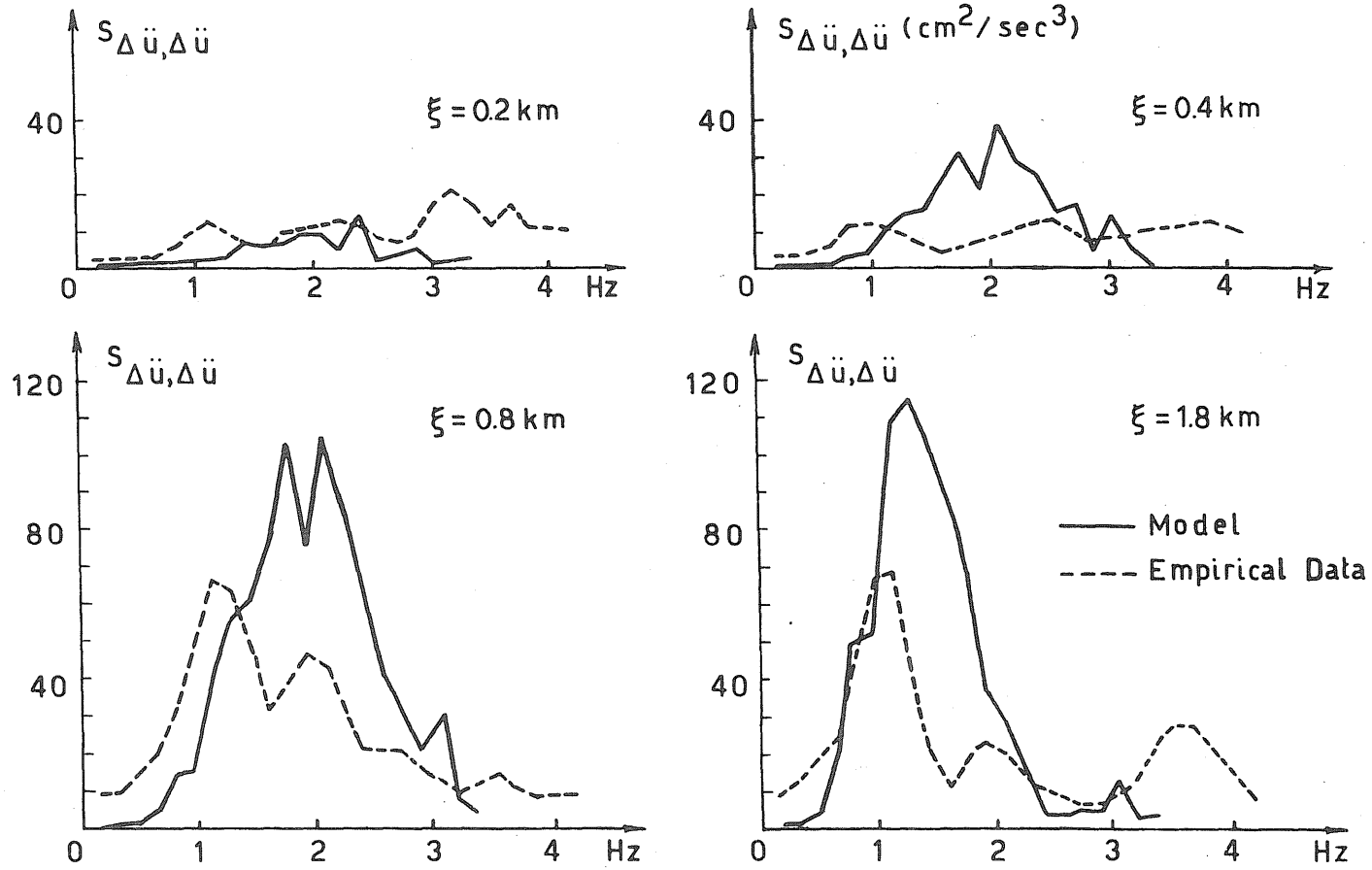

Figure 3.14 Power Spectral Densities of Differential Acceleration

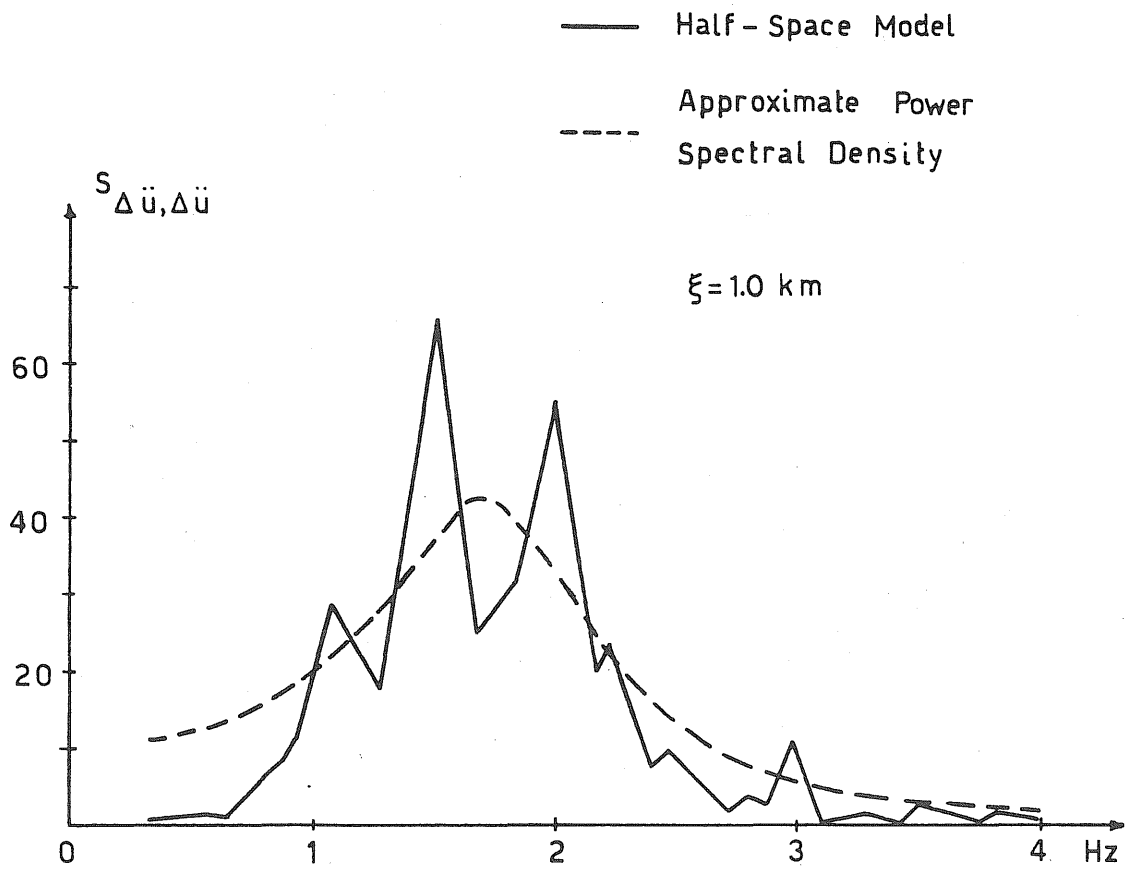

Figure 3.15 Comparison of Analytical Power Spectral Density with Empirical Curve (Differential Motions in Vertical Direction)

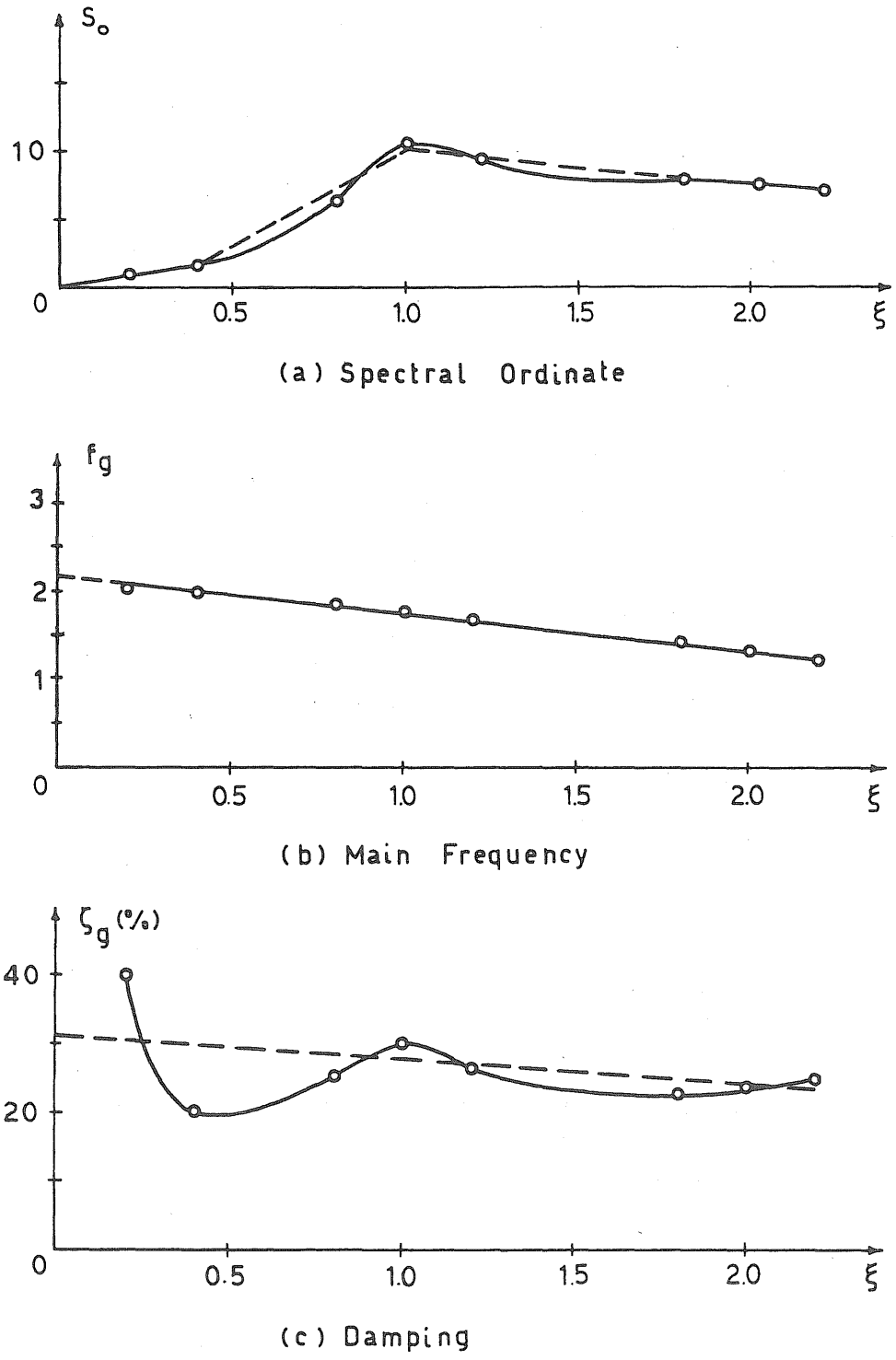

Figure 3.16 Variation of Parameters of Vertical Motions with Separation Distance

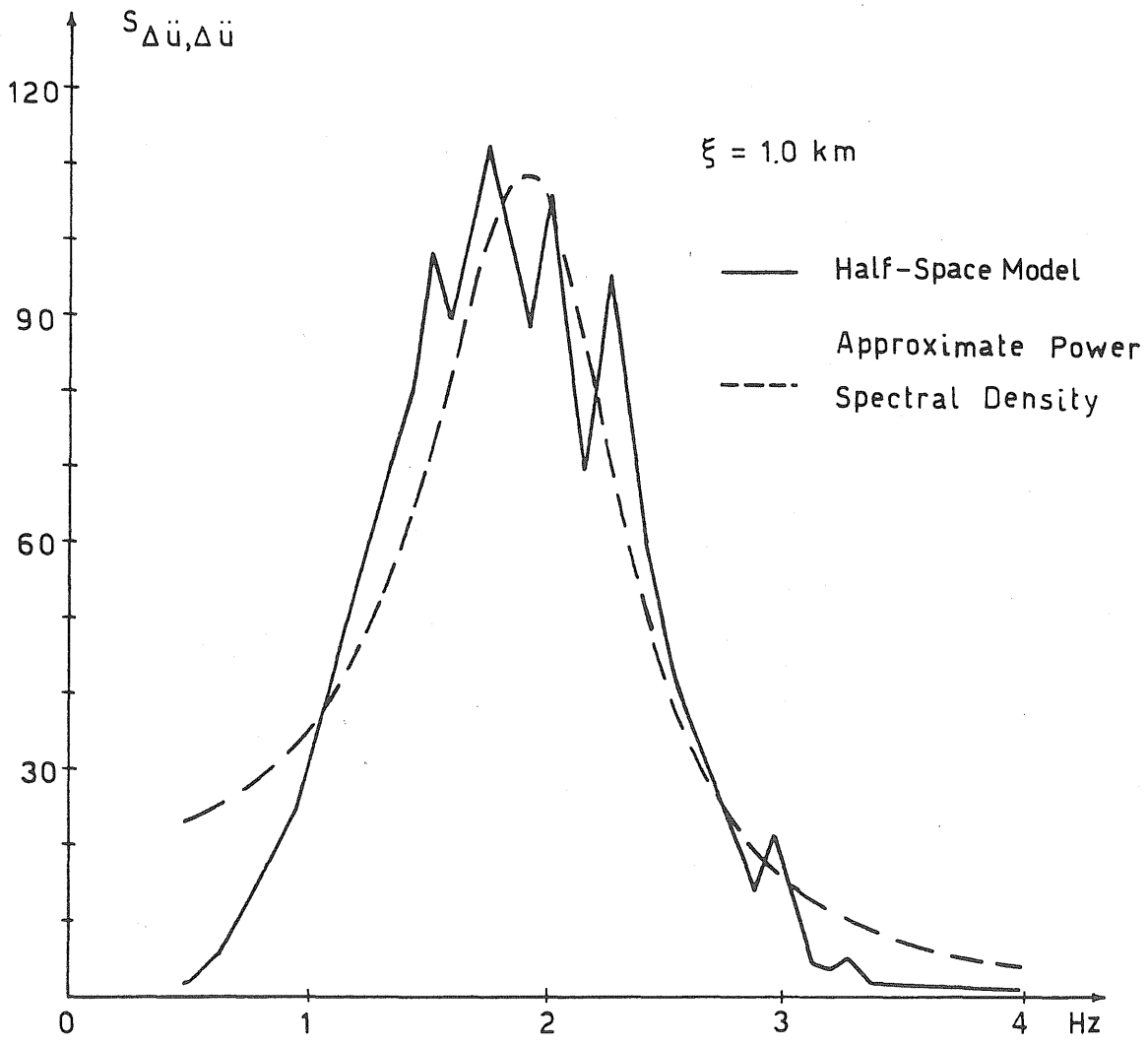

Figure 3.17 Comparison of Analytical Power Spectral Density with Empirical Curve (Differential Motions Along Epicentral Direction)

Figure 3.18 Variation of Parameters of Motions Along Epicentral Direction with Separation Distance

Figure 3.19 Comparison of Analytical Power Spectral Density with Empirical Curve (Differential Motions Normal to Epicentral Direction)

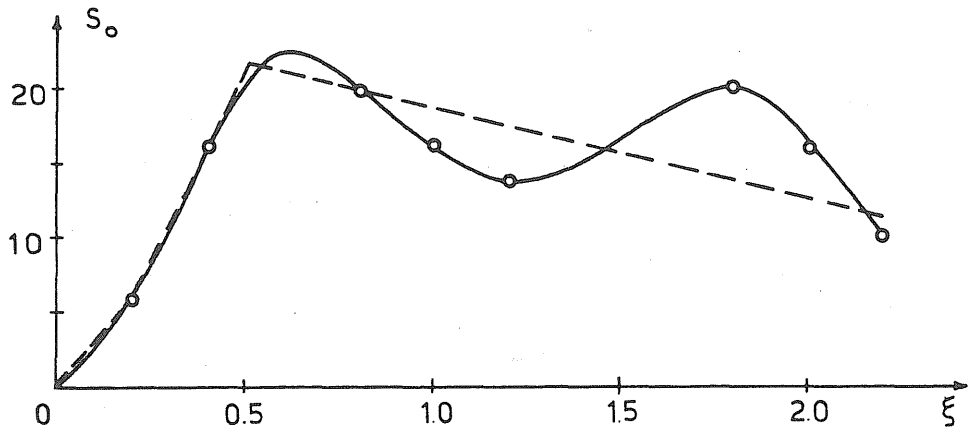

(a) Spectal Ordinate

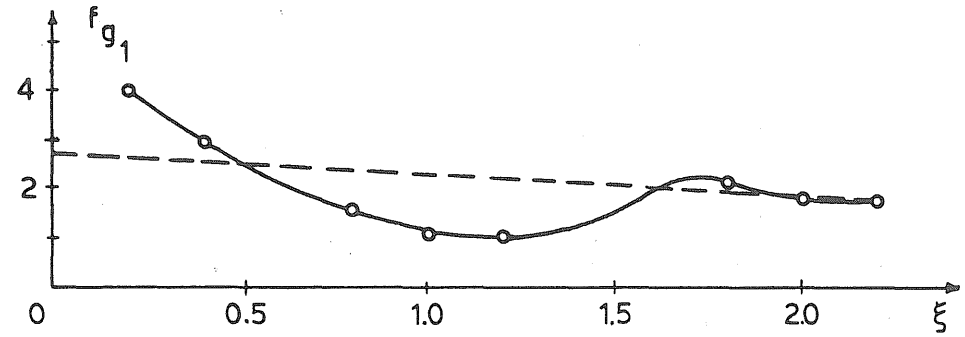

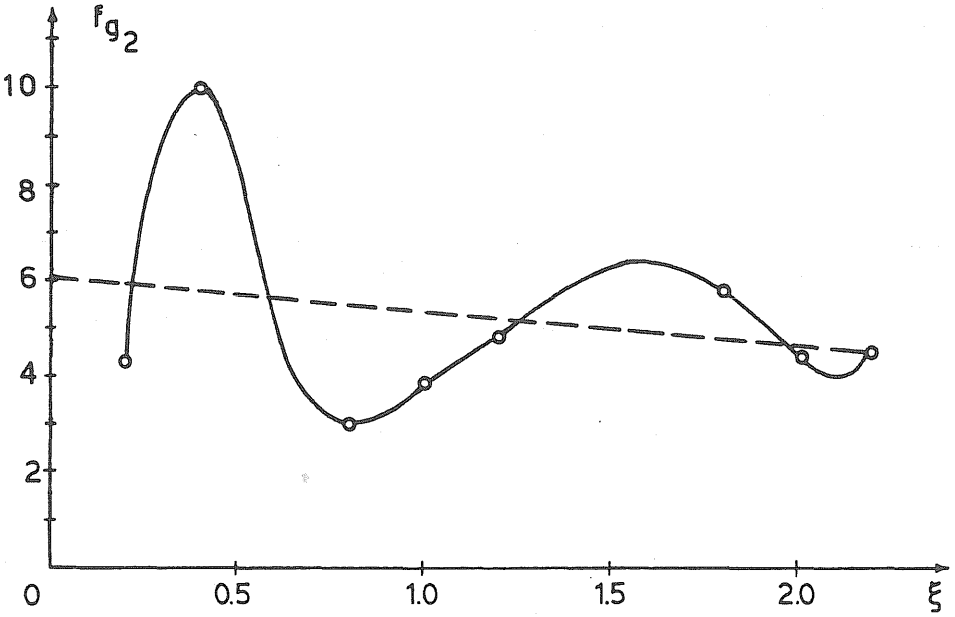

(b) Main Frequencies .

Figure 3.20 Variation of Parameters of Motions Normal to Epicentral Direction with Separation Distance

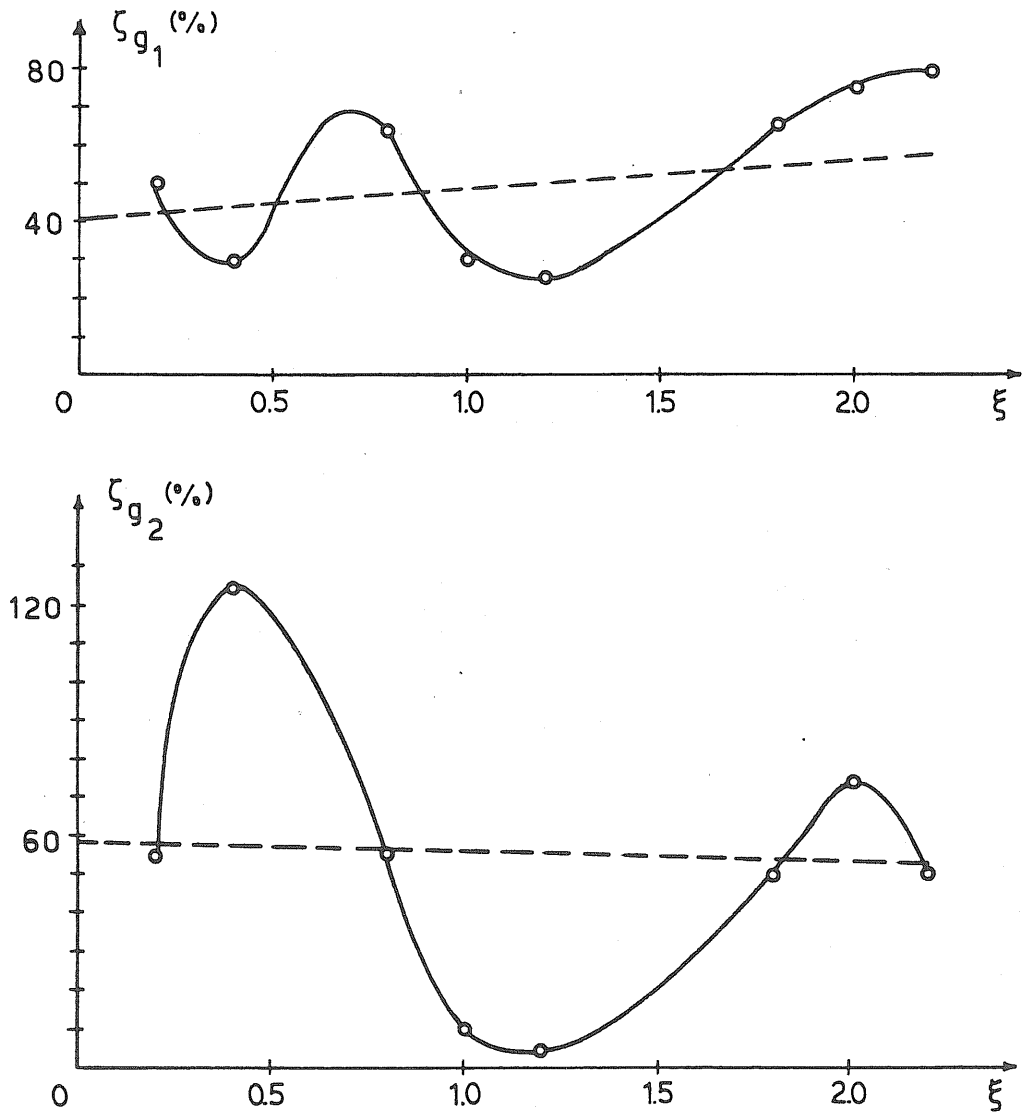

(c) Damping Coefficients

Figure 3.20 (Cont'd.)

CHAPTER 4

APPLICATIONS TO PIPELINES

4.1 Introduction

The continuing performance of pipelines during an earthquake is of vital importance to the health and safety of urban population; e.g., the operational integrity of a water distribution system is essential for fire fighting after an earthquake. Also, in order to minimize the hazard of potential explosion, gas and oil pipelines must remain intact after an earthquake. Pipeline damage may be caused by fault ruptures, soil liquefaction, landslide, or ground shaking during an earthquake.

Since pipelines are long structures that may extend over great distances along or close to the ground surface, the usual assumption of equal support motion is generally not valid. Nelson and Weidlinger (1977) introduced the "interference response spectra" in an attempt to take the spatial variation of ground motions into account. The model is based on the differential motion of a two-degree of freedom pipeline, in which two pipe segments behave as rigid bodies that are supported by springs and dashpots as shown in Fig. 4.1. The base motion at the left support is a given acceleration time history, whereas the input at the right support is the same acceleration time history delayed by the travel time of the motion between the supports; i.e., equal to ℓ/v, where ℓ is the distance between the centers of gravity of the two pipe segments and v is the velocity of the predominant wave. Strictly speaking, however, this assumption is not consistent with the propagation of earthquake waves, since the

accelerograms are the result of contributions of many different types of waves, that are reflected and refracted in the ground medium, and do not consist solely of a surface wave with constant propagation velocity.

Shinozuka and Kawakami (1977) developed a stochastic model to evaluate the spatial variations of strong ground motion for a continuous pipeline. A one-dimensional propagating shear wave model was used; the compressional and surface waves, and the multiple reflections and refractions that occur in a layered medium because of the various angles of incidence of waves originating from the bedrock are neglected.

The model presented in Chapters 2 and 3 is two-dimensional, in contrast to the one-dimensional models described above. The various waves contained in a strong earthquake ground motion, as presented in this model, are compressional, shear (SV- and SH-), and head waves.

The pipelines examined in this study are subjected to two different kinds of input base motions. First the ground motions at the supports are assumed to be fully correlated; this represents the conventional deterministic approach. Secondly, the spatial variation of ground motions is considered, by evaluating the response of pipelines subjected to partially correlated input motions at the supports.

The effect of differential ground motion on the joints of a pipeline is examined in Sect. 4.2, whereas continuous pipelines on elastic foundations are considered in Sect. 4.3.

4.2 Differential Motions Between Pipe Segments

Most damage of pipelines reported during earthquakes occurs at the joints of the pipes; therefore, the differential motions between the pipe segments are of great importance in the earthquake-resistant design of pipelines. These differential motions along and normal to the pipeline axis, namely in the axial, lateral, and vertical directions, may be examined separately.

4.2.1 Joints Subjected to Excitation Along Pipeline Axis

Deterministic Analysis -- The model considered for evaluating the differential motions of pipelines subjected to earthquake excitations along the pipeline axis is that developed by Nelson and Weidlinger (1977). The model shown in Fig. 4.1 consists of two pipe segments, which are assumed to behave as rigid bodies; the pipe segments, each of mass, m, are connected with a spring of stiffness, k_p, and a dashpot of damping, c_p; soil-structure interaction is represented by springs and dashpots of stiffness and damping k_g and c_g, respectively. The ground displacements at the two supports are denoted by $y_{G_1}(t)$ and $y_{G_2}(t)$, whereas the responses of the masses of the pipe segments are $y_1(t)$ and $y_2(t)$.

The equations of motion of the system are

$$m\ddot{y}_1 + c_p(\dot{y}_1-\dot{y}_2) + k_p(y_1-y_2) + c_g(\dot{y}_1-\dot{y}_{G_1}) + k_g(y_1-y_{G_1}) = 0 \qquad (4.1)$$

$$m\ddot{y}_2 + c_p(\dot{y}_2-\dot{y}_1) + k_p(y_2-y_1) + c_g(\dot{y}_2-\dot{y}_{G_2}) + k_g(y_2-y_{G_2}) = 0 \qquad (4.2)$$

By adding Eqs. 4.1 and 4.2 and rearranging terms,

$$m(\ddot{y}_1+\ddot{y}_2) + c_g(\dot{y}_1+\dot{y}_2) + k_g(y_1+y_2) = c_g(\dot{y}_{G_1}+\dot{y}_{G_2}) + k_g(y_{G_1}+y_{G_2}) \qquad (4.3)$$

Equation 4.3 is the equation of motion of the rigid body mode, in which the distance ℓ between the mass centers of the pipe segments remains constant.

Subtracting Eq. 4.2 from Eq. 4.1 yields

$$m(\ddot{y}_1-\ddot{y}_2) + (c_g+2c_p)(\dot{y}_1-\dot{y}_2) + (k_g+2k_p)(y_1-y_2)$$

$$= c_g(\dot{y}_{G_1}-\dot{y}_{G_2}) + k_g(y_{G_1}-y_{G_2}) \qquad (4.4)$$

or,

$$\Delta\ddot{y} + 2\zeta\omega_o\Delta\dot{y} + \omega_o^2\Delta y = \frac{c_g}{m}\Delta\dot{y}_G + \frac{k_g}{m}\Delta y_G \tag{4.5}$$

where:

$\Delta y = y_1 - y_2$, the differential displacement between the pipe segments;

$$2\zeta\omega_o = \frac{c_g + 2c_p}{m} \quad ;$$

$$\omega_o^2 = \frac{k_g + 2k_p}{m} \quad ;$$

and,

$$\Delta y_G = y_{G_1} - y_{G_2} \quad .$$

At this point the following assumption is made

$$\frac{c_p}{c_g} = \frac{k_p}{k_g} = \lambda \tag{4.6}$$

and the parameter α is introduced,

$$\alpha = \frac{k_g}{k_g + 2k_p} = \frac{c_g}{c_g + 2c_p} \tag{4.7}$$

Then, the equation of differential motions becomes

$$\Delta\ddot{y} + 2\zeta\omega_o\Delta\dot{y} + \omega_o^2\Delta y = \alpha(2\zeta\omega_o\Delta\dot{y}_G + \omega_o^2\Delta y_G) \tag{4.8}$$

Δy may be evaluated by means of Duhamel's integral, namely;

$$\Delta y(t) = \int_0^t h(t-\tau)\, f(\tau)\, d\tau \qquad (4.9)$$

where:

$h(t) = \dfrac{1}{\omega_o\sqrt{1-\zeta^2}}\, e^{-\zeta\omega_o t} \sin \omega_o\sqrt{1-\zeta^2}\, t$, the impulse response function of the system;

$f(t) = \alpha\left(2\zeta\omega_o\, \Delta\dot{y}_G(t) + \omega_o^2\, \Delta y_G(t)\right)$, is the seismic input to the system;

and,

ω_o, ζ = the natural frequency and damping coefficient, respectively.

Stochastic Analysis -- The autocorrelation function of the differential motions between two pipe segments is defined as,

$$R_{\Delta y,\Delta y}(\tau) = E[\Delta y(t)\, \Delta y(t+\tau)]$$

$$= E\left[\int_{-\infty}^{\infty} f(t-\tau_1)\, h(\tau_1)\, d\tau_1 \int_{-\infty}^{\infty} f(t+\tau-\tau_2)\, h(\tau_2)\, d\tau_2\right] \qquad (4.10)$$

where, E represents the expected value, and

$f(t)$ = seismic input to the system (Eq. 4.9);

τ = the elapsed time difference.

Interchanging expectation and integration, the autocorrelation function for Δy becomes,

$$R_{\Delta y,\Delta y}(\tau) = \iint_{-\infty}^{\infty} h(\tau_1)\, h(\tau_2)\, R_{ff}(\tau+\tau_1-\tau_2)\, d\tau_1\, d\tau_2 \qquad (4.11)$$

where $R_{ff}(\tau)$ is the autocorrelation function of the seismic input, which may be evaluated as follows

$$R_{ff}(\tau) = E[f(t)\ f(t+\tau)]$$

$$= \alpha^2\ E[(2\zeta\omega_o\Delta\dot{y}_G(t) + \omega_o^2\Delta y_G(t))\ (2\zeta\omega_o\Delta\dot{y}_G(t+\tau) + \omega_o^2\Delta y_G(t+\tau))]$$

$$= \alpha^2[4\zeta^2\omega_o^2\ R_{\Delta\dot{y}_G,\Delta\dot{y}_G}(\tau) + 2\zeta\omega_o^3\ (R_{\Delta y_G,\Delta\dot{y}_G}(\tau)$$

$$+ R_{\Delta\dot{y}_G,\Delta y_G}(\tau)) + \omega_o^4\ R_{\Delta y_G,\Delta y_G}(\tau)] \qquad (4.12)$$

where:

$R_{\Delta y,_G\Delta y_G}(\tau)$ = the autocorrelation function of the differential displacement;

$R_{\Delta\dot{y}_G,\Delta\dot{y}_G}(\tau)$ = the autocorrelation function of the differential velocity;

and,

$R_{\Delta\dot{y}_G,\Delta y_G}(\tau)$, $R_{\Delta y_G,\Delta\dot{y}_G}(\tau)$ = the cross-correlation functions between the differential velocity and displacement.

Taking the Fourier transform of Eq. 4.12, the power spectral density of the input motion becomes

$$S_{ff}(\omega) = \alpha^2[4\zeta^2\omega_o^2\ S_{\Delta\dot{y}_G,\Delta\dot{y}_G}(\omega) + 2\zeta\omega_o^3\ (S_{\Delta y_G,\Delta\dot{y}_G}(\omega)$$

$$+ S_{\Delta\dot{y}_G,\Delta y_G}(\omega)) + \omega_o^4\ S_{\Delta y_G,\Delta y_G}(\omega)]$$

$$= \frac{\alpha^2}{\omega^4}\ (4\zeta^2\omega_o^2\omega^2 + \omega_o^4)\ S_{\Delta\ddot{y}_G,\Delta\ddot{y}_G}(\omega) \qquad (4.13)$$

Finally, with Eq. 4.13 the Fourier transform of Eq. 4.11 yields the power spectral density of the differential displacement when a pipe is subjected to earthquake excitations along the pipeline axis; thus,

$$S_{\Delta y,\Delta y}(\omega) = \frac{\alpha^2}{\omega^4} (4\zeta^2\omega_o^2\omega^2 + \omega_o^4) \left|H(\omega)\right|^2 S_{\Delta\ddot{y}_G,\Delta\ddot{y}_G}(\omega) \tag{4.14}$$

where:

$$\left|H(\omega)\right|^2 = \frac{1}{(\omega_o^2-\omega^2)^2 + 4\zeta^2\omega_o^2\omega^2} ;$$

and $S_{\Delta\ddot{y}_G,\Delta\ddot{y}_G}(\omega)$ is the power spectral density of the differential acceleration (see Eqs. 2.34 and 2.36, or Eq. 3.5).

4.2.2 Joints Subjected to Excitation Normal to Pipeline Axis

The structural model used to evaluate the differential motion when a pipeline is subjected to earthquake excitations normal to the pipeline axis, namely lateral or vertical motions, is shown in Fig. 4.2. The structural model is similar to the one Nelson and Weidlinger (1977) introduced in their interference response spectra; in addition to the translational motions, $x_1(t)$ and $x_2(t)$, of the mass centers of the pipe segments, the rotations $\theta_1(t)$ and $\theta_2(t)$ have been added.

The equations of motion of the system are,

$$m\ddot{x}_1 + c_g\dot{x}_1 + k_g x_1 + c_p(\dot{x}_1-\dot{x}_2+\ell'\dot{\theta}_1+\ell'\dot{\theta}_2) + k_p(x_1-x_2+\ell'\theta_1+\ell'\theta_2)$$

$$= c_g\dot{x}_{G_1} + k_g x_{G_1} \tag{4.15}$$

$$m\ddot{x}_2 + c_g\dot{x}_2 + k_g x_2 - c_p(\dot{x}_1-\dot{x}_2+\ell'\dot{\theta}_1+\ell'\dot{\theta}_2) - k_p(x_1-x_2+\ell'\theta_1+\ell'\theta_2)$$

$$= c_g\dot{x}_{G_2} + k_g x_{G_2} \tag{4.16}$$

$$J\ddot{\theta}_1 + c_p\ell'(\dot{x}_1-\dot{x}_2+\ell'\dot{\theta}_1+\ell'\dot{\theta}_2) + k_p\ell'(x_1-x_2+\ell'\theta_1+\ell'\theta_2) = 0 \tag{4.17}$$

and,

$$J\ddot{\theta}_2 + c_p\ell'(\dot{x}_1-\dot{x}_2+\ell'\dot{\theta}_1+\ell'\dot{\theta}_2) + k_p\ell'(x_1-x_2+\ell'\theta_1+\ell'\theta_2) = 0 \qquad (4.18)$$

where:

ℓ' = $\ell/2$, in which ℓ is the distance between the mass centers of the two pipe segments;

m, J = the mass and the moment of inertia of each segment;

k_p, c_p = the stiffness and damping between the pipe segments;

k_g, c_g = the stiffness and damping of the soil; and

$x_{G_1}(t)$, $x_{G_2}(t)$ = the input displacements at the two supports.

In matrix form Eqs. 4.15 through 4.18 become,

$$[M]\{\ddot{x}\} + [C]\{\dot{x}\} + [K]\{x\} = \{F(t)\} \qquad (4.19)$$

where:

$$[M] = \begin{bmatrix} m & 0 & 0 & 0 \\ 0 & m & 0 & 0 \\ 0 & 0 & J & 0 \\ 0 & 0 & 0 & J \end{bmatrix} ;$$

$$[C] = \begin{bmatrix} c_g+c_p & -c_p & c_p\ell' & c_p\ell' \\ -c_p & c_g+c_p & -c_p\ell' & -c_p\ell' \\ c_p\ell' & -c_p\ell' & c_p\ell'^2 & c_p\ell'^2 \\ c_p\ell' & -c_p\ell' & c_p\ell'^2 & c_p\ell'^2 \end{bmatrix} ;$$

$$[K] = \begin{bmatrix} k_g+k_p & -k_p & k_p\ell' & k_p\ell' \\ -k_p & k_g+k_p & -k_p\ell' & -k_p\ell' \\ k_p\ell' & -k_p\ell' & k_p\ell'^2 & k_p\ell'^2 \\ k_p\ell' & -k_p\ell' & k_p\ell'^2 & k_p\ell'^2 \end{bmatrix} ;$$

$$\{x\} = \begin{Bmatrix} x_1 \\ x_2 \\ \theta_1 \\ \theta_2 \end{Bmatrix} \quad ;$$

and,

$$\{F(t)\} = \begin{Bmatrix} c_g \dot{x}_{G_1}(t) + k_g x_{G_1}(t) \\ c_g \dot{x}_{G_2}(t) + k_g x_{G_2}(t) \\ 0 \\ 0 \end{Bmatrix} .$$

The natural frequencies and mode shapes of the system are:

$$\omega_1^2 = 0 \quad ; \quad [\phi_1] = [0 \quad 0 \quad -1 \quad 1] \quad ;$$

$$\omega_3^2 = \frac{k_g}{m} \quad ; \quad [\phi_3] = [1 \quad 1 \quad 0 \quad 0] \quad ;$$

$$\omega_{2,4}^2 = \frac{2k_p \ell'^2 m + k_g J + 2k_p J \pm \sqrt{(2k_p \ell'^2 m + k_g J + 2k_p J)^2 - 8k_g k_p \ell'^2 mJ}}{2mJ} ;$$

$$[\phi_{2,4}] = [1 \quad -1 \quad A_{II,IV} \quad B_{II,IV}] \quad ; \qquad (4.20)$$

in which,

$$A_{II,IV} = \frac{\ell'(m\omega_{2,4}^2 - k_g)}{J\omega_{2,4}^2} \quad ;$$

and,

$$B_{II,IV} = \frac{mJ\omega_{2,4}^2 - (k_g + 2k_p)\, J\omega_{2,4}^2 - k_p \ell'^2 m\omega_{2,4}^2 + k_g k_p \ell'^2}{k_p \ell' J \omega_{2,4}^2}$$

The subscripts 2,4 and II,IV imply that the quantities are evaluated for the second and fourth modes, respectively.

If stiffness proportional damping is assumed, and

$$\{x\} = [\Phi]\{y\} \tag{4.21}$$

then, the equations of motion, Eqs. 4.15 through 4.18, become,

$$m_i \ddot{y}_i(t) + c_i \dot{y}_i(t) + k_i y_i(t) = f_i(t) \quad ; \quad i=1,2,3,4 \tag{4.22}$$

where:

$$\zeta_i = \frac{c_i}{2m_i\, \omega_i} \quad ;$$

$$m_i = [\Phi]^T [M][\Phi]_i \quad ;$$

$$c_i = [\Phi]^T [C][\Phi]_i \quad ;$$

$$k_i = [\Phi]^T [K][\Phi]_i \quad ;$$

and,

$$\{f_i(t)\} = \begin{Bmatrix} 0 \\ c_g\left(\dot{x}_{G_1}(t) - \dot{x}_{G_2}(t)\right) + k_g\left(x_{G_1}(t) - x_{G_2}(t)\right) \\ c_g\left(\dot{x}_{G_1}(t) + \dot{x}_{G_2}(t)\right) + k_g\left(x_{G_1}(t) + x_{G_2}(t)\right) \\ c_g\left(\dot{x}_{G_1}(t) - \dot{x}_{G_2}(t)\right) + k_g\left(x_{G_1}(t) - x_{G_2}(t)\right) \end{Bmatrix}.$$

Each $y_i(t)$, i = 1,2,3,4, may now be obtained in terms of the Duhamel's integral,

$$y_i(t) = \frac{1}{m_i} \int_0^t h_i(t-\tau)\, f_i(\tau)\, d\tau \tag{4.23}$$

from which $x_1(t)$, $x_2(t)$, $\theta_1(t)$ and $\theta_2(t)$ may be obtained through Eq. 4.21.

The differential motion between the pipe segments is

$$\Delta x(t) = x_1(t) - x_2(t) + \ell'\theta_1(t) + \ell'\theta_2(t) \tag{4.24}$$

Substituting $x_1(t)$, $x_2(t)$, $\theta_1(t)$ and $\theta_2(t)$ from Eq. 4.21, Eq. 4.24 becomes,

$$\Delta x(t) = C_{II}\, y_2(t) + C_{IV}\, y_4(t) \tag{4.25}$$

where $C_{II,IV} = 2 + \ell'\, A_{II,IV} + \ell'\, B_{II,IV}$.

The power spectral density of the differential displacement, when the earthquake excitation is normal to the pipeline axis, becomes (see Appendix A for details)

$$S_{\Delta x,\Delta x}(\omega) = C_{II}^2\, S_{y_2y_2}(\omega) + C_{II}C_{IV}\left(S_{y_2y_4}(\omega) + S_{y_4y_2}(\omega)\right) + C_{IV}^2\, S_{y_4y_4}(\omega) \tag{4.26}$$

where C_{II} and C_{IV} are given by Eq. 4.25 and $S_{y_2y_2}(\omega)$, $S_{y_2y_4}(\omega)$, $S_{y_4y_2}(\omega)$ and $S_{y_4y_4}(\omega)$ are given by

$$S_{y_jy_\ell}(\omega) = \frac{1}{m_j m_\ell} H_j^*(\omega)\, H_\ell(\omega)\, S_{f_jf_\ell}(\omega) \quad ; \quad j,\ell = 2 \text{ or } 4 \tag{4.27}$$

in which, $H_j(\omega)$, $H_\ell(\omega)$ are the frequency transfer functions of the system.

The cross spectral density of the input for the generalized coordinates j and ℓ, $S_{f_j f_\ell}(\omega)$ may be found to be

$$S_{f_j f_\ell}(\omega) = \left[\frac{c_g^2}{\omega^2} + \frac{k_g^2}{\omega^4} \right] S_{\Delta\ddot{x}_G, \Delta\ddot{x}_G}(\omega) \tag{4.28}$$

Equations 4.26 through 4.28 define the spectrum of differential displacement between the pipe segments when subjected to earthquake excitations normal to the pipeline axis.

4.2.3 Effect of Differential Ground Motion

The orientation of the axis of the pipelines examined in this study is assumed to coincide with the epicentral direction, namely the direction from Station 006 to Station 012 of the SMART-1 array as shown in Fig. 3.1. Therefore, the input in the axial direction is the motion along the epicentral direction, whereas the input in the lateral direction is the excitation normal to the epicentral direction.

Loh, Ang, and Wen (1983) used the interference response spectra to evaluate the differential axial motion between two pipe segments for the earthquake of January 29, 1981 recorded at the SMART-1 array; 5% of critical damping was assumed, although the damping of pipelines may be much higher (Hindy and Novak, 1980). The same structural model is also used here for frequencies of 0.5, 1, 2 and 3 Hz with 5% of critical damping. The method of interference response spectra evaluates the maximum response in the deterministic domain. For comparison, the mean value and standard deviation of the maximum response during the same earthquake are evaluated with the stochastic analysis presented herein.

Table 4.1 shows the results obtained with the interference response spectra, denoted by Δ_{max}; the results of the stochastic analysis are also presented for the mean maximum differential displacement, μ_{x_m}, and corresponding standard deviation, σ_{x_m}, over the duration of strong ground

motion (Longuet-Higgins, 1952; Davenport, 1964). The results of the stochastic analysis are the response corresponding to the base motions obtained with the half-space model. The method of interference response spectra generally gives results that are lower than those of the stochastic analysis; this suggests that the interference response spectra tend to underestimate the differential motion between the pipe segments, particularly for pipes with frequencies higher than 1 Hz.

Tables 4.2 through 4.4 show the differential displacements between pipe segments for the axial, lateral, and vertical motions. The stiffness and damping of the connection between the pipe segments is half the stiffness and damping of the soil. The natural frequency of the system subjected to axial motion is 1 Hz. The frequency of the third mode of the system subjected to lateral and vertical motions is also 1 Hz; the third frequency of the system and the ratio of the stiffness of the connection between the pipe segments to the stiffness of the soil allow the evaluation of the remaining frequencies. The input motions in all directions are the results of the half-space model, obtained from Eqs. 2.34 and 2.36, as well as those described by the approximate power spectral densities for differential accelerations (Eqs. 3.5 through 3.9). The results obtained with the approximate power spectral density of differential acceleration are in reasonable agreement with the results of the half-space model.

The response in the vertical direction is smaller than the response in the axial or lateral direction. The axial and lateral responses are equally important in the seismic design of the joints, as pointed out in the report of the U. S. Department of Commerce (1973) with regard to the San Fernando earthquake of February 9, 1971.

If the motion at two adjacent supports is assumed to be perfectly correlated, the input to the systems would be zero, which would result in a zero differential motion between the pipe segments, i.e., a stress-free rigid body motion. This, however, would contradict the observation that most damage of pipelines during earthquakes occurred at the joints (U. S. Department of Commerce, 1973). Therefore, it is important that the differential motions be considered in the design and safety evaluation of pipelines.

Differential Response Spectrum -- The differential response spectrum, similar in purpose to the interference response spectrum, is introduced here. The differential response spectrum represents the maximum response as a function of the natural frequency of a system; it is based on the response in the axial direction of the model presented in Sect. 4.2.1. The response is given by Eq. 4.14, whereas the input motion is the approximate power spectral density of Eqs. 3.5 and 3.8.

Figure 4.3 shows the mean maximum differential displacements obtained with the differential response spectrum for separation distances 0.2, 0.8, 1.0 and 1.8 km. The response of the same system subjected to input motions obtained through the half-space model (Eqs. 2.34 and 2.36) are also shown for comparison. The maximum differential displacements for the two input motions are in good agreement particularly for short separation distance ℓ = 0.2 km. The differences in the lower frequency range may be attributed to the fact that the spectral amplitudes of the approximate power spectral density are higher than those corresponding to the half-space model in this frequency range; in this way it is believed that the approximate power spectral density provides a better approximation for the spectra of the actual earthquake than the half-space model (see Sect. 3.3). The maximum relative displacement decreases with frequency, and generally increases with separation up to a distance of 1.0 km which is related to the correlation length. Loh, Ang, and Wen (1983) indicated that the correlation length is approximately 2.0 km.

Figure 4.4 shows the differential response spectrum for the mean maximum differential displacement and the corresponding mean plus one standard deviation obtained with the approximate power spectral density of differential ground acceleration.

4.3 Response of Continuous Pipelines

The effect of the differential motion on a continuous pipeline is examined in this section for axial and lateral motions. Again, fully and partially correlated input motions are considered; the latter representing motions expected during an earthquake.

4.3.1 Axial Response of Continuous Pipelines

The model used to evaluate the response statistics of a long continuous pipeline is shown in Fig. 4.5; the pipe rests on elastic foundations and its end supports allow a rigid body motion in the axial direction. Buckling is not included in the analysis.

If $v(y,t)$ denotes the absolute displacement as a function of the coordinate along the axis of the pipeline, and $v_g(y,t)$ denotes the ground excitation, the equation of motion of the pipe becomes

$$m \frac{\partial^2 v(y,t)}{\partial t^2} + C_A \frac{\partial v(y,t)}{\partial t} + K_A v(y,t) - E_p A \frac{\partial^2 v(y,t)}{\partial y^2}$$

$$= C_A \frac{\partial v_g(y,t)}{\partial t} + K_A v_g(y,t) \qquad (4.29)$$

where:

m = the mass per unit length of the pipe;

C_A, K_A = the damping and stiffness of the soil, respectively; and

E_P, A = the modulus of elasticity and cross sectional area of the pipe, respectively.

The internal damping of the pipe has been neglected, as it is much smaller than the damping derived from the soil (Hindy and Novak, 1980).

Letting the damping and the input ground motions equal zero, and considering that the pipe has stress-free end conditions, the natural frequencies and mode shapes of the pipe become,

$$\omega_j = \sqrt{\frac{K_A}{m}} \sqrt{1 + \frac{E_p A}{K_A} \frac{(j-1)^2 \pi^2}{\ell^2}} \quad ;$$

$$\phi_j(y) = \cos \frac{(j-1)\pi y}{\ell} \qquad (4.30)$$

$$S_{\sigma_A(y_\alpha),\sigma_A(y_\beta)}(\omega) = \frac{E_p^2\pi^2}{m^2\ell^2}\left[\frac{C_A^2}{\omega^2} + \frac{K_A^2}{\omega^4}\right]\sum_{i=1}^{N}\sum_{j=1}^{N}(i-1)(j-1)$$

$$\cdot \sin\frac{(i-1)\pi y_\alpha}{\ell}\sin\frac{(j-1)\pi y_\beta}{\ell}H_i^*(\omega)\,H_j(\omega)\,\frac{1}{L_iL_j}$$

$$\cdot \int_0^\ell\int_0^\ell \phi_i(y_1)\,\phi_j(y_2)\,S_{\ddot{v}_g(y_1),\ddot{v}_g(y_2)}(\omega)\,dy_1\,dy_2 \qquad (4.38)$$

where $\sigma_A(y_\alpha)$ stands for axial stress at point y_α. The corresponding cross spectral density of the axial strains $\varepsilon_A(y)$ is

$$S_{\varepsilon_A(y_\alpha),\varepsilon_A(y_\beta)}(\omega) = \frac{S_{\sigma_A(y_\alpha),\sigma_A(y_\beta)}(\omega)}{E_p^2} \qquad (4.39)$$

4.3.2 Transverse Response of Continuous Pipelines

The response in the direction normal to the pipeline axis can be evaluated with the model shown in Fig. 4.6; the pipe is assumed to rest on elastic foundations, and its end conditions allow a rigid body motion in the transverse direction.

If the absolute displacement in the transverse direction is denoted by $w(y,t)$, where y is the coordinate along the axis of the pipeline, and $u_g(y,t)$ is the ground excitation in the transverse direction, the equation of motion of the pipeline becomes

$$m \frac{\partial^2 w(y,t)}{\partial t^2} + C_T \frac{\partial w(y,t)}{\partial t} + K_T w(y,t) + E_p I \frac{\partial^4 w(y,t)}{\partial y^4}$$

$$= C_T \frac{\partial u_g(y,t)}{\partial t} + K_T u_g(y,t) \qquad (4.40)$$

where:

C_T, K_T = the damping and stiffness of the soil, respectively; and

E_P, I = the modulus of elasticity and moment of inertia of the pipe, respectively.

Again, internal damping of the pipe is neglected (Hindy and Novak, 1980).

The equation for the free, undamped vibration follows from Eq. 4.40 with $C_T = \dot{u}_g = u_g = 0$, namely;

$$m \frac{\partial^2 w(y,t)}{\partial t^2} + K_T w(y,t) + E_P I \frac{\partial^4 w(y,t)}{\partial y^2} = 0 \qquad (4.41)$$

Taking the boundary conditions

$$w'(0,t) = w'''(0,t) = w'(\ell,t) = w'''(\ell,t) = 0 \qquad (4.42)$$

into account, and describing the free vibration by

$$w(y,t) = u(y) \exp(i\omega t) \qquad (4.43)$$

in which,

$$u(y) = C_1 \cosh\left(\frac{\lambda y}{\ell}\right) + C_2 \sinh\left(\frac{\lambda y}{\ell}\right) + C_3 \cos\left(\frac{\lambda y}{\ell}\right) + C_4 \sin\left(\frac{\lambda y}{\ell}\right),$$

the natural frequencies and mode shapes of the structure become,

$$\omega_j = \sqrt{\frac{K_T}{m}} \sqrt{1 + \frac{E_p I}{K_T} \frac{(j-1)^4 \pi^4}{\ell^4}} \quad ;$$

$$\phi_j(y) = \cos \frac{(j-1)\pi y}{\ell} \qquad (4.44)$$

The absolute displacement may then be written as,

$$w(y,t) = \sum_{i=1}^{N} \phi_i(y)\, q_i(t) \tag{4.45}$$

and the uncoupled equations of motion become,

$$m_j \ddot{q}_j(t) + c_j \dot{q}_j(t) + k_j q_j(t)$$

$$= C_T \int_0^{\ell} \phi_j(y) \dot{u}_g(y,t)\, dy + K_T \int_0^{\ell} \phi_j(y) u_g(y,t)\, dy \tag{4.46}$$

where:

$$m_j = mL_j \quad ; \quad c_j = C_T L_j \quad ; \quad k_j = K_T L_j + E_p I L_j \frac{(j-1)^4 \pi^4}{\ell^4} \quad ;$$

and,

$$L_j = \begin{cases} \ell/2 & \text{if} \quad j \neq 1 \\ \ell & \text{if} \quad j = 1 \end{cases}$$

Letting

$$\frac{c_j}{m_j} = 2\zeta_j \omega_j \tag{4.47}$$

and recalling that

$$\frac{k_j}{m_j} = \frac{K_T}{m}\left(1 + \frac{E_p I}{K_T} \frac{(j-1)^4 \pi^4}{\ell^4}\right) = \omega_j^2 \tag{4.48}$$

the equations of motion for the generalized coordinates become,

$$\ddot{q}_j(t) + 2\zeta_j \omega_j \dot{q}_j(t) + \omega_j^2 q_j(t) = B_j(t) \tag{4.49}$$

in which,

$$B_j(t) = \frac{C_T}{mL_j} \int_0^{\ell} \phi_j(y)\, \dot{u}_g(y,t)\, dy + \frac{K_T}{mL_j} \int_0^{\ell} \phi_j(y)\, u_g(y,t)\, dy \ .$$

$q_j(t)$ may then be evaluated by means of the Duhamel's integral, and the total response is given by Eq. 4.45.

The cross spectral density of the transverse response at points y_α and y_β may be evaluated with a procedure similar to the one described in Appendix B and has the following form:

$$S_{w(y_\alpha),w(y_\beta)}(\omega) = \frac{1}{m^2} \left[\frac{C_T^2}{\omega^2} + \frac{K_T^2}{\omega^4} \right] \sum_{i=1}^{N} \sum_{j=1}^{N} \frac{\phi_i(y_\alpha)\, \phi_j(y_\beta)}{L_i L_j}$$

$$\cdot H_i^*(\omega)\, H_j(\omega) \int_0^{\ell}\int_0^{\ell} \phi_i(y_1)\, \phi_j(y_2)\, S_{\ddot{u}_g(y_1),\ddot{u}_g(y_2)}(\omega)\, dy_1\, dy_2 \qquad (4.50)$$

The power spectral density at point y can be obtained by substituting $y_\alpha = y_\beta = y$.

The power spectral density of the maximum bending stress, $\sigma_T(y_\alpha)$, in the pipeline is given by the following equation:

$$S_{\sigma_T(y_\alpha),\sigma_T(y_\beta)}(\omega) = \left(\frac{E_p R}{m}\right)^2 \frac{\pi^4}{\ell^4} \left[\frac{C_T^2}{\omega^2} + \frac{K_T^2}{\omega^4} \right]$$

$$\cdot \sum_{i=1}^{N} \sum_{j=1}^{N} (i-1)^2\, (j-1)^2\, \phi_i(y_\alpha)\, \phi_j(y_\beta)\, H_i^*(\omega)\, H_j(\omega)$$

$$\cdot \int_0^{\ell}\int_0^{\ell} \phi_i(y_1)\, \phi_j(y_2)\, S_{\ddot{u}_g(y_1),\ddot{u}_g(y_2)}(\omega)\, dy_1\, dy_2 \qquad (4.51)$$

in which R is the pipe radius. The corresponding cross spectral density of the maximum bending strains $\varepsilon_T(y)$ is

$$S_{\varepsilon_T(y_\alpha),\varepsilon_T(y_\beta)}(\omega) = \frac{S_{\sigma_T(y_\alpha),\sigma_T(y_\beta)}(\omega)}{E_p^2} \tag{4.52}$$

4.3.3 Numerical Results

As indicated in Sect. 4.2, the spatial variation of ground motion has a significant effect on the joints of a pipeline. This section evaluates the displacements, stresses and strains induced in long, continuous pipelines subjected to earthquake ground motions.

The following properties and dimensions are used in a specific numerical analysis to demonstrate the effects of spatial variation of ground motions on a continuous pipeline.

Modulus of elasticity: $E_p = 2.07 \times 10^{10} \frac{N}{m^2}$ $(3 \times 10^6$ psi)

Density of pipe: $\rho_p = 2.2 \times 10^3 \frac{kg}{m^3}$ $(1.37 \times 10^2$ lb/ft$^3)$

Radius of pipe: $R = 1$ m (3.3 ft)

Thickness of pipe: $t = 0.15\ R$ (4.53)

According to Novak and Hindy (1977) and Hindy and Novak (1980) the damping of the soil can be very high; accordingly, the damping coefficient for the first mode is assumed to be

$$\zeta_1 = 0.80 \tag{4.54}$$

The damping coefficients of the higher modes are given by Eq. 4.33, for either axial or transverse motion.

The stiffness of the soil is given by

$$\frac{E_p}{K_A} = \frac{E_p}{K_T} = 2.63 \times 10^5 \qquad (4.55)$$

The different pipeline configurations examined in the analysis are relatively long; they were considered, however, for determining the effect of loss of correlation as the length increases.

The pipeline was examined for input motions along and normal to the axial direction. Two different cases of input motion were examined each time, namely perfectly and partially correlated motions. The pipeline axis is considered to coincide with the epicentral direction, namely the direction from Station 006 to Station 012 (Fig. 3.1).

The integrals in Eqs. 4.37, 4.38, 4.50 and 4.51, require the continuous distribution of the cross spectral densities of the input motions; however, the results of the analysis in Chapter 3 provide information at discrete points only, namely the stations along the diameter from 006 to 012 (Fig. 3.1). Linear interpolation between stations is used to obtain the motions at intermediate stations.

The number of modes required to evaluate the response of the pipelines -- i.e., beyond which an additional mode would not contribute significantly to the response -- depended highly on the slenderness of the pipe and the direction of the excitation. The dominant modes were determined by increasing their number by one each time, until no further increase in the displacements or stresses was observed. The transverse direction required a higher number of modes, as was also indicated by Hindy and Novak (1980). The displacements in both directions were dominated by the corresponding first modes, whereas the evaluation of the stresses required a higher number of modes.

For the double integrations of Eqs. 4.37, 4.38, 4.50 and 4.51, Gaussian integration was used. Since the number of modes used in the analysis varied with the slenderness of the pipe and the direction of the excitation, the number of integration points varied as well; their number

was such that at least two or three integration points lay between the zeros of the mode shapes.

Effect of Differential Motion -- Tables 4.5 through 4.9 summarize the results of the pipeline examination; in particular, Tables 4.5 through 4.7 show the maximum axial displacements, stresses and strains at various points along the pipeline axis for lengths of 200, 400, and 800 m, respectively, whereas Tables 4.8 and 4.9 present the maximum displacements, bending stresses and strains in the transverse direction for lengths of 200 and 400 m.

Tables 4.5 through 4.9 indicate that the displacements obtained from the fully and partially correlated input motions are approximately the same. This is due to the fact that the dominant mode for either input is the first mode, which is a rigid body mode. This mode, however, is the only one excited when fully correlated support motion is examined, and yields zero stress and strain distribution along the pipeline. On the other hand, the response corresponding to the partially correlated motion consists of the first rigid body mode and higher modes, which may seem insignificant as far as displacements are concerned, but are very important in the stress and strain distributions.

In the analysis of long lifelines, it is controversial whether the axial or the transverse response is dominant. For example, Hindy and Novak (1980) concluded that the axial response is more dominant; this, however, is based on the assumption that the input motions in the axial and transverse directions are equal. Comparison of the results in Tables 4.5 and 4.8, which correspond to a pipeline of length 200 m, indicates that the response in the transverse direction is more significant. This result agrees with the conclusions of Sakuari and Takahashi (1969) that if the diameters of pipelines are large, the bending stresses become as important as the axial stresses. Comparison of Tables 4.6 and 4.9 shows that the axial stresses at the midspan of the pipeline are higher than the corresponding bending stresses. Tables 4.8 and 4.9, indicate that the bending stresses do not vary with length, whereas from Tables 4.5 and 4.6 a significant increase in the axial stress may be observed for longer pipelines. A pipeline of ℓ = 800 m was examined; although such a length is

not realistic, the result is used to confirm a further increase in the axial stress (Table 4.7). At the two ends of the pipeline the bending stresses dominate and the axial stresses vanish, due to the boundary conditions assumed in the analysis.

In the analysis, the radius of the pipeline was held constant, while its length was increased. The stresses in the pipeline depend on the slenderness of the pipe, namely the ratio of the length to the radius; as the slenderness of the pipe increases, the dominance of the axial stress also increases.

Loh, Ang, and Wen (1983) examined a continuous pipeline subjected to axial excitation. The axial strain in the pipe was assumed to be proportional to the ground strain (Shinozuka, Takada, and Kawakami, 1977), which was evaluated from the earthquake data recorded at the SMART-1 array. They indicated that the order of magnitude of the axial strains is approximately 10^{-5}, which is in reasonable agreement with the results of the present analysis (Tables 4.5 through 4.7). Furthermore, the deformation of the pipeline follows the ground deformation, as indicated also by Sakurai and Takahashi (1969).

Table 4.1 Differential Axial Motion Between Pipe Segments (ζ = 5%)

		By Stochastic Analysis		By Interference Response Spectrum
Frequency [Hz]	ℓ [km]	μ_{x_m} [cm]	σ_{x_m} [cm]	Δ_{max} [cm]
0.5	0.2	0.761	0.262	0.80
	0.8	1.852	0.559	2.50
	1.0	2.377	0.724	3.50
	1.8	3.980	1.207	3.50
1.0	0.2	0.970	0.240	0.75
	0.8	2.896	0.667	2.50
	1.0	3.545	0.820	3.50
	1.8	5.086	1.181	2.60
2.0	0.2	0.944	0.193	0.50
	0.8	2.494	0.474	1.00
	1.0	2.778	0.535	0.75
	1.8	2.391	0.504	0.85
3.0	0.2	0.701	0.153	0.30
	0.8	1.342	0.259	0.45
	1.0	1.575	0.317	0.60
	1.8	1.776	0.403	0.45

Table 4.2 Maximum Relative Displacements (in cm) Between Pipe Segments Under Axial Excitation

	Half-Space Model		Approximate Differential Power Spectral Density	
ℓ [m]	μ_{x_m}	σ_{x_m}	μ_{x_m}	σ_{x_m}
20	0.106	0.019	0.109	0.028
50	0.147	0.039	0.172	0.045
100	0.217	0.059	0.244	0.063
200	0.329	0.092	0.412	0.113
400	0.424	0.101	0.853	0.234

Table 4.3 Maximum Relative Displacements (in cm) Between Pipe Segments Under Transverse Excitation

	Half-Space Model		Approximate Differential Power Spectral Density	
ℓ [m]	μ_{x_m}	σ_{x_m}	μ_{x_m}	σ_{x_m}
20	0.102	0.024	0.148	0.036
50	0.161	0.038	0.234	0.057
100	0.229	0.054	0.331	0.081
200	0.325	0.077	0.450	0.111
400	0.613	0.147	0.772	0.189

Table 4.4 Maximum Relative Displacements (in cm) Between Pipe Segments Under Vertical Excitation

	Half-Space Model		Approximate Differential Power Spectral Density	
ℓ [m]	μ_{x_m}	σ_{x_m}	μ_{x_m}	σ_{x_m}
20	0.043	0.009	0.062	0.014
50	0.067	0.014	0.099	0.022
100	0.096	0.020	0.140	0.031
200	0.135	0.028	0.201	0.044
400	0.248	0.051	0.289	0.064

Table 4.5 Axial Displacement, Stress and Strain for a Continuous Pipeline (Length ℓ = 200 m)

	Partially Correlated Motion					Fully Correlated Motion
	0	$\ell/4$	$\ell/2$	$3\ell/4$	ℓ	$0 \leq y \leq \ell$
$\mu_{u_{max}}$ (cm)	1.401	1.401	1.401	1.401	1.401	1.409
$\sigma_{u_{max}}$ (cm)	0.395	0.395	0.396	0.396	0.396	0.397
$\mu_{\sigma_{max}}$ (N/m^2)	0.0	1.352×10^4	1.810×10^4	1.354×10^4	0.0	0.0
$\sigma_{\sigma_{max}}$ (N/m^2)	0.0	2.522×10^3	3.368×10^3	2.528×10^3	0.0	0.0
$\mu_{\varepsilon_{max}}$	0.0	6.529×10^{-7}	8.745×10^{-7}	6.539×10^{-7}	0.0	0.0
$\sigma_{\varepsilon_{max}}$	0.0	1.218×10^{-7}	1.627×10^{-7}	1.221×10^{-7}	0.0	0.0

Table 4.6 Axial Displacement, Stress and Strain for a Continuous Pipeline (Length ℓ = 400 m)

	Partially Correlated Motion					Fully Correlated Motion
	0	$\ell/4$	$\ell/2$	$3\ell/4$	ℓ	$0 \leq y \leq \ell$
$\mu_{u_{max}}$ (cm)	1.377	1.382	1.381	1.381	1.381	1.369
$\sigma_{u_{max}}$ (cm)	0.388	0.390	0.390	0.390	0.389	0.380
$\mu_{\sigma_{max}}$ (N/m^2)	0.0	4.689×10^4	6.174×10^4	4.808×10^4	0.0	0.0
$\sigma_{\sigma_{max}}$ (N/m^2)	0.0	8.629×10^3	1.140×10^4	8.913×10^3	0.0	0.0
$\mu_{\varepsilon_{max}}$	0.0	2.265×10^{-6}	2.983×10^{-6}	2.323×10^{-6}	0.0	0.0
$\sigma_{\varepsilon_{max}}$	0.0	4.168×10^{-7}	5.509×10^{-7}	4.306×10^{-7}	0.0	0.0

Table 4.7 Axial Displacement, Stress and Strain for a Continuous Pipeline (Length ℓ = 800 m)

	Partially Correlated Motion					Fully Correlated Motion
	0	$\ell/4$	$\ell/2$	$3\ell/4$	ℓ	$0 \leq y \leq \ell$
$\mu_{u_{max}}$ (cm)	1.364	1.343	1.318	1.330	1.347	1.360
$\sigma_{u_{max}}$ (cm)	0.376	0.376	0.375	0.372	0.370	0.379
$\mu_{\sigma_{max}}$ (N/m^2)	0.0	1.463×10^5	1.955×10^5	1.446×10^5	0.0	0.0
$\sigma_{\sigma_{max}}$ (N/m^2)	0.0	2.846×10^4	3.822×10^4	2.808×10^4	0.0	0.0
$\mu_{\varepsilon_{max}}$	0.0	7.067×10^{-6}	9.443×10^{-6}	6.985×10^{-6}	0.0	0.0
$\sigma_{\varepsilon_{max}}$	0.0	1.375×10^{-6}	1.846×10^{-6}	1.357×10^{-6}	0.0	0.0

Table 4.8 Transverse Displacement, Bending Stress and Strain for a Continuous Pipeline (Length ℓ = 200 m)

	Partially Correlated Motion					Fully Correlated Motion
	0	$\ell/4$	$\ell/2$	$3\ell/4$	ℓ	$0 \leq y \leq \ell$
$\mu_{u_{max}}$ (cm)	2.501	2.492	2.483	2.474	2.471	2.485
$\sigma_{u_{max}}$ (cm)	1.053	1.049	1.042	1.035	1.030	1.402
$\mu_{\sigma_{max}}$ (N/m^2)	6.360×10^4	4.389×10^4	4.385×10^4	4.383×10^4	6.314×10^4	0.0
$\sigma_{\sigma_{max}}$ (N/m^2)	1.305×10^4	9.153×10^3	9.166×10^3	9.178×10^3	1.306×10^4	0.0
$\mu_{\varepsilon_{max}}$	3.072×10^{-6}	2.120×10^{-6}	2.118×10^{-6}	2.117×10^{-6}	3.050×10^{-6}	0.0
$\sigma_{\varepsilon_{max}}$	6.306×10^{-7}	4.421×10^{-7}	4.428×10^{-7}	4.434×10^{-7}	6.309×10^{-7}	0.0

Table 4.9 Transverse Displacement, Bending Stress and Strain for a Continuous Pipeline (Length ℓ = 400 m)

	Partially Correlated Motion					Fully Correlated Motion
	0	$\ell/4$	$\ell/2$	$3\ell/4$	ℓ	$0 \leq y \leq \ell$
$\mu_{u_{max}}$ (cm)	2.499	2.483	2.468	2.488	2.521	2.508
$\sigma_{u_{max}}$ (cm)	1.054	1.042	1.030	1.030	1.038	1.403
$\mu_{\sigma_{max}}$ (N/m^2)	6.333×10^4	4.437×10^4	4.614×10^4	4.647×10^4	6.769×10^4	0.0
$\sigma_{\sigma_{max}}$ (N/m^2)	1.297×10^4	9.288×10^3	9.364×10^3	9.671×10^3	1.380×10^4	0.0
$\mu_{\varepsilon_{max}}$	3.059×10^{-6}	2.143×10^{-6}	2.229×10^{-6}	2.245×10^{-6}	3.270×10^{-6}	0.0
$\sigma_{\varepsilon_{max}}$	6.265×10^{-7}	4.487×10^{-7}	4.524×10^{-7}	4.672×10^{-7}	6.666×10^{-7}	0.0

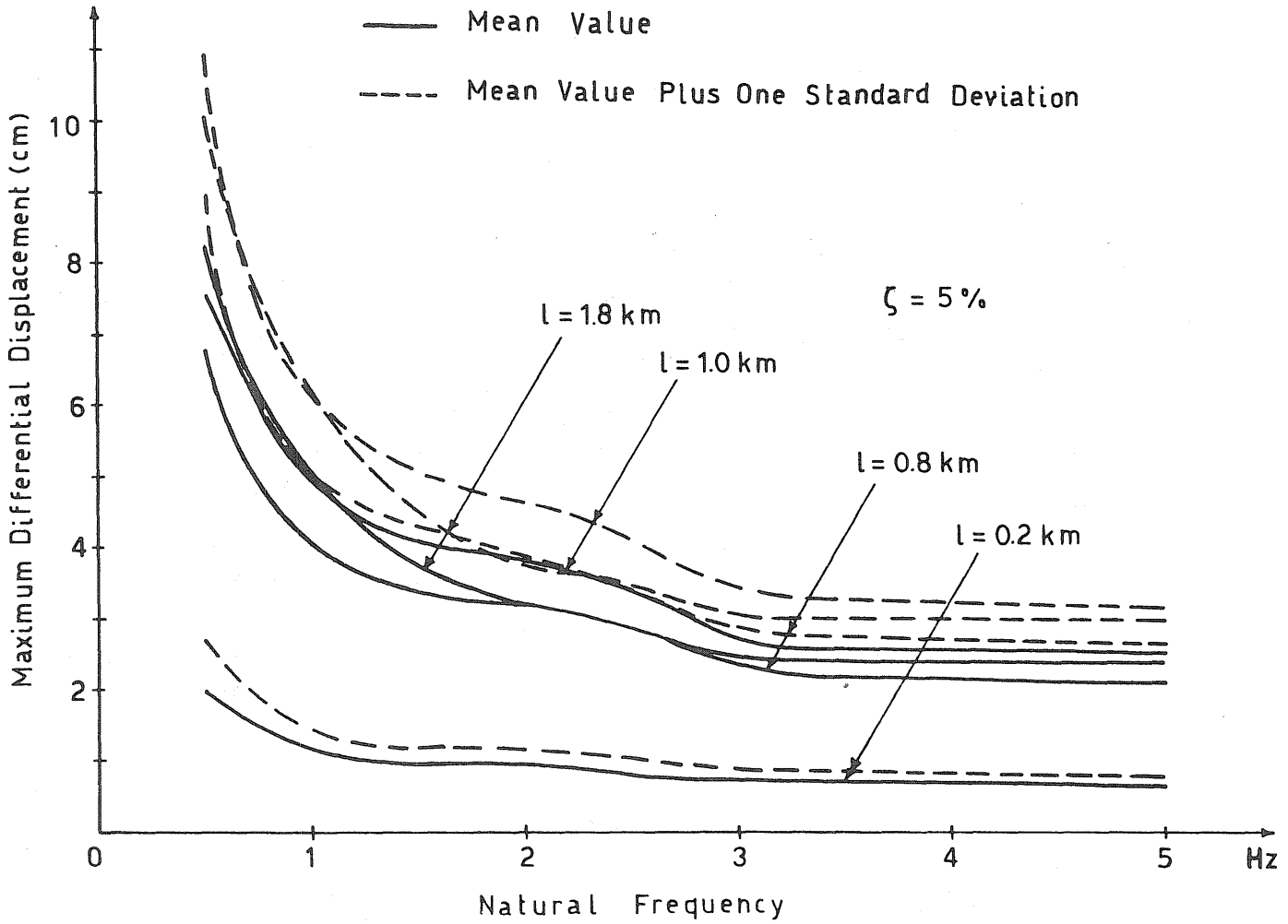

Figure 4.4 Differential Displacement Response Spectrum by Approximate Power Spectral Density

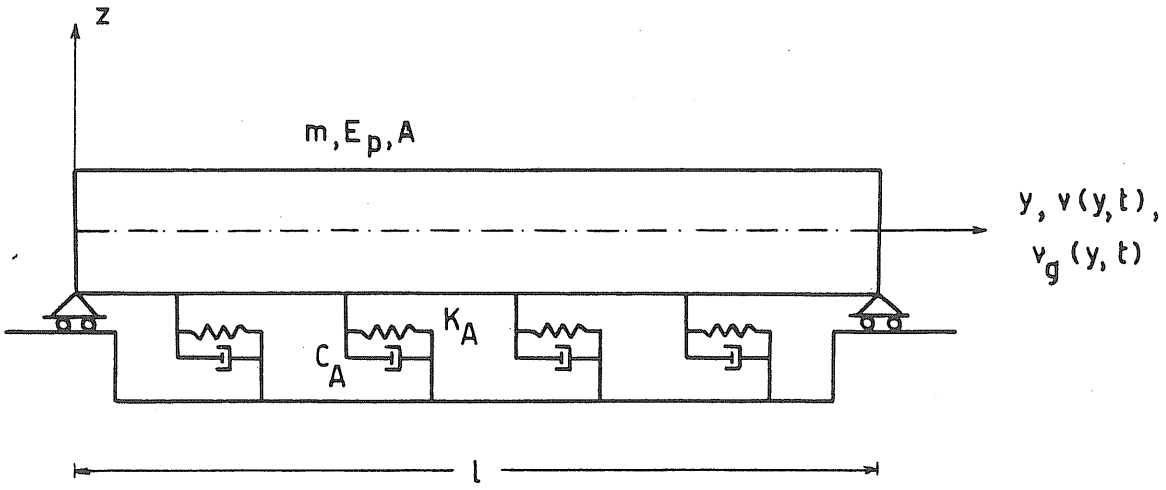

Figure 4.5 Structural Model for Continuous Pipelines -- Axial Motion

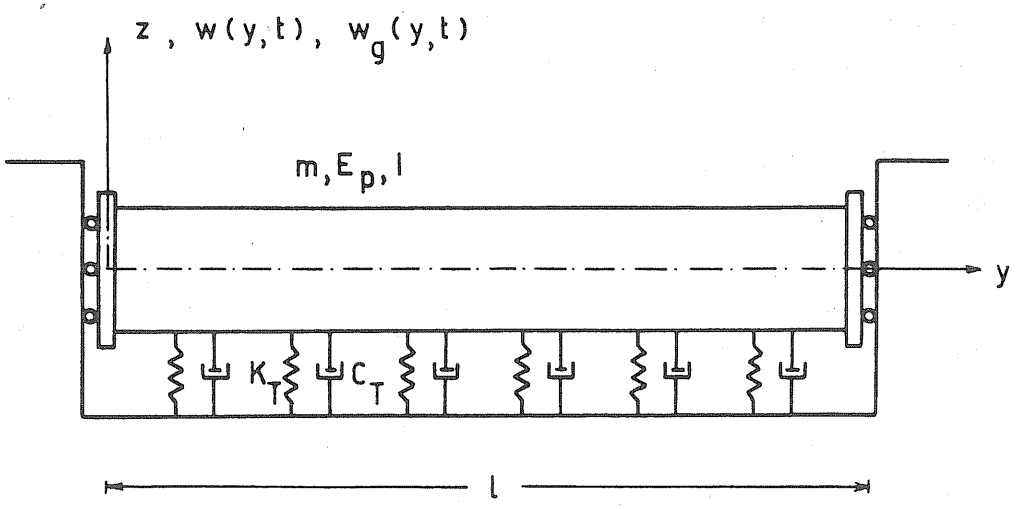

Figure 4.6 Structural Model for Continuous Pipelines -- Transverse Motion

CHAPTER 5

APPLICATIONS TO LONG BEAMS

5.1 Introduction

During many major earthquakes, bridges have been reported to be damaged excessively (Iwasaki, Penzien, and Clough, 1972). The effects of spatially varying ground excitations are of major importance to the seismic performance and safety of bridges (Hall and Newmark, 1979). Bogdanoff, Goldberg, and Schiff (1965) indicated that the differential ground motion should not be ignored when considering the response and safety of long structures; Johnson and Galletly (1972) compared the response of a highway bridge to uniform and moving ground excitation by means of a three-dimensional mathematical model and concluded that the moving ground excitation should be considered in the seismic design of bridges on multiple supports. Masri (1976) described the exact solution for the transient response of viscously damped Bernoulli-Euler beams with arbitrary boundary conditions subjected to propagating boundary excitations, and showed that for certain combinations of the system parameters and support motion the beam response to propagating support motions can be significantly higher than when subjected to uniform (non-propagating) support motions.

Simple single-span, simply-supported beams are examined in this chapter. The structures are subjected to excitations in the axial, lateral and vertical directions. The lateral direction is examined using two models -- in one case the structure is considered to behave as a shear-beam

model; the other case considers a Bernoulli-Euler beam. In the vertical direction, the structure is modeled as a Bernoulli-Euler beam.

A shear-beam model assumes that the shear force is proportional to the slope of the deformation at each point (Newmark and Rosenblueth, 1971), whereas the Bernoulli-Euler beam model includes the effect of moments in the equation of motion. Since the vertical direction is the direction of gravity loads, the contribution of moments ought to be included in the analysis, whereas for the lateral direction the simplification associated with the shear-beam model may be appropriate. The lateral direction was examined with the two different beam models, in order to evaluate a comparison of the responses of the two systems.

Again, two different types of excitations are examined; in one case, the motion at the two supports is assumed to be perfectly correlated, and in the second case the motion is considered to be partially correlated using the results of Chapters 2 and 3. The effects of soil-structure interaction are neglected; the supports are considered to follow the ground motion without affecting the seismic excitation.

5.2 Axial Motion of Beams

The model used to evaluate the axial response of a single-span beam is shown in Fig. 5.1. The input ground motions at the two supports are denoted by $f_1(t)$ and $f_2(t)$. If $u(y,t)$ denotes the total displacement along the axis of the beam, $u_s(y,t)$ the quasi-static displacement, and $u_D(y,t)$ the dynamic displacement, and if strain velocity (internal) damping is assumed, the equation of motion becomes

$$\rho \frac{\partial^2 u_D(y,t)}{\partial t^2} - E \frac{\partial^2 u_D(y,t)}{\partial y^2} - C_s \frac{\partial^3 u_D(y,t)}{\partial t \, \partial y^2}$$

$$= - \rho \left[\left(1 - \frac{y}{\ell}\right) \ddot{f}_1(t) + \frac{y}{\ell} \ddot{f}_2(t) \right] \qquad (5.1)$$

where:

ρ = the mass density;

E = the elastic modulus;

C_s = damping; and

y = the coordinate along the beam axis.

Letting $C_s = f_1(t) = f_2(t) = 0$ and making use of the boundary conditions $u_D(0,t) = u_D(\ell,t) = 0$ the natural frequencies and mode shapes of the structure become, respectively,

$$\omega_j = \frac{j\pi}{\ell}\sqrt{\frac{E}{\rho}} \quad ; \quad \omega_j = j\,\omega_1$$

$$\phi_j(y) = \sin\frac{j\pi y}{\ell} \tag{5.2}$$

The total response then becomes (Mindlin and Goodman, 1950),

$$u(y,t) = u_s(y,t) + u_D(y,t) \tag{5.3}$$

in which,

$$u_s(y,t) = (1 - \frac{y}{\ell})\, f_1(t) + \frac{y}{\ell}\, f_2(t) \quad ; \tag{5.4}$$

and,

$$u_D(y,t) = \sum_{i=1}^{N} \phi_i(y)\, q_i(t) \tag{5.5}$$

where:

$q_i(t)$ = the generalized coordinate;

$\phi_i(y)$ = the mode shape; and

N = the number of modes used in the analysis.

By substituting Eq. 5.5 into Eq. 5.1, multiplying both sides by $\phi_j(y)$ and by using the orthogonality conditions, the equations of motion for the generalized coordinates become,

$$\ddot{q}_j(t) + \frac{C_s}{E}\omega_j^2\,\dot{q}_j(t) + \omega_j^2\,q_j(t) = \frac{-2}{j\pi}\left[\ddot{f}_1(t) - \cos j\pi\,\ddot{f}_2(t)\right] \tag{5.6}$$

With the assumption that

$$\frac{C_s}{E}\omega_j^2 = 2\zeta_j\omega_j \quad ; \quad \zeta_j = \frac{\zeta_1}{\omega_1}\omega_j \tag{5.7}$$

in which ζ_j is the damping coefficient, the equations of motion become

$$\ddot{q}_j(t) + 2\zeta_j\omega_j\,\dot{q}_j(t) + \omega_j^2\,q_j(t) = \frac{-2}{j\pi}\left[\ddot{f}_1(t) - \cos j\pi\,\ddot{f}_2(t)\right] \tag{5.8}$$

The generalized coordinates $q_j(t)$ may then be evaluated by means of the convolution integral; namely,

$$q_j(t) = \frac{-2}{j\pi}\int_0^t h_j(t-\tau)\left[\ddot{f}_1(\tau) - \cos j\pi\,\ddot{f}_2(\tau)\right]d\tau \tag{5.9}$$

where,

$$h_j(t) = \frac{1}{\omega_j\sqrt{1-\zeta_j^2}}\,e^{-\zeta_j\omega_j t}\sin\omega_j\sqrt{1-\zeta_j^2}\,t$$

is the impulse response function. Equations 5.3, 5.4, 5.5 and 5.9 define the axial response of the beam.

The cross spectral density functions of the quasi-static and dynamic displacements at points y_α and y_β along the axis of the beam are as follows (Appendix C):

$$S_{u_s(y_\alpha),u_s(y_\beta)}(\omega) = \frac{1}{\omega^4}\{(1 - \frac{y_\alpha}{\ell})(1 - \frac{y_\beta}{\ell})\, S_{\ddot{f}_1\ddot{f}_1}(\omega)$$

$$+ (1 - \frac{y_\alpha}{\ell})\,\frac{y_\beta}{\ell}\, S_{\ddot{f}_1\ddot{f}_2}(\omega) + \frac{y_\alpha}{\ell}(1 - \frac{y_\beta}{\ell})\, S_{\ddot{f}_2\ddot{f}_1}(\omega)$$

$$+ \frac{y_\alpha}{\ell}\,\frac{y_\beta}{\ell}\, S_{\ddot{f}_2\ddot{f}_2}(\omega)\} \qquad (5.10)$$

$$S_{u_s(y_\alpha),u_D(y_\beta)}(\omega) = \frac{1}{\omega^2}\sum_{k=1}^{N}\frac{2}{k\pi}\cdot\sin\frac{k\pi y_\beta}{\ell}\, H_k(\omega)$$

$$\cdot\{(1 - \frac{y_\alpha}{\ell})\,[S_{\ddot{f}_1\ddot{f}_1}(\omega) - \cos k\pi\, S_{\ddot{f}_1\ddot{f}_2}(\omega)]$$

$$+ \frac{y_\alpha}{\ell}\,[S_{\ddot{f}_2\ddot{f}_1}(\omega) - \cos k\pi\, S_{\ddot{f}_2\ddot{f}_2}(\omega)]\} \qquad (5.11)$$

$$S_{u_D(y_\alpha),u_s(y_\beta)}(\omega) = \frac{1}{\omega^2}\sum_{j=1}^{N}\frac{2}{j\pi}\sin\frac{j\pi y_\alpha}{\ell}\, H_j^*(\omega)$$

$$\cdot\{(1 - \frac{y_\beta}{\ell})\,[S_{\ddot{f}_1\ddot{f}_1}(\omega) - \cos j\pi\, S_{\ddot{f}_2\ddot{f}_1}(\omega)]$$

$$+ \frac{y_\beta}{\ell}\,[S_{\ddot{f}_1\ddot{f}_2}(\omega) - \cos j\pi\, S_{\ddot{f}_2\ddot{f}_2}(\omega)]\} \qquad (5.12)$$

and,

$$S_{u_D(y_\alpha),u_D(y_\beta)}(\omega) = \sum_{j=1}^{N}\sum_{k=1}^{N} \frac{4}{jk\pi^2} \sin\frac{j\pi y_\alpha}{\ell} \sin\frac{k\pi y_\beta}{\ell}$$

$$\cdot H_j^*(\omega)\, H_k(\omega) \left[S_{\ddot{f}_1\ddot{f}_1}(\omega) - \cos k\pi\, S_{\ddot{f}_1\ddot{f}_2}(\omega)\right.$$

$$\left. - \cos j\pi\, S_{\ddot{f}_2\ddot{f}_1}(\omega) + \cos j\pi \cos k\pi\, S_{\ddot{f}_2\ddot{f}_2}(\omega)\right] \qquad (5.13)$$

where:

$S_{\ddot{f}_m\ddot{f}_n}(\omega)$ = the cross spectral density of accelerations at supports m and n (m, n = 1 or 2); and

$H_j(\omega)$, $H_k(\omega)$ = the frequency transfer functions for the j^{th} and k^{th} modes, respectively.

The cross spectral density of the axial displacements at two points along the axis of the beam becomes

$$S_{u(y_\alpha),u(y_\beta)}(\omega) = S_{u_s(y_\alpha),u_s(y_\beta)}(\omega) + S_{u_s(y_\alpha),u_D(y_\beta)}(\omega)$$

$$+ S_{u_D(y_\alpha),u_s(y_\beta)}(\omega) + S_{u_D(y_\alpha),u_D(y_\beta)}(\omega) \qquad (5.14)$$

where the four terms on the right-hand side are given by Eqs. 5.10 through 5.13.

An important additional consideration in the evaluation of the response of beams is the axial force at the end supports. The axial force is proportional to the first derivative of the displacement time history; therefore, u'(y,t) -- the derivative of the displacement with respect to the axial coordinate -- is a measure of the axial force. The cross spectral densities of u'(y,t) are found to be,

$$S_{u'(y_\alpha),u'(y_\beta)}(\omega) = \frac{1}{\ell^2}\left\{\frac{1}{\omega^4}\left(S_{\ddot{f}_1\ddot{f}_1}(\omega) - S_{\ddot{f}_1\ddot{f}_2}(\omega) - S_{\ddot{f}_2\ddot{f}_1}(\omega) + S_{\ddot{f}_2\ddot{f}_2}(\omega)\right)\right.$$

$$+ \frac{2}{\omega^2}\sum_{j=1}^{N}\cos\frac{j\pi y_\alpha}{\ell}H_j^*(\omega)\left(-S_{\ddot{f}_1\ddot{f}_1}(\omega) + \cos j\pi\, S_{\ddot{f}_2\ddot{f}_1}(\omega)\right.$$

$$\left. + S_{\ddot{f}_1\ddot{f}_2}(\omega) - \cos j\pi\, S_{\ddot{f}_2\ddot{f}_2}(\omega)\right)$$

$$+ \frac{2}{\omega^2}\sum_{k=1}^{N}\cos\frac{k\pi y_\beta}{\ell}H_k(\omega)\left(-S_{\ddot{f}_1\ddot{f}_1}(\omega) + \cos k\pi\, S_{\ddot{f}_1\ddot{f}_2}(\omega)\right.$$

$$\left. + S_{\ddot{f}_2\ddot{f}_1}(\omega) - \cos k\pi\, S_{\ddot{f}_2\ddot{f}_2}(\omega)\right)$$

$$+ 4\sum_{j=1}^{N}\sum_{k=1}^{N}\cos\frac{j\pi y_\alpha}{\ell}\cos\frac{k\pi y_\beta}{\ell}H_j^*(\omega)\,H_k(\omega)$$

$$\left(S_{\ddot{f}_1\ddot{f}_1}(\omega) - \cos k\pi\, S_{\ddot{f}_1\ddot{f}_2}(\omega) - \cos j\pi\, S_{\ddot{f}_2\ddot{f}_1}(\omega)\right.$$

$$\left.\left. + \cos j\pi\cos k\pi\, S_{\ddot{f}_2\ddot{f}_2}(\omega)\right)\right\} \qquad (5.15)$$

5.3 Transverse Motion of Beams

5.3.1 Shear-Beam Model

The shear-beam model used to describe the transverse motion of a single-span beam is shown in Fig. 5.2, where $w(y,t)$ denotes the total lateral displacement, $w_s(y,t)$ the quasi-static displacement, and $w_D(y,t)$ the dynamic displacement. In this case, $f_1(t)$ and $f_2(t)$ denote the input ground displacements at the two supports in the transverse direction. The equation of motion of the shear-beam is,

$$\rho \frac{\partial^2 w_D(y,t)}{\partial t^2} - k'G \frac{\partial^2 w_D(y,t)}{\partial y^2} - C_s \frac{\partial^3 w_D(y,t)}{\partial t\, \partial y^2}$$

$$= - \rho \left[(1 - \frac{y}{\ell}) \ddot{f}_1(t) + \frac{y}{\ell} \ddot{f}_2(t) \right] \tag{5.16}$$

where:

k' = a numerical factor depending on the shape of the cross section;

G = the shear modulus;

and strain rate damping is assumed.

A close examination of Eqs. 5.1 and 5.16 shows that the only difference between the equations for axial and transverse motions is the coefficient of the second derivative with respect to y. Therefore, the equations of Sect. 5.2 also hold for transverse motion with the modulus of elasticity E in Eqs. 5.2, 5.6 and 5.7 replaced by k'G.

Therefore, the cross spectral density function of the displacement in the transverse direction is given by,

$$S_{w(y_\alpha),w(y_\beta)}(\omega) = \frac{1}{\omega^4} \{ (1 - \frac{y_\alpha}{\ell})(1 - \frac{y_\beta}{\ell}) S_{\ddot{f}_1 \ddot{f}_1}(\omega) + (1 - \frac{y_\alpha}{\ell}) \frac{y_\beta}{\ell} S_{\ddot{f}_1 \ddot{f}_2}(\omega)$$

$$+ \frac{y_\alpha}{\ell} (1 - \frac{y_\beta}{\ell}) S_{\ddot{f}_2 \ddot{f}_1}(\omega) + \frac{y_\alpha}{\ell} \frac{y_\beta}{\ell} S_{\ddot{f}_2 \ddot{f}_2}(\omega) \}$$

$$+ \frac{1}{\omega^2} \sum_{k=1}^{N} \frac{2}{k\pi} \sin \frac{k\pi y_\beta}{\ell} H_k(\omega) \{ (1 - \frac{y_\alpha}{\ell}) [S_{\ddot{f}_1 \ddot{f}_1}(\omega)$$

$$- \cos k\pi\, S_{\ddot{f}_1 \ddot{f}_2}(\omega)] + \frac{y_\alpha}{\ell} [S_{\ddot{f}_2 \ddot{f}_1}(\omega) - \cos k\pi\, S_{\ddot{f}_2 \ddot{f}_2}(\omega)] \}$$

$$+ \frac{1}{\omega^2} \sum_{j=1}^{N} \frac{2}{j\pi} \sin \frac{j\pi y_\alpha}{\ell} H_j^*(\omega) \{ (1 - \frac{y_\beta}{\ell}) [S_{\ddot{f}_1 \ddot{f}_1}(\omega)$$

If the damping, and the excitations $f_1(t)$ and $f_2(t)$ at the two supports are equal to zero, the natural frequencies and mode shapes of the beam can be found to be,

$$\omega_j = \left(\frac{j\pi}{\ell}\right)^2 \sqrt{\frac{EI}{m}} \qquad ; \qquad \omega_j = j^2 \omega_1$$

$$\phi_j(y) = \sin \frac{j\pi y}{\ell} \tag{5.21}$$

The total response then becomes (Mindlin and Goodman, 1950),

$$w(y,t) = w_s(y,t) + w_D(y,t) \tag{5.22}$$

where:

$$w_s(y,t) = \left(1 - \frac{y}{\ell}\right) f_1(t) + \frac{y}{\ell} f_2(t) \quad ; \tag{5.23}$$

and,

$$w_D(y,t) = \sum_{i=1}^{N} \phi_i(y)\, q_i(t) \tag{5.24}$$

Under the assumption that:

$$\frac{C_s}{E} \omega_j^2 = 2\zeta_j \omega_j \qquad ; \qquad \zeta_j = \frac{\zeta_1}{\omega_1} \omega_j \tag{5.25}$$

the equations of motion for the generalized coordinates become,

$$\ddot{q}_j(t) + 2\zeta_j \omega_j \dot{q}_j(t) + \omega_j^2 q_j(t) = \frac{-2}{j\pi} \left[\ddot{f}_1(t) - \cos j\pi\, \ddot{f}_2(t)\right] \tag{5.26}$$

The generalized coordinates may then be evaluated by means of the convolution integral, namely;

$$q_j(t) = \frac{-2}{j\pi} \int_0^t h_j(t-\tau) \left[\ddot{f}_1(\tau) - \cos j\pi \, \ddot{f}_2(\tau)\right] d\tau \tag{5.27}$$

The cross spectral density function of the total displacement in the transverse direction obtained with the Bernoulli-Euler beam model is,

$$\begin{aligned}
S_{w(y_\alpha),w(y_\beta)}(\omega) = \frac{1}{\omega^4} \Big\{ & (1 - \tfrac{y_\alpha}{\ell})(1 - \tfrac{y_\beta}{\ell}) \, S_{\ddot{f}_1\ddot{f}_1}(\omega) + (1 - \tfrac{y_\alpha}{\ell}) \tfrac{y_\beta}{\ell} \, S_{\ddot{f}_1\ddot{f}_2}(\omega) \\
& + \tfrac{y_\alpha}{\ell} (1 - \tfrac{y_\beta}{\ell}) \, S_{\ddot{f}_2\ddot{f}_1}(\omega) + \tfrac{y_\alpha}{\ell} \tfrac{y_\beta}{\ell} \, S_{\ddot{f}_2\ddot{f}_2}(\omega) \Big\} \\
& + \frac{1}{\omega^2} \sum_{k=1}^{N} \frac{2}{k\pi} \sin \frac{k\pi y_\beta}{\ell} H_k(\omega) \Big\{ (1 - \tfrac{y_\alpha}{\ell}) \left[S_{\ddot{f}_1\ddot{f}_1}(\omega) \right. \\
& \left. - \cos k\pi \, S_{\ddot{f}_1\ddot{f}_2}(\omega) \right] + \tfrac{y_\alpha}{\ell} \left[S_{\ddot{f}_2\ddot{f}_1}(\omega) - \cos k\pi \, S_{\ddot{f}_2\ddot{f}_2}(\omega) \right] \Big\} \\
& + \frac{1}{\omega^2} \sum_{j=1}^{N} \frac{2}{j\pi} \sin \frac{j\pi y_\alpha}{\ell} H_j^*(\omega) \Big\{ (1 - \tfrac{y_\beta}{\ell}) \left[S_{\ddot{f}_1\ddot{f}_1}(\omega) \right. \\
& \left. - \cos j\pi \, S_{\ddot{f}_2\ddot{f}_1}(\omega) \right] + \tfrac{y_\beta}{\ell} \left[S_{\ddot{f}_1\ddot{f}_2}(\omega) - \cos j\pi \, S_{\ddot{f}_2\ddot{f}_2}(\omega) \right] \Big\} \\
& + \sum_{j=1}^{N} \sum_{k=1}^{N} \frac{4}{jk\pi^2} \sin \frac{j\pi y_\alpha}{\ell} \sin \frac{k\pi y_\beta}{\ell} H_j^*(\omega) \, H_k(\omega) \left[S_{\ddot{f}_1\ddot{f}_1}(\omega) \right. \\
& - \cos k\pi \, S_{\ddot{f}_1\ddot{f}_2}(\omega) - \cos j\pi \, S_{\ddot{f}_2\ddot{f}_1}(\omega) \\
& \left. + \cos j\pi \cos k\pi \, S_{\ddot{f}_2\ddot{f}_2}(\omega) \right]
\end{aligned} \tag{5.28}$$

For a Bernoulli-Euler beam a measure of the shear force is the third derivative of the displacement with respect to the axial coordinate. The cross spectral density of $w'''(y,t)$ is,

$$S_{w'''(y_\alpha),w'''(y_\beta)}(\omega) = \sum_{j=1}^{N} \sum_{k=1}^{N} \frac{4j^2k^2\pi^4}{\ell^6} \cos\frac{j\pi y_\alpha}{\ell} \cos\frac{k\pi y_\beta}{\ell}$$

$$\cdot H_j^*(\omega)\, H_k(\omega) \left[S_{\ddot{f}_1\ddot{f}_1}(\omega) - \cos k\pi\, S_{\ddot{f}_1\ddot{f}_2}(\omega)\right.$$

$$\left. - \cos j\pi\, S_{\ddot{f}_2\ddot{f}_1}(\omega) + \cos j\pi \cos k\pi\, S_{\ddot{f}_2\ddot{f}_2}(\omega)\right] \qquad (5.29)$$

The corresponding moment is proportional to the curvature $w''(y,t)$; the cross spectral density of $w''(y,t)$ is,

$$S_{w''(y_\alpha),w''(y_\beta)}(\omega) = \sum_{j=1}^{N} \sum_{k=1}^{N} \frac{4jk\pi^2}{\ell^4} \sin\frac{j\pi y_\alpha}{\ell} \sin\frac{k\pi y_\beta}{\ell}$$

$$\cdot H_j^*(\omega)\, H_k(\omega) \left[S_{\ddot{f}_1\ddot{f}_1}(\omega) - \cos k\pi\, S_{\ddot{f}_1\ddot{f}_2}(\omega)\right.$$

$$\left. - \cos j\pi\, S_{\ddot{f}_2\ddot{f}_1}(\omega) + \cos j\pi \cos k\pi\, S_{\ddot{f}_2\ddot{f}_2}(\omega)\right] \qquad (5.30)$$

5.4 Effect of Differential Motion

The spatial variation of ground motions plays a significant role in the seismic safety evaluation of long structures on multiple supports. This study compares the displacements and forces induced in long structures, idealized as simply-supported beams, subjected to fully and partially correlated seismic motions applied at the supports.

In particular, four different span lengths are examined, namely 20, 50, 100, and 200 m. Although spans of 100 m and 200 m are not realistic

for simply-supported beams, they are considered in the analysis to evaluate the effect of further loss of correlation as the span length increases. The values of the input motions for beams of length $\ell \leq 100$ m are obtained through linear interpolation of the spectral densities between the stations of the array. The fundamental natural frequencies for the beams of $\ell \leq 50$ m are 0.80, 0.48, and 0.24 Hz for axial, lateral and vertical motions, respectively, whereas the corresponding fundamental natural frequencies of the longer beams are 0.27, 0.16, and 0.08 Hz for axial, lateral and vertical motions. The damping coefficient of the first mode is 10% of critical (Abdel-Ghaffar, 1977). The natural frequencies and damping coefficients of the higher modes can be obtained from Eqs. 5.2, 5.7, 5.21 and 5.25.

The number of modes required, i.e., beyond which additional modes would not contribute significantly to the response, is nine for the axial direction, nine for the lateral direction when the shear-beam model is used, and three for the Bernoulli-Euler beam in both the lateral and vertical directions.

The response in the transverse direction, when examined by the two different beam models, namely the shear-beam and Bernoulli-Euler beam, is shown in Table 5.1. The results show a comparison of the root mean square (rms) absolute displacement, σ_w, and rms velocity, $\sigma_{\dot{w}}$, in the transverse direction for partially correlated motion obtained with the two models; the two models appear to give approximately the same response.

Tables 5.2 through 5.4 show the mean maximum dynamic displacements at $\ell/4$, $\ell/2$ and $3\ell/4$ of the beam (Longuet-Higgins, 1952; Davenport, 1964). The results at the midspan of the beam indicate that the response corresponding to the fully correlated support motion is slightly higher than that of the partially correlated support motion. At the midspan of the beam, the total response consists of symmetric modes only, see e.g., Eq. 5.13. However, as can be seen from the same equation, the contribution of the input spectra for every mode is higher for the fully correlated motion than for the partially correlated motion. The response at $3\ell/4$ is in general slightly higher for the partially correlated motion than for the fully correlated motion. This may be attributed to the fact, that for the

fully correlated motion, only the symmetric modes are excited, whereas the partially correlated motion excites all modes.

Table 5.5 shows the effect of correlation (between partial and full correlation) for axial forces (Eq. 5.15) and Table 5.6 for the shear forces (Eq. 5.18) obtained with the shear-beam model. Tables 5.7 and 5.9 show similar results for the mean maximum moments (Eq. 5.30), and Tables 5.8 and 5.10 for the mean maximum shear forces (Eq. 5.29) at the two supports for the transverse and vertical directions obtained with the Bernoulli-Euler beam. Since the fully correlated motion excites the symmetric modes only, the forces and moments are symmetric with respect to the midspan of the beam. The values of the mean maximum axial and shear forces at the supports associated with the fully correlated input motions lie between the corresponding values of the forces associated with the partially correlated input motions (Tables 5.5, 5.6, 5.8, and 5.10). This may also be attributed to the effect of the antisymmetric modes, which are excited only when partially correlated motion is applied. As far as moments are concerned (Tables 5.7 and 5.9), the curvature at $\ell/4$ or $3\ell/4$ is higher for partially correlated motions than for fully correlated motions. The curvature at the midspan, however, is always higher for the fully correlated input motion.

The responses associated with fully and partially correlated input motions indicate only slight differences. This agrees with the results of Masri (1976), who evaluated the curvature response spectrum for a simply-supported beam for uniform and propagating boundary conditions (Fig. 5.3). In Fig. 5.3, T_a indicates the delay in the arrival time of the wave train from one support to the other, T_1 is the fundamental period of the beam, and S_o is the maximum amplitude of the wave train. In this analysis, the fundamental period of the beams ranges between 2 sec to 12.5 sec for transverse or vertical motions, whereas the ground may allow small delay times for the arrival of the wave train at the other support. Masri (1976) indicated that for $T_a/T_1 > 0.125$, all locations along the length of the beam have reduced curvatures, whereas for $T_a/T_1 < 0.125$ (Fig. 5.3) the curvature at $\ell/4$ and $3\ell/4$ is slightly higher for the propagating support motion (equivalent to partially correlated motion). This agrees with the

results presented in Tables 5.7 and 5.9, since the values of T_a/T_1 in this analysis fall in the range $T_a/T_1 < 0.125$. Furthermore, as can be seen from Fig. 5.3, the curvature at the midspan of the beam is always higher for the equal support motion; this is also observed in the results of Tables 5.7 and 5.9.

Table 5.1 Transverse RMS Displacement and Velocity at Midspan of Beam (in cm) -- Partially Correlated Motion

Length [m]	Shear Beam Model		Bernoulli-Euler Beam Model	
	σ_w	$\sigma_{\dot{w}}$	σ_w	$\sigma_{\dot{w}}$
20	2.690	5.188	2.691	5.146
50	2.682	5.162	2.683	5.119
100	3.821	3.368	3.821	3.376
200	3.801	3.349	3.802	3.356

Table 5.2 Axial Dynamic Displacements (in cm)

Length [m]	Correlation	Point	μ_{u_m}	σ_{u_m}
20	Partial	$\ell/4$ $\ell/2$ $3\ell/4$	1.861 2.675 1.883	0.449 0.641 0.453
	Full	$\ell/4$ $\ell/2$ $3\ell/4$	1.873 2.678 1.873	0.451 0.641 0.451
50	Partial	$\ell/4$ $\ell/2$ $3\ell/4$	1.852 2.670 1.886	0.448 0.640 0.453
	Full	$\ell/4$ $\ell/2$ $3\ell/4$	1.872 2.677 1.872	0.451 0.641 0.451
100	Partial	$\ell/4$ $\ell/2$ $3\ell/4$	2.314 3.149 2.338	0.739 1.106 0.748
	Full	$\ell/4$ $\ell/2$ $3\ell/4$	2.329 3.155 2.329	0.743 1.107 0.743
200	Partial	$\ell/4$ $\ell/2$ $3\ell/4$	2.332 3.181 2.366	0.749 1.124 0.762
	Full	$\ell/4$ $\ell/2$ $3\ell/4$	2.355 3.190 2.355	0.755 1.124 0.755

Table 5.3 Transverse Dynamic Displacements (in cm)

Length [m]	Correlation	Point	μ_{w_m}	σ_{w_m}
20	Partial	$\ell/4$	2.549	0.797
		$\ell/2$	3.671	1.147
		$3\ell/4$	2.585	0.804
	Full	$\ell/4$	2.570	0.801
		$\ell/2$	3.676	1.148
		$3\ell/4$	2.570	0.801
50	Partial	$\ell/4$	2.525	0.791
		$\ell/2$	3.652	1.141
		$3\ell/4$	2.582	0.802
	Full	$\ell/4$	2.560	0.798
		$\ell/2$	3.663	1.144
		$3\ell/4$	2.560	0.798
100	Partial	$\ell/4$	4.153	2.186
		$\ell/2$	5.583	3.410
		$3\ell/4$	4.184	2.209
	Full	$\ell/4$	4.181	2.190
		$\ell/2$	5.599	3.396
		$3\ell/4$	4.181	2.190
200	Partial	$\ell/4$	4.118	2.177
		$\ell/2$	5.541	3.406
		$3\ell/4$	4.161	2.208
	Full	$\ell/4$	4.163	2.178
		$\ell/2$	5.573	3.380
		$3\ell/4$	4.163	2.178

Table 5.4 Vertical Dynamic Displacements (in cm)

Length [m]	Correlation	Point	μ_{w_m}	σ_{w_m}
20	Partial	$\ell/4$	1.614	0.536
		$\ell/2$	2.318	0.756
		$3\ell/4$	1.628	0.534
	Full	$\ell/4$	1.621	0.535
		$\ell/2$	2.319	0.756
		$3\ell/4$	1.621	0.535
50	Partial	$\ell/4$	1.608	0.536
		$\ell/2$	2.316	0.756
		$3\ell/4$	1.631	0.533
	Full	$\ell/4$	1.620	0.534
		$\ell/2$	2.318	0.756
		$3\ell/4$	1.620	0.534
100	Partial	$\ell/4$	2.833	1.632
		$\ell/2$	3.875	2.505
		$3\ell/4$	2.846	1.628
	Full	$\ell/4$	2.843	1.626
		$\ell/2$	3.881	2.497
		$3\ell/4$	2.843	1.626
200	Partial	$\ell/4$	2.814	1.628
		$\ell/2$	3.852	2.500
		$3\ell/4$	2.834	1.622
	Full	$\ell/4$	2.831	1.618
		$\ell/2$	3.863	2.485
		$3\ell/4$	2.831	1.618

Table 5.5 Axial Force Parameters (in cm)

Length [m]	Correlation	Support	μ_{x_m}	σ_{x_m}
20	Partial	1 2	8.261 8.293	1.992 1.999
	Full	1 2	8.279	1.997
50	Partial	1 2	8.245 8.298	1.989 1.998
	Full	1 2	8.277	1.996
100	Partial	1 2	12.472 12.419	3.201 3.192
	Full	1 2	12.444	3.197
200	Partial	1 2	12.605 12.539	3.246 3.232
	Full	1 2	12.556	3.237

NOTE: Mean Maximum Axial Force = $\frac{AE}{\ell} \mu_{x_m}$

where,

A = area of beam;

E = elastic modulus; and

ℓ = span length.

Table 5.6 Shear Force Parameters (in cm) -- Shear-Beam Model

Length [m]	Correlation	Support	μ_{x_m}	σ_{x_m}
20	Partial	1 2	11.539 11.600	3.404 3.425
	Full	1 2	11.574	3.417
50	Partial	1 2	11.469 11.566	3.380 3.415
	Full	1 2	11.529	3.403
100	Partial	1 2	22.887 22.798	8.176 8.217
	Full	1 2	22.862	8.189
200	Partial	1 2	22.790 22.684	8.138 8.187
	Full	1 2	22.770	8.154

NOTE: Mean Maximum Shear Force = $\frac{k'G}{\ell} \mu_{x_m}$

where,

k' = numerical factor depending on shape of cross section;

G = shear modulus; and

ℓ = span length.

Table 5.7 Moment Parameters (in cm) -- Transverse Direction (Bernoulli-Euler Model)

Length [m]	Correlation	Point	μ_{x_m}	σ_{x_m}
20	Partial	$\ell/4$	2.549	0.798
		$\ell/2$	3.704	1.138
		$3\ell/4$	2.574	0.802
	Full	$\ell/4$	2.558	0.803
		$\ell/2$	3.710	1.138
		$3\ell/4$	2.558	0.803
50	Partial	$\ell/4$	2.539	0.790
		$\ell/2$	3.682	1.133
		$3\ell/4$	2.578	0.796
	Full	$\ell/4$	2.548	0.799
		$\ell/2$	3.697	1.134
		$3\ell/4$	2.548	0.799
100	Partial	$\ell/4$	4.316	1.968
		$\ell/2$	6.150	2.990
		$3\ell/4$	4.219	2.112
	Full	$\ell/4$	4.250	2.402
		$\ell/2$	6.198	2.960
		$3\ell/4$	4.250	2.402
200	Partial	$\ell/4$	4.314	1.941
		$\ell/2$	6.079	3.004
		$3\ell/4$	4.224	2.106
	Full	$\ell/4$	4.223	2.037
		$\ell/2$	6.171	2.945
		$3\ell/4$	4.223	2.037

NOTE: Mean Maximum Moment = $\frac{EI\pi^2}{\ell^2} \mu_{x_m}$

where,

E = elastic modulus;

I = moment of inertia; and

ℓ = span length.

Table 5.8 Shear Force Parameters (in cm) -- Transverse Direction (Bernoulli-Euler Model)

Length [m]	Correlation	Support	μ_{x_m}	σ_{x_m}
20	Partial	1 2	3.682 3.651	1.080 1.108
	Full	1 2	3.660	1.096
50	Partial	1 2	3.683 3.642	1.066 1.106
	Full	1 2	3.645	1.092
100	Partial	1 2	7.403 6.826	2.333 2.477
	Full	1 2	7.226	2.341
200	Partial	1 2	7.380 6.552	2.351 2.594
	Full	1 2	7.182	2.338

NOTE: Mean Maximum Shear Force = $\frac{EI\pi^3}{\ell^3}\mu_{x_m}$

where,

E = elastic modulus;

I = moment of inertia; and

ℓ = span length.

Table 5.9 Moment Parameters (in cm) -- Vertical Direction (Bernoulli-Euler Model)

Length [m]	Correlation	Point	μ_{x_m}	σ_{x_m}
20	Partial	$\ell/4$	1.625	0.510
		$\ell/2$	2.500	0.743
		$3\ell/4$	1.628	0.518
	Full	$\ell/4$	1.623	0.515
		$\ell/2$	2.502	0.743
		$3\ell/4$	1.623	0.515
50	Partial	$\ell/4$	1.628	0.507
		$\ell/2$	2.497	0.743
		$3\ell/4$	1.632	0.519
	Full	$\ell/4$	1.622	0.514
		$\ell/2$	2.500	0.742
		$3\ell/4$	1.622	0.514
100	Partial	$\ell/4$	3.548	1.205
		$\ell/2$	4.643	1.953
		$3\ell/4$	3.446	1.241
	Full	$\ell/4$	3.500	1.220
		$\ell/2$	4.654	1.947
		$3\ell/4$	3.500	1.220
200	Partial	$\ell/4$	3.554	1.194
		$\ell/2$	4.612	1.948
		$3\ell/4$	3.410	1.244
	Full	$\ell/4$	3.486	1.214
		$\ell/2$	4.634	1.937
		$3\ell/4$	3.486	1.214

NOTE: Mean Maximum Moment = $\frac{EI\pi^2}{\ell^2}\,\mu_{x_m}$

where,

E = elastic modulus;

I = moment of inertia; and

ℓ = span length.

Table 5.10 Shear Force Parameters (in cm) -- Vertical Direction (Bernoulli-Euler Model)

Length [m]	Correlation	Support	μ_{x_m}	σ_{x_m}
20	Partial	1 2	2.681 2.587	0.656 0.660
	Full	1 2	2.633	0.657
50	Partial	1 2	2.709 2.562	0.655 0.663
	Full	1 2	2.632	0.657
100	Partial	1 2	6.954 6.636	1.727 1.684
	Full	1 2	6.816	1.705
200	Partial	1 2	6.977 6.527	1.730 1.668
	Full	1 2	6.793	1.698

NOTE: Mean Maximum Shear Force = $\frac{EI\pi^3}{\ell^3} \mu_{x_m}$

where,

E = elastic modulus;

I = moment of inertia; and

ℓ = span length.

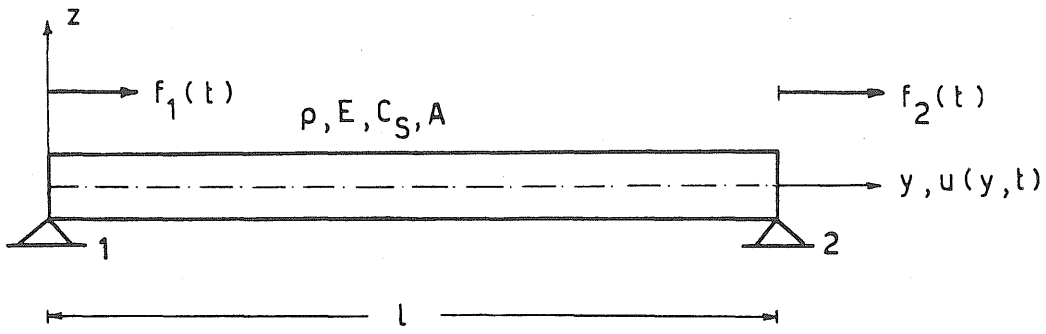

Figure 5.1 Structural Model for Beams -- Axial Motion

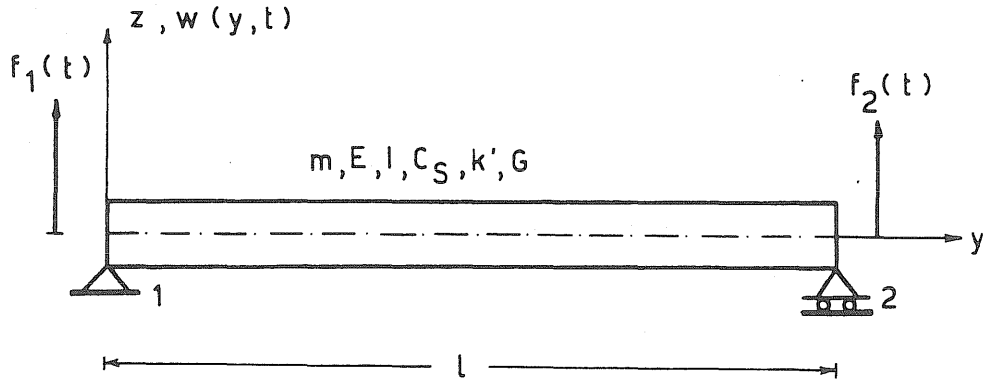

Figure 5.2 Structural Model for Beams -- Transverse and Vertical Motion

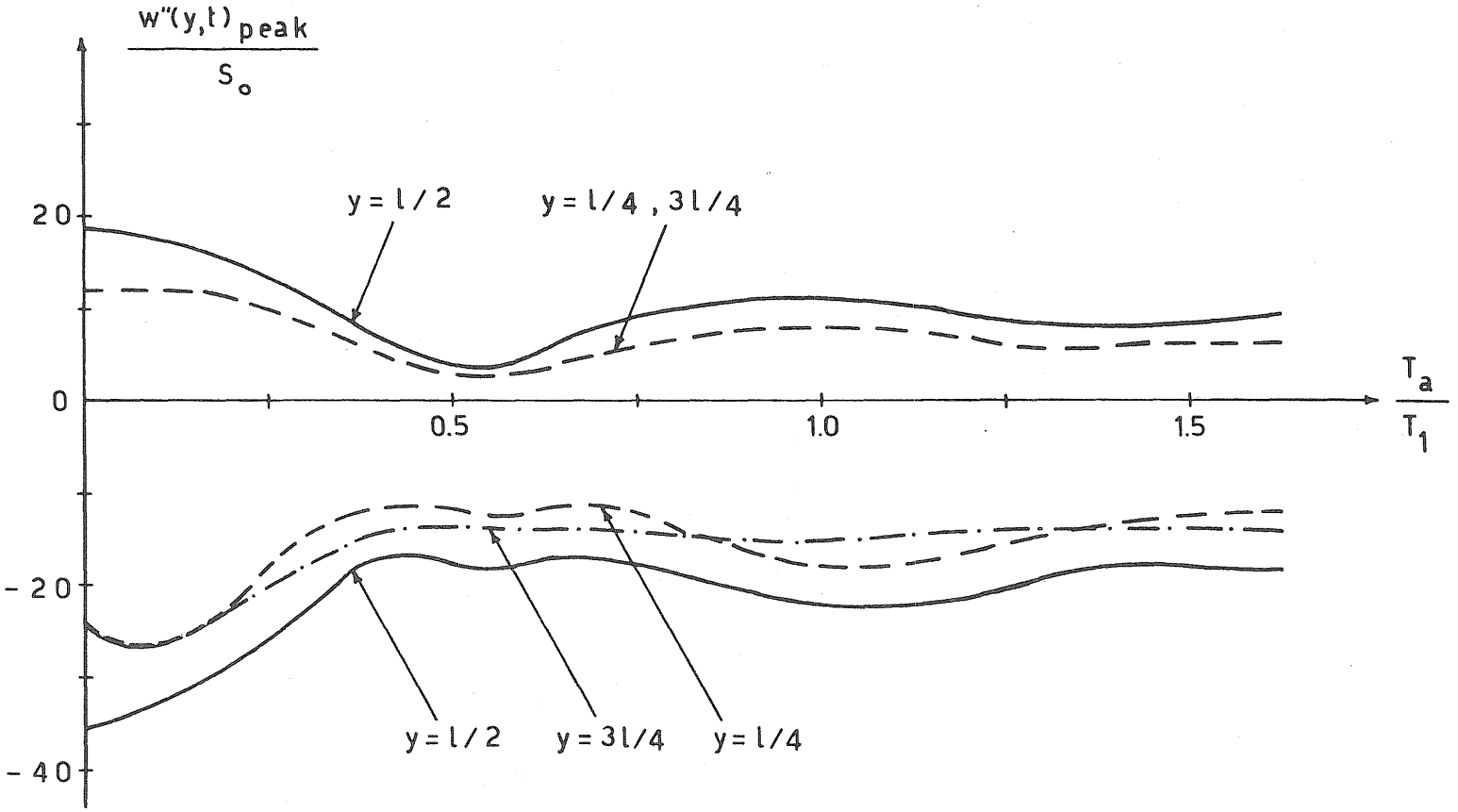

Figure 5.3 Curvature Response Spectrum (Masri, 1976)

CHAPTER 6

SUMMARY AND CONCLUSIONS

6.1 Seismic Ground Motion Model

6.1.1 Summary

A model is presented for determining the stochastic characteristics of earthquake ground motions. The model is based on the assumption that the excitation at the earthquake source (fault rupture) may be represented by a stochastic random process for which a power spectral density is assigned; this power spectral density is a function of the earthquake magnitude and the characteristics of the surrounding medium. The excitation at the source is transmitted to the ground surface by means of a frequency transfer function, which is obtained from an analytical wave propagation solution and a system identification technique. The model allows the evaluation of the power spectral density functions of ground motions at various points on the surface, the cross spectral density functions between two different points or two different directions, and the evaluation of the spatial variation of ground motions.

The model does not rely directly on previous earthquake data; instead, the input to the model is the earthquake magnitude, the orientation of existing faults, the distance of the site from the fault, and the characteristics of the ground.

The results of the model have been compared with data from an actual earthquake, the earthquake of January 29, 1981 recorded at the SMART-1

array, located in Lotung, Taiwan. These results include power spectral densities for acceleration at the stations of the array lying along the epicentral direction, cross-correlation coefficients between the motions in the directions along and normal to the epicentral direction, the spatial correlation coefficients, as well as the power spectral densities of differential acceleration. The results are in reasonable agreement with the empirical data of the single earthquake.

6.1.2 Conclusions

On the basis of this study, the following conclusions concerning the seismic ground model may be drawn:

1. The model may be used to predict the power spectral density of the acceleration at the ground surface. Any difference between the results of the model and the empirical data from a single earthquake can be attributed to the assumptions made in the analysis, namely the assumption of an elastic, homogeneous and isotropic half-space and the idealization of the three-dimensional problem with a two-dimensional wave propagation model.

2. The cross-correlation coefficients in two different directions are in reasonable agreement with the results from the earthquake data.

3. Where comparison is possible, the spatial variations of the ground motions are in reasonable agreement with the empirical results of one earthquake.

4. The power spectral densities for differential motions obtained with the model have the same trend as those of the empirical data.

The model may also be extended to layered media.

6.2 Effect of Differential Motion on Lifelines

6.2.1 Summary

Several lifeline problems were examined in this study. These include differential motions between pipe segments, the displacements, stresses

and strains of continuous pipelines, and displacements and forces in single-span simply-supported long structures (idealized as beams).

In each case the effects of correlated motions were examined; the motion at the various supports was considered to be either fully correlated or partially correlated, the latter representing the seismic ground motions obtained by the wave propagation analysis. Various lengths of the lifelines were used to examine the effect of differential motion. In all cases the excitations in three different directions were considered, namely the axial, transverse, and vertical motions. The axial motion is assumed to coincide with the epicentral direction.

6.2.2 Conclusions

On the basis of the results obtained, the following conclusions may be observed:

Joints of Pipelines -- As far as the joints of a pipeline are concerned, the differential ground motion is of major importance. Whereas the fully correlated support motion will yield zero differential displacements and forces between the pipe segments, the partially correlated support motion can give high differential displacements. This agrees with observations made from past earthquakes, where most of the damage to pipelines occurred at the joints, thus contradicting the assumption that fully correlated input motion is a safe approach in the seismic evaluation of pipelines. This would also imply that the evaluation of the differential motion by means of the interference response spectra may be on the unsafe side.

The examination of the transverse response indicated that it may be as important as the axial response. This is consistent with observed seismic damages of pipelines, in which damages at the joints were equally attributed to compression-tension forces and shear forces. As expected, the motion in the vertical direction is smaller than in the other two.

The proposed Differential Response Spectrum predicts the maximum differential motion between the pipe segments as a function of the system frequency.

Continuous Pipelines -- For a continuous pipeline, the differential seismic motion is of major importance. The fully correlated motion at the supports excites the first mode only, which is a rigid body mode, and thus yields zero stresses and strains, which contradicts observed damage in pipelines. On the other hand, the partially correlated input motion excites all modes, and results in relatively high stresses and strains. The displacements resulting from the two different input motions are approximately the same, as the major contribution to the displacements comes from the first (rigid body) mode.

For continuous pipelines, it is debatable as to which direction is the more important -- the axial or transverse direction. The results of this study show that for relatively stiff pipelines the transverse direction is dominant. As the length increases, the response in the transverse direction tends to remain constant, whereas the response in the axial direction increases. Therefore, in the analysis of stiff pipelines (e.g., large diameter pipes) the transverse direction should not be neglected.

Long Beams -- The effect of differential ground motions is not as significant for single-span, simply-supported beams as it is for pipelines. The axial and shear forces at one support of the beam, as well as the bending moments at its quarter points along the span become slightly higher when subjected to partially correlated input motions.

Although not examined here, it is generally believed that the differential ground motions are important in the consideration of multi-span beam structures. This analysis shows that the partially correlated ground motions yield slightly higher forces and moments than those of fully correlated input motions even for simply-supported beams.

The general conclusion, based on the three different lifeline structural systems examined herein, is that the spatial variation of ground motions plays an important role in the seismic safety evaluation of long horizontal structures.

6.3 Suggestions for Further Study

On the basis of this work, the following suggestions for further study can be made.

1. The analytical model presented herein has been validated for a single earthquake; consequently, the approximate power spectral density of differential accelerations is valid for site conditions similar to those of the SMART-1 array and earthquakes of magnitude approximately 6.3. Validation of the model with data from other earthquakes is necessary, before more general power spectral densities can be suggested. For example, the approximate power spectral densities in this study depend only on separation distances. Other factors such as soil conditions and earthquake magnitude may be included as well and may be of major importance to the seismic safety evaluation of long lifelines.

2. The model presented herein assumes that the three-dimensional wave propagation problem during an earthquake may be decomposed into a plane strain and an antiplane problem, in which the medium is considered to be elastic, homogeneous and isotropic. A three-dimensional model, which will take into account the inelastic parameters and the anisotropy of the ground should provide better results for predicting the spatial ground motions from earthquakes.

APPENDIX A

POWER SPECTRAL DENSITY OF DIFFERENTIAL MOTION BETWEEN THE PIPE SEGMENTS FOR EXCITATION NORMAL TO THE PIPELINE AXIS

The autocorrelation function of the differential motion between the pipe segments is defined as,

$$R_{\Delta x,\Delta x}(\tau) = E[\Delta x(t)\ \Delta x(t+\tau)]$$

$$= E\{[C_{II}\ y_2(t) + C_{IV}\ y_4(t)]\ [C_{II}\ y_2(t+\tau) + C_{IV}\ y_4(t+\tau)]\}$$

$$= C_{II}^2\ R_{y_2y_2}(\tau) + C_{II}C_{IV}\ (R_{y_2y_4}(\tau) + R_{y_4y_2}(\tau))$$

$$+ C_{IV}^2\ R_{y_4y_4}(\tau) \qquad (A.1)$$

where C_{II} and C_{IV} are defined in Eq. 4.25, and $y_2(t)$ and $y_4(t)$ denote the responses of the generalized coordinates due to the excitations $x_{G_1}(t)$ and $x_{G_2}(t)$ at the supports.

The generalized response $y_i(t)$ is given by Eq. 4.23; for the two modes of interest, namely the second and the fourth, the exciting forces are given by (Eq. 4.22),

$$f_2(t) = f_4(t) = c_g\left(\dot{x}_{G_1}(t) - \dot{x}_{G_2}(t)\right) + k_g\left(x_{G_1}(t) - x_{G_2}(t)\right) \qquad (A.2)$$

where $x_{G_1}(t)$, $x_{G_2}(t)$ and their derivatives are random processes.

The cross-correlation function $R_{f_j f_\ell}(\tau)$, where j and ℓ are equal to either 2 or 4, is given by

$$R_{f_j f_\ell}(\tau) = E\left[f_j(t)\ f_\ell(t+\tau)\right] \qquad (A.3)$$

where $f_j(t)$ and $f_\ell(t+\tau)$ are given by Eq. A.2, and E denotes expected value.

The cross-correlation function $R_{y_j y_\ell}(\tau)$ becomes then,

$$R_{y_j y_\ell}(\tau) = E\left[y_j(t)\ y_\ell(t+\tau)\right]$$

$$= \frac{1}{m_j m_\ell} \int_{-\infty}^{\infty}\int h_j(\tau_1)\ h_\ell(\tau_2)\ R_{f_j f_\ell}(\tau+\tau_1-\tau_2)\ d\tau_1\ d\tau_2 \qquad (A.4)$$

where m_j and m_ℓ are given by Eq. 4.22.

The power spectral density of the differential displacement between the pipe segments, when the earthquake excitation is normal to the pipeline axis, may, then, be evaluated by taking the Fourier transform of Eqs. A.1, A.3 and A.4.

APPENDIX B

POWER SPECTRAL DENSITY OF DISPLACEMENTS (CONTINUOUS PIPELINES)

The procedure for obtaining the power spectral density of displacements for continuous pipelines will be described for axial motion only. The corresponding power spectral density for transverse motion may be evaluated following a similar procedure.

The cross-correlation function between the displacement at two different points along the axis of the pipeline is given by,

$$R_{v(y_\alpha),v(y_\beta)}(\tau) = R_{v(y_\alpha),v(y_\beta)}(t_k,t_\ell)$$

$$= E\Big[\sum_{i=1}^{N} \phi_i(y_\alpha)\, q_i(t_k) \sum_{j=1}^{N} \phi_j(y_\beta)\, q_j(t_\ell)\Big]$$

$$= \sum_{i=1}^{N}\sum_{j=1}^{N} \phi_i(y_\alpha)\, \phi_j(y_\beta)\, R_{q_i q_j}(t_k,t_\ell) \qquad \text{(B.1)}$$

where:

$v(y_\alpha)$, $v(y_\beta)$ = the displacements evaluated at y_α and y_β along the pipeline axis;

$R_{q_i q_j}(t_k,t_\ell)$ = the cross-correlation function between the generalized coordinates;

t_k, t_ℓ = time instances; and

$\tau = t_\ell - t_k$, is the time lag.

The cross-correlation function $R_{q_i q_j}(t_k, t_\ell)$ is

$$R_{q_i q_j}(t_k, t_\ell) = \int_{-\infty}^{\infty}\int h_i(t_k - \tau_k)\, h_j(t_\ell - \tau_\ell)\, R_{A_i A_j}(\tau_k, \tau_\ell)\, d\tau_k\, d\tau_\ell \qquad (B.2)$$

in which the cross-correlation function $R_{A_i A_j}(\tau_k, \tau_\ell)$ is given by

$$R_{A_i A_j}(\tau_k, \tau_\ell) = \frac{C_A^2}{m^2 L_i L_j} \int_0^\ell \int_0^\ell \phi_i(y_1)\, \phi_j(y_2)\, R_{\dot{v}_g(y_1), \dot{v}_g(y_2)}(\tau_k, \tau_\ell)\, dy_1 dy_2$$

$$+ \frac{C_A K_A}{m^2 L_i L_j} \int_0^\ell \int_0^\ell \phi_i(y_1)\, \phi_j(y_2)\, R_{\dot{v}_g(y_1), v_g(y_2)}(\tau_k, \tau_\ell)\, dy_1 dy_2$$

$$+ \frac{K_A C_A}{m^2 L_i L_j} \int_0^\ell \int_0^\ell \phi_i(y_1)\, \phi_j(y_2)\, R_{v_g(y_1), \dot{v}_g(y_2)}(\tau_k, \tau_\ell)\, dy_1 dy_2$$

$$+ \frac{K_A^2}{m^2 L_i L_j} \int_0^\ell \int_0^\ell \phi_i(y_1)\, \phi_j(y_2)\, R_{v_g(y_1), v_g(y_2)}(\tau_k, \tau_\ell)\, dy_1 dy_2 \qquad (B.3)$$

where:

$R_{\dot{v}_g(y_1), \dot{v}_g(y_2)}(\tau_k, \tau_\ell)$; $R_{\dot{v}_g(y_1), v_g(y_2)}(\tau_k, \tau_\ell)$;

$R_{v_g(y_1), \dot{v}_g(y_2)}(\tau_k, \tau_\ell)$; and $R_{v_g(y_1), v_g(y_2)}(\tau_k, \tau_\ell)$

are the cross-correlation functions of the ground velocities, between velocity and displacement, displacement and velocity, and displacements, respectively.

The cross spectral density function of the displacement in the axial direction along the axis of the pipeline is then simply the Fourier transform of Eq. B.1, namely

$$S_{v(y_\alpha),v(y_\beta)}(\omega) = \sum_{i=1}^{N} \sum_{j=1}^{N} \phi_i(y_\alpha)\, \phi_j(y_\beta)\, S_{q_i q_j}(\omega) \qquad \text{(B.4)}$$

where $S_{q_i q_j}(\omega)$ is the Fourier transform of Eq. B.2,

$$S_{q_i q_j}(\omega) = H_i^*(\omega)\, H_j(\omega)\, S_{A_i A_j}(\omega) \qquad \text{(B.5)}$$

where:

$H_j(\omega)$ = the frequency transfer function, i.e.,

$$H_j(\omega) = \frac{1}{\omega_j^2 - \omega^2 + 2\zeta_j \omega_j \omega i} \quad ;$$

and, finally, $S_{A_i A_j}(\omega)$ is given by

$$S_{A_i A_j}(\omega) = \frac{1}{m^2 L_i L_j} \left[\frac{C_A^2}{\omega^2} + \frac{K_A^2}{\omega^4} \right] \int_0^{\ell} \int_0^{\ell} \phi_i(y_1)\, \phi_j(y_2)$$

$$\cdot\, S_{\ddot{v}_g(y_1),\ddot{v}_g(y_2)}(\omega)\, dy_1\, dy_2 \qquad \text{(B.6)}$$

which was obtained by taking the Fourier transform of Eq. B.3.

APPENDIX C

POWER SPECTRAL DENSITY OF AXIAL DISPLACEMENTS (BEAMS)

The cross-correlation function of the total displacement in the axial direction between two points along the axis of the beam is given by,

$$R_{u(y_\alpha),u(y_\beta)}(\tau) = R_{u(y_\alpha),u(y_\beta)}(t_1,t_2)$$

$$= R_{u_s(y_\alpha),u_s(y_\beta)}(t_1,t_2) + R_{u_s(y_\alpha),u_D(y_\beta)}(t_1,t_2)$$

$$+ R_{u_D(y_\alpha),u_s(y_\beta)}(t_1,t_2) + R_{u_D(y_\alpha),u_D(y_\beta)}(t_1,t_2) \quad \text{(C.1)}$$

where:

$u(y_\alpha,t_1)$, $u(y_\beta,t_2)$ = the total displacements at points y_α and y_β along the axis of the beam evaluated at time instance t_1 and t_2, respectively, as given by Eq. 5.3;

$u_s(y_\alpha,t_1)$, $u_s(y_\beta,t_2)$ = the quasi-static displacements as given by Eq. 5.4;

$u_D(y_\alpha,t_1)$, $u_D(y_\beta,t_2)$ = the dynamic displacements as given by Eq. 5.5; and

$\tau = t_2 - t_1$, is the time lag.

The four terms on the right-hand side of Eq. C.1 are,

$$R_{u_s(y_\alpha),u_s(y_\beta)}(t_1,t_2) = (1 - \frac{y_\alpha}{\ell})(1 - \frac{y_\beta}{\ell})\, R_{f_1f_1}(t_1,t_2)$$

$$+ (1 - \frac{y_\alpha}{\ell})\, \frac{y_\beta}{\ell}\, R_{f_1f_2}(t_1,t_2) + \frac{y_\alpha}{\ell}\,(1 - \frac{y_\beta}{\ell})\, R_{f_2f_1}(t_1,t_2)$$

$$+ \frac{y_\alpha}{\ell}\, \frac{y_\beta}{\ell}\, R_{f_2f_2}(t_1,t_2) \qquad (C.2)$$

$$R_{u_s(y_\alpha),u_D(y_\beta)}(t_1,t_2) = \sum_{k=1}^{N} \frac{-2}{k\pi} \sin \frac{k\pi y_\beta}{\ell}$$

$$\cdot \{(1 - \frac{y_\alpha}{\ell}) \int_{-\infty}^{\infty} h_k(\tau_2)\, [R_{f_1\ddot{f}_1}(t_1,t_2-\tau_2)$$

$$- \cos k\pi\, R_{f_1\ddot{f}_2}(t_1,t_2-\tau_2)]\, d\tau_2 + \frac{y_\alpha}{\ell} \int_{-\infty}^{\infty} h_k(\tau_2)$$

$$\cdot [R_{f_2\ddot{f}_1}(t_1,t_2-\tau_2) - \cos k\pi\, R_{f_2\ddot{f}_2}(t_1,t_2-\tau_2)]\, d\tau_2\} \qquad (C.3)$$

$$R_{u_D(y_\alpha),u_s(y_\beta)}(t_1,t_2) = \sum_{j=1}^{N} \frac{-2}{j\pi} \sin \frac{j\pi y_\alpha}{\ell}$$

$$\cdot \{(1 - \frac{y_\beta}{\ell}) \int_{-\infty}^{\infty} h_j(\tau_1)\, [R_{\ddot{f}_1f_1}(t_1-\tau_1,t_2)$$

$$- \cos j\pi\, R_{\ddot{f}_2f_1}(t_1-\tau_1,t_2)]\, d\tau_1 + \frac{y_\beta}{\ell} \int_{-\infty}^{\infty} h_j(\tau_1)$$

$$\cdot [R_{\ddot{f}_1f_2}(t_1-\tau_1,t_2) - \cos j\pi\, R_{\ddot{f}_2f_2}(t_1-\tau_1,t_2)]\, d\tau_1\} \qquad (C.4)$$

and,

$$R_{u_D(y_\alpha),u_D(y_\beta)}(t_1,t_2) = \sum_{j=1}^{N}\sum_{k=1}^{N} \frac{4}{jk\pi^2} \sin\frac{j\pi y_\alpha}{\ell} \sin\frac{k\pi y_\beta}{\ell}$$

$$\cdot \int_{-\infty}^{\infty}\int h_j(\tau_1)\, h_k(\tau_2) \left[R_{\ddot{f}_1\ddot{f}_1}(t_1-\tau_1,t_2-\tau_2)\right.$$

$$- \cos k\pi\, R_{\ddot{f}_1\ddot{f}_2}(t_1-\tau_1,t_2-\tau_2) - \cos j\pi\, R_{\ddot{f}_2\ddot{f}_1}(t_1-\tau_1,t_2-\tau_2)$$

$$\left. + \cos j\pi \cos k\pi\, R_{\ddot{f}_2\ddot{f}_2}(t_1-\tau_1,t_2-\tau_2)\right] d\tau_1\, d\tau_2 \qquad (C.5)$$

where:

$h_j(t)$, $h_k(t)$ = the impulse response functions for the j^{th} and k^{th} mode, respectively, as defined in Eq. 5.9;

$R_{f_m f_n}(\tau)$ = the cross-correlation function of the input displacements at supports m and n (m and n take values from 1 to 2);

and double dot denotes second derivative with respect to time.

The cross spectral density functions of the quasi-static and dynamic displacements may be obtained by taking the Fourier transform of Eqs. C.2 through C.5, while the cross spectral density of the total response is given by the Fourier transform of Eq. C.1.

LIST OF REFERENCES

1. Abdel-Ghaffar, A. M., "Studies on the Effect of Differential Motion of Two Foundations Upon the Response of the Superstructure of a Bridge," Earthquake Engineering Research Laboratory Report No. EERL 77-02, California Institute of Technology, Pasadena, California, January 1977.

2. Aki, K., "Scaling Law of Seismic Spectrum," Jour. Geophys. Res., Vol. 72, No. 4, pp. 1217-1231, February 1967.

3. Andrews, D. J., "A Stochastic Source Model 2 Time-Dependent Case," Jour. Geophys. Res., Vol. 86, No. B11, pp. 10821-10834, November 1981.

4. Beck, J. L., "Determining Models of Structures from Earthquake Records," Earthquake Engineering Research Laboratory Report No. EERL 78-01, California Institute of Technology, Pasadena, California, June 1978.

5. Bendat, J. S., Principles and Applications of Random Noise Theory, Robert E. Krieger Publishing Company, Huntington, New York, 1977.

6. Bogdanoff, J. L., Goldberg, J. E., and Schiff, A. J., "The Effect of Ground Transmission Time on the Response of Long Structures," Bull. Seism. Soc. Am., Vol. 55, No. 3, pp. 627-640, June 1965.

7. Bolt, B. A., Loh, C. H., Penzien, J., Tsai, Y. B., and Yeh, Y. T., "Preliminary Report on the SMART 1 Strong Motion Array in Taiwan," Earthquake Engineering Research Center Report No. UCB/EERC 82-13, University of California, Berkeley, California, August 1982.

8. Boore, D. M., and Joyner, W. B., "The Influence of Rupture Incoherence on Seismic Directivity," Bull. Seism. Soc. Am., Vol. 68, No. 2, pp. 283-300, April 1978.

9. Davenport, A. G., "The Distribution of Largest Values of a Random Function with Application to Gust Loading," Proceedings, Institute of Civil Engineers, London, Vol. 28, Paper No. 6739, pp. 187-196, June 1964.

10. Donovan, N. C., and Bornstein, A. E., "Uncertainties in Seismic Risk Procedures," Jour. Geotech. Div., ASCE, Vol. 104, No. GT7, pp. 869-887, July 1978.

11. Dravinski, M., "Evaluation of Strong Ground Motion Using Boundary Integral Equation Approach," in Earthquake Source Modeling, Ground Motion and Structural Response, editor S. K. Datta, ASME, PVP-Vol. 80, AMD-Vol. 60, pp. 61-80, 1984.

12. Farewell, T. E., and Robinson, A. R., "Wave Propagation in an Elastic Half-Space Due to Couples Applied at a Point Beneath the Surface," Civil Engineering Studies, Scientific Research Series No. 411, University of Illinois at Urbana-Champaign, Urbana, Illinois, August 1974.

13. Hall, W. J., and Newmark, N. M., "Seismic Design of Bridges--An Overview of Research Needs," Proceedings, Workshop on Earthquake Resistance of Highway Bridges, Palo Alto, California, pp. 164-181, January 1979.

14. Hanks, T. C., "b Values and $\omega^{-\gamma}$ Seismic Source Models: Implications for Tectonic Stress Variations Along Active Crystal Fault Zones and the Estimation of High Frequency Strong Ground Motion," Jour. Geophys. Res., Vol. 84, No. B5, pp. 2235-2242, May 1979.

15. Hanks, T. C., and Kanamori, H., "A Moment Magnitude Scale," Jour. Geophys. Res., Vol. 84, No. B5, pp. 2348-2350, May 1979.

16. Hanks, T. C., and McGuire, R. K., "The Character of High-Frequency Strong Ground Motion," Bull. Seism. Soc. Am., Vol. 71, No. 6, pp. 2071-2095, December 1981.

17. Harada, T., "Probabilistic Modeling of Spatial Variation of Strong Earthquake Ground Displacements," Proceedings, Eighth World Conference on Earthquake Engineering, San Francisco, Vol. II, pp. 605-612, July 1984.

18. Harichandran, R., and Vanmarcke, E., "Space-Time Variation of Earthquake Ground Motion," Research Report R84-12, Department of Civil Engineering, Massachusetts Institute of Technology, Cambridge, Massachusetts, September 1984.

19. Haskell, N. A., "Total Energy and Energy Spectral Density of Elastic Wave Radiation from Propagating Faults," Bull. Seism. Soc. Am., Vol. 54, No. 6, pp. 1811-1841, December 1964.

20. Haskell, N. A., "Total Energy and Energy Spectral Density of Elastic Wave Radiation from Propagating Faults. Part II. A Statistical Source Model," Bull. Seism. Soc. Am., Vol. 56, No. 1, pp. 125-140, February 1966.

21. Hindy, A., and Novak, M., "Pipeline Response to Random Ground Motion," Jour. Eng. Mech. Div., ASCE, Vol. 106, No. EM2, pp. 339-360, April 1980.

22. Housner, G. W., "Properties of Strong Ground Motion Earthquakes," Bull. Seism. Soc. Am., Vol. 45, pp. 197-218, 1955.

23. Housner, G. W., and Jennings, P. C., "Generation of Artificial Earthquakes," Jour. Eng. Mech. Div., ASCE, Vol. 90, No. EM1, pp. 113-151, February 1964.

24. Iwasaki, T., Penzien, J., and Clough, R., "Literature Survey-Seismic Effects on Highway Bridges," Earthquake Engineering Research Center Report No. EERC 72-11, University of California, Berkeley, California, November 1972.

25. Jennings, P. C., and Wood, J. H., "Earthquake Damage to Freeway Structures," in Engineering Features of the San Fernando Earthquake, February 9, 1971, editor P. C. Jennings, Report No. EERL 71-02, California Institute of Technology, Pasadena, California, June 1971.

26. Johnson, N. E., and Galletly, R. D., "The Comparison of the Response of a Highway Bridge to Uniform Ground Shock and Moving Ground Excitation," The Shock and Vibration Bull., No. 42, Part 2, pp. 75-85, January 1972.

27. Johnson, J. J., and Robinson, A. R., "Wave Propagation in a Half-Space Due to an Interior Point Load Parallel to the Surface," Civil Engineering Studies, Structural Research Series No. 388, University of Illinois at Urbana-Champaign, Urbana, Illinois, July 1972.

28. Joyner, W. B., "A Scaling Law for the Spectra of Large Earthquakes," Bull. Seism. Soc. Am., Vol. 74, No. 4, pp. 1167-1188, August 1984.

29. Kanai, K., "Semi-Empirical Formula for the Seismic Characteristics of the Ground," Bull. Earthq. Res. Inst., University of Tokyo, Tokyo, Japan, Vol. 35, pp. 307-325, June 1957.

30. Kanamori, H., "Determination of Effective Tectonic Stress Associated with Earthquake Faulting. The Tottori Earthquake of 1943," Phys. Earth Planet. Interiors, Vol. 5, pp. 426-434, October 1972.

31. Kanamori, H., and Anderson, D. L., "Theoretical Basis of Some Empirical Relations in Seismology," Bull. Seism. Soc. Am., Vol. 65, No. 5, pp. 1073-1095, October 1975.

32. Lin, Y. K., Probabilistic Theory of Structural Dynamics, Robert E. Krieger Publishing Company, Huntington, New York, 1976.

33. Loh, C. H., personal communication, 1984a.

34. Loh, C. H., "Study of Spatial Variation of SMART-1 Array Data, and the Effects of Wave Propagation on Buried Pipelines," Civil Engineering Studies, National Central University, Department of Civil Engineering, Chung-Li, Taiwan, March 1984b.

35. Loh, C. H., Ang, A. H-S., and Wen, Y. K., "Spatial Correlation Study of Strong Motion Array Data with Application to Lifeline Earthquake Engineering," Civil Engineering Studies, Structural Research Series No. 503, University of Illinois at Urbana-Champaign, Urbana, Illinois, March 1983.

36. Longuet-Higgins, M. S., "On the Statistical Distribution of the Heights of Sea Waves," Jour. of Marine Research, Vol. 3, pp. 245-266, 1952.

37. Masri, S. F., "Response of Beams to Propagating Boundary Excitation," Earthq. Eng. and Struc. Dyn., Vol. 4, No. 5, pp. 497-509, July-September 1976.

38. Mindlin, R. D., and Goodman, L. E., "Beam Vibrations with Time-Dependent Boundary Conditions," Jour. of Applied Mechanics, Vol. 17, No. 3, pp. 377-380, December 1950.

39. Mohammadi, J., and Ang, A. H-S., "A Method for the Analysis of Seismic Reliability of Lifeline Systems," Civil Engineering Studies, Structural Research Series No. 474, University of Illinois at Urbana-Champaign, Urbana, Illinois, February 1980.

40. Nelson, I., and Weidlinger, P., "Development of Interference Response Spectra for Lifelines Seismic Analysis," Grant Report No. 2, Weidlinger Associates, New York, New York, July 1977 [for National Science Foundation (RANN), Grant No. ENV P76-9838].

41. Newmark, N. M., and Hall, W. J., "Seismic Design Criteria for Nuclear Reactor Facilities," Proceedings, Fourth World Conference on Earthquake Engineering, Santiago, Chile, Vol. 2, Session B-4, pp. 37-50, January 1969.

42. Newmark, N. M., and Rosenblueth, E., Fundamentals of Earthquake Engineering, Prentice-Hall, Inc., Englewood Cliffs, New Jersey, 1971.

43. Novak, M., and Hindy, A., "Seismic Response of Buried Pipelines," Advances in Civil Engineering through Engineering Mechanics, ASCE, pp. 44-47, May 1977.

44. Papageorgiou, A. S., and Aki, K., "A Specific Barrier Model for the Quantitative Description of Inhomogeneous Faulting and the Prediction of Strong Ground Motion. I. Description of the Model," Bull. Seism. Soc. Am., Vol. 73, No. 3, pp. 693-722, June 1983a.

45. Papageorgiou, A. S., and Aki, K., "A Specific Barrier Model for the Quantitative Description of Inhomogeneous Faulting and the Prediction of Strong Ground Motion. II. Applications of the Model," Bull. Seism. Soc. Am., Vol. 73, No. 4, pp. 953-978, August 1983b.

46. Sakurai, A., and Takahashi, T., "Dynamic Stresses of Underground Pipelines During Earthquakes," Proceedings, Fourth World Conference on Earthquake Engineering, Santiago, Chile, Vol. 2, Session B-4, pp. 81-95, January 1969.

47. Sato, R., "Stress Drop for a Finite Fault," Jour. Phys. Earth., Vol. 20, No. 4, pp. 397-407, 1972.

48. Seyyedian-Choobi, M., and Robinson, A. R., "Motion on the Surface of a Layered Elastic Half-Space Produced by a Buried Dislocation Pulse," Civil Engineering Studies, Structural Research Series No. 421, University of Illinois at Urbana-Champaign, Urbana, Illinois, November 1975.

49. Shinozuka, M., and Kawakami, H., "Ground Characteristics and Free Field Strains," Technical Report No. CU-2, Department of Civil Engineering and Engineering Mechanics, Columbia University in the City of New York, New York, August 1977.

50. Shinozuka, M., Takada, S., and Kawakami, H., "Risk Analysis of Underground Network Systems," Proceedings, U.S.-Southeast Asia Symposium on Engineering for Natural Hazards Protection, Manila, Philippines, pp. 44-58, 1977.

51. Tajimi, H., "A Statistical Method for Determining the Maximum Response of a Building Structure During an Earthquake," Proceedings, Second World Conference on Earthquake Engineering, Tokyo and Kyoto, Japan, Vol. 2, pp. 781-797, July 1960.

52. Thompson, J. C., and Robinson, A. R., "Exact Solution of Some Dynamic Problems of Indentation and Transient Loadings of an Elastic Half-Space," Civil Engineering Studies, Structural Research Series No. 350, University of Illinois at Urbana-Champaign, Urbana, Illinois, September 1969.

53. Thomson, W. T., Theory of Vibration with Applications, Prentice-Hall, Inc., Englewood Cliffs, New Jersey, 1981.

54. U. S. Department of Commerce, San Fernando, California Earthquake of February 9, 1971, Washington, D. C., 1973.